Dnyaneshwar Gramonnati Mandal's

HON. BALASAHEB JADHAV ARTS, COMMERCE AND SCIENCE COLLEGE

Ale, Tal. Junnar, Dist. Pune (412411)

Affiliated to : Savitribai Phule Pune University, Pune

One day MULTIDISCIPLINARY NATIONAL CONFERENCE

on

"ADVANCED MATERIALS, TECHNOLOGY, APPLICATIONS AND EDUCATION" [AMTAE-2021] (Multidisciplinary)

organized by

DEPARTMENT OF PHYSICS

Saturday 16th October 2021

National Conference on "Advanced Materials, Technology, Applications and Education"

Saturday Date: 16/10/2021

List of Paper Publications

Paper No.	Name of Researcher	Paper Title	Name of College
P-1	R. S. Shaikh L. S. Ravangave	Chemically Synthesized ZnO and Al, Ag and Cd Doped ZnO Nanoparticles at higher temperature 600^0C, study of Antibacterial Activity.	Department of Physics S.G.B.S. College, Purna (Jn.) Dt: Parbhani (Nanded University)
P-2	Prakash Rajaram Chavan	Statistical Analysis of HDFC and ICICI Bank Stocks	Department of Statistics Smt. KasturbaiWalchand College, Sangli (Kolhapur University)
P-3	D. M. Markad M. L. Muluk D. D. Muluk S. K. Ranyewale	Assessing The Suitability Of Beach Tourism At Achara and Devbaug Area in Malvan Tehsil, Sindhudurg District of Maharashtra, India	Dept of Geography Hutatma Rajguru Mahavidyalaya, Rajgurunagar (Pune University)
P-4	M. A. Patil, S. G. Thube, V. M. Nikale, Y. A. Pathak	Growth and Characterizations of Single Crystals of Pure and L-Alanine Doped Zinc Tris-Thiourea Sulphate	Department of Physics, Dada Patil Mahavidyalaya, Karjat Dist- Ahmednagar (Pune University)
P-5	Rohit R. Motkar, Nitin. D. Sali	Design and Development of low cost Spin Coating system for thin film development	Department of Physics, Ahmednagar College, Ahmednagar (Pune University)
P-6	Arun Garde Jitendra A. Borse	Electro-optical properties of Cu-doped ZnS thin film used as window layer in solar cell	Department of Physics, S P H Arts, Science and Commerce College, Nampur (Pune University)
P-7	Raghunath K. Sonawane, Kailas. H. Kapadnis, Arun B. Nikumbh, Vishnu A. Adole Kailaspati K.Jadhav	Interpretation of Viscometric, Thermodynamic and Acoustic properties of sodium fluoride in aqueous solutions of Dextrose at different molarities and temperatures	Research Centre in Chemistry, M.G. Vidyamandir's L.V.H. College, Nashik (Pune University)
P-8	Surekha Munde, Kranti Zakde, A. R. Khan, Y. H. Shaikh	Concentration-Dependent Diffusion Constant For Mass Transport Through Membranes	P.E.S College of Engineering, Aurangabad (Aurangabad University)
P-9	Dilip D. Muluk Arjun Musmade	An Assessment of District-wise Urbanization Growth of Maharashtra	Dept. of Geography, Hutatma Rajguru Mahavidyalaya, Rajgurunagar (Pune University)
P-10	Deshmane Jini Subhash Prakash Rajaram Chavan	An Analysis of the Determinants of Rural and Urban migration in Maharashtra state	Department of Zoology, Smt. Kasturbai Walchand College, Sangli (Kolhapur University)
P-11	Nirmala Kakade, Shobha Rupanar, Rituja Satpute	Study of Thermal Analytical Characteristics of Gymnemasylvestre plant by TGA-DTA technique	DadapatilRajale Arts, Science and Commerce College, Adinathnagar, Pathardi (Pune University)

P-12	Kaje Shraddha Shirke-Awachat	The Internet-Based Classroom Education For Visual Arts: Challenges & Opportunities	Faculty of Art & Design, Vishwakarma University, Pune
P-13	Chavan V. S.	Study of pH of Rhizospheric and Non-Rhizospheric soil of Lablab purpureus (L)	Department of Botany, Anandibai Pradhan Science College, Nagothane, Roha, Dist-Raigad (Mumbai University)
P-14	Vijay S. Raykar	A Theoretical and Experimental Study of Temperature Dependent Thermal Conductivity Enhancement of Functionalized Nanofluids	Department of Physics, G. M. Vedak College of Science, Tala (Mumbai University)
P-15	H. S. Koli, B. B. Bahule Khursheed Ahmed	Plant mediated biosynthesis, characterization and antioxidant activity of silver and copper nanoparticles employing root extract of Cyperus pertenuis	Department of Chemistry, Abeda Inamdar College, Pune. (Pune University)
P-16	Biplob Sarkar, Bitopan Das, Ankur Nath	Looking at the high-energy X-ray universe-An overview	Department of Applied Sciences, Tezpur University, Napaam, (Tezpur University, Assam)
P-17	Mahendra Shinde	Study of Synthesis and Applications of Zinc sulphide (ZnS) Thin Films: Review	Department of Physics, M.J.M. Arts, Commerce and Science College, Karanjali, Tal: Peth, Dist: Nashik (Pune University)
P-18	Goswami Vishal H.	Study of Assisting Tools like Pin-on-Disc to Determine Tribological Factors of Microhardness and Coefficients of Friction for Thin Film Coatings on Industrial Tools	Patkar, Varde College, Goregaon(W), Mumbai (Mumbai University)
P-19	Neerja	Dielectric and Mobility Profile of NADAC-ADC Co-Polymer	Department of Physics, DAV College, Amritsar (Punjab University)
P-20	Abullais Nehal Ahmed	Induced Transient Current Measurements and Characteristics of Transducer by Squeezing Piezoelectric Substances	Dept. of Physics, J.A.T. Arts, Science and Commerce College (For Women), Malegaon, Dist. Nashik (Pune University)
P-21	Kothawade N.B. Dhanwate S. V.	A Novel Multifunctional Binary Oxide Tio_2: Moo_3 Thin Films Deposited by Spray Pyrolysis Method	Department of Physics, Arts, Commerce and Science College, Kalwan (Manur) Dist. Nashik (Pune University)
P-22	Rupali Ajesh Gulalkari	Thermo Study of Commercial Samples of *Lohabhasma*	Dept of Chemistry BJS'S ASC College, Wagholi Pune. (Pune University)
P-23	Jayashree S. Patil	Development of an Extractive and Spectrophotometric determination of Strontium(II) with N,N''-bis (O-hydroxy-acetophenone) ethylenediimine (HAPED) derivative as an analytical reagent	Department of Chemistry, J.S.M. College, Alibag, Raigad. (Mumbai University)
P-24	R. N. Wadalkar S. P. Bakale	Study of Human Body Response for the Classical Ragas used for Releasing Tension, Played on Wind Instrument Shehnai using Psycho-Physiological Method	Department of Physics, Swami Mukatanand College of Science, Yeola (Pune University)

P-25	B. Kalyani	Role of Heavy Metal Oxide on Vanadium Doped Lithium Borate based Quaternary Glasses	University College for Women, Koti, (Hyderabad University)
P-26	Quadri F B Naseem Deshpande Sangeeta Shinde	Nanoparticles and Their Applications in Agriculture	Dr. Rafiq Zakaria College for Women, Aurangabad (Aurangabad University)
P-27	Vaishali S. Raut	A Short Review on Effect of Nanosizing on Biological Activities of Some Herbal Medicinal Plants based Nanoparticles.	Department of Chemistry K.V.N. Naik College, Nashik (Pune University)
P-28	Swarali Hinge, Digvijay Gore, G. R. Pansare	Optimization of Gamma Ray Spectroscopy Technique for Measurement of Nuclear Pollution of Water samples due to Uranium and Thorium salts	Department of Physics, Haribhai V. Desai College, Pune (Pune University)
P-29	S.R. Navale, S. K. Thorat S.N. Dalvi	Theoretical drying time from drying characteristics	S.N. Arts, D.J.M. Commerce and B.N. Sarada Science College, Sangamner,(PUNE UNIVERSITY)
P-30	Sangita Meshram, U. B. Tumberphale, P. G. Gawali	Dielectric Properties Of Allyl Amine And 2- Butoxyethanol Using Microwave Frequency 9.85 Ghz At Room Temperature	B. N. Bandodkar Science College, Thane (Mumbai University)
P-31	Sangita Shinde, Pallavi Nalle, P. Kute, Firdos Quadri N. D. Chaudhari	Facile Synthesis and Characterization of Copper Oxide (CuO) Nanoparticles via Sol-Gel Method	Pratishthan Mahavidyalaya, Paithan, Aurangabad (Aurangabad University)
P-32	Sukhada Pande, G.R. Pansare	Study of Exposure Dose of Gamma Radiations on Output Response of Silicon Solar Cell Panel	Haribhai V. Desai College, Pune(Pune University)
P-33	Tejas C. Gaikwad	Synthesis Of Nanocrystalline Zirconia By Various Chemical Methods : Review	MJM Arts, Commerce and Science College Karanjali, Nashik (Pune University)
P-34	Sharad Bangayya Ashok Kanade	RGB color space based Machine Vision system for classification of Guava fruits	P.V.P. College, Pravaranagar (Pune University)
P-35	G. R. Mahajan, Y. S. Joshi K. S. Kanse A. C. Kumbharkhane	Dielectric relaxation studies of potentised homeopathic medicine in the frequency range of 20 Hz to 2 MHz	Shri Datta Arts, Commerce and Science College Hadgaon,Nanded
P-36	Ajit Suryawanshi Dhammpal Suryawanshi, Anjali Rajbhoj	Spectroscopic Studies of Metal Complexes of Cu (II), Ni (II), Co (II), Cr (III) and Fe (III) Complexes	Hon. B. J. College, Ale (Pune University)
P-37	Savita V. Thakare	Investigation of antimicrobial properties and characterization of silver nanoparticles initiated via silver effluent	K.S.K.W. Arts, Science and Commerce College CIDCO Nashik (Pune University)
P-38	Bhausaheb R. Ghorpade	Studies On Glycogen Content And Haemolymph Lipid Profile In Freshwater Crab, *BarytelphusaGuerini* In Relation To Reproduction	Shri Anand College, Pathardi Dist. Ahmednagar (Pune University)

P-39	Ashok Kanade Arvind Shaligram	Development of metal oxide semiconductor gas sensor based system (E-Nose) for tropical fruit sorting	P.V.P. College, Pravaranagar (Pune University)
P-40	R S Indumathi, M R Rajesh Kanna, H. L. Parashivamurthy, Manjula C. Gudgeri , Niranjan K M C	Topological Indices Of 2-Deoxy–D-Glucose For Covid-19	MIT Mysore, Belwadi
P-41	Dr. Kritika Ms. Shweta	Employability and Employment Rate of Commerce Students in India: Comparison with Other Streams	Chaudhary Bansilal University, Bhiwani
P-42	J. R. Wadkar , R. G. Metkar , B. B. Pandit	Heat Transfer Analysis Of A Straight Fin With Temperature Dependent Properties	Swami Ramanand Teerth Marathwada University, Nanded
P-43	Patil D. N.	Ethan botanical study of Nagzira Wildlife Sanctuary, Gondia	BJS's A.S.C. College, Wagholi, Pune (Pune University)
P-44	D G Rathod, D N Rander, K S Kanse, Y S Joshi, A C Kumbharkhane	Study of dielectric and electrical properties of aqueous L-phenylalanine in the frequency range of 20 Hz to 2 MHz	Lal Bahadur Shastri Mahavidyalaya, Dharmabad, Dist. Nanded (Nanded University)
P-45	Sagar Pardhi, Milind Bhandare Madhav Sarode	Synthesis and Characterization of Bismuth Ferrite (BFO) Prepared by Auto Combustion Method for Photovoltaic Application	Department of Physics, Mahatma Phule Mahavidyalaya Pimpri, Pune (Pune University)
P-46	Dhumane N. R.	Comparative studies of SHG efficiency of L-Alanine and Glycine doped BisThiourea Cadmium Chloride (BTCC) single crystal	Shri Anand College, Pathardi Dist.-Ahmednagar (Pune University)
P-47	Bagade Aditi J. Temkar Vaishnavi S, Suse Sachin N.	Development of Multigrain Instant Porridge	Dept. of B. Voc. Food processing and Quality Management, A. A. College, Manchar. Pune (MH) (Pune University)
P-48	Yogeshwar Kaldante, Manohar Chaskar	Photocatalytic degradation of Xylenol Orange dye over hydrothermally synthesized Zinc Oxide	Department of Chemistry, PDEA's Baburaoji Gholap College, Sangvi, Pune, (Pune University)
P-49	Jagdeesh Pataiya, Lokesh Jharbade, Nilesh Dhurve, Neetu Paliwal, Manoj Singh Rana, Satish Bagde	Properties of Samarium Polonide with Nacl-type Structure	Department of Physics, Dr. Bhimrao Ambedkar Govt. College, Alma, (M.P.), India
P-50	Afroj Dange, Shraddha Mahakal	Development of Smart Energy Meter for Billing System Using ESP32	Annasaheb Awate College, Manchar, Pune (Pune University)
P-51	Shraddha Mahakal	Structural Influence of Serine on ZnO Nanostructures	Annasaheb Awate College, Manchar, Pune 410503 (Pune University)

P-52	S. P. Kamble	Dielectric constant, Density and Refractive Index Study on Mixing Properties of Carbon Tetrachloride-Acetone Binary Liquid Mixtures	Department of Physics, C.T. Bora College, Shirur Dist. Pune. (M.S.) (Pune University)
P-53	B.Y. Pagare R. R. Bhosale S.K. Narwade	Solar photocatalytic degradation of methylene blue using Sb-doped TiO_2 nanoparticles	Department of Chemistry, Shri Anand College, Pathardi, Ahmednagar (Pune University)
P-54	Mithilesh Chavan, Sunil Gaikwad, Tushar Ghorpade, Vilas Ugale Dipesh Karmarkar	Estimation of Socio-economic Coastal Vulnerability Index for Coastal Villages of Dapoli Tahsil, Ratnagiri District, Maharashtra	Dept. of Geography, Sir Parashurambhau College, Pune (Pune University)
P-55	U.D. Patil, D.M. Nerkar, Neetu Paliwal	Bio-Inspired Heteroatom Doped Engineering of Graphene Nanomaterial for its Adsorption and Absorbing Performance with Facile Recycling	Department of Physics, Annasaheb Awate College, Manchar, Tal: Ambegaon Dist.: Pune (Pune University)
P-56	Pradeepkumar R, Pragathi G, Rajesh Kanna M.R	Applications Of Probability On Cowry Shell Game	The Gsss Institute Of Engineering And Technology For Women, Mysuru
P-57	Roopa S., M R Rajesh Kanna	Studies on Topological Properties of Verapami	Department Of Mathematics, Sri D. Devaraja Urs Government First Grade College, Hunsur, Karnataka
P-58	V. B. Sanap, M. S. Patil, A. D. Suryawanshi, B. H. Pawar	Study of Chemically Deposited Nickel Sulfide Thin Films	Department of Physics, Yeshwantrao Chavan College, Sillod, Dist. Aurangabad (M.S) (Aurangabad University|)
P-59	Sayyad Shahim K., Gachande B. D. Shaikh N. F.	Biosynthesis, characterization, and antibacterial activity o*f* silver nanoparticles from an endophytic fungus *Alanphillipsiaaloeigena*	Post Graduate Department of Botany, N.E.S. Science College, Nanded. (Nanded University)
P-60	Dhumane N. R.	Dielectric studies of Glycine doped Zinc (Tris) Thiourea Sulfate Single Crystal	Department of Physics, Shri Anand College, Pathardi, (Pune University) Ahmednagar, MS, India
P-61	Rajendra Jagtap Sanjay Gaikwad	Synthesis, Characterization and Molecular Docking of Condensed Molecules of Halogen Derivatives of Some Naturally Occurring Quinones and Phenylene Diamines	Pimpri Chinchwad College of Engineering, Nigdi (Pune University)
P-62	Ashok Datir, Naseem Deshpande	Copper Phthalocyanine Based Humidity Sensor	Agasti Arts, Commerce and Dadasaheb Rupwate Science College, Akole, Ahmednagar (Pune University)
P-63	Avadhut Kardile, M. Moulavi, Amar Katkar, R. B. Bhise, Ramakant Joshi, P. N. Shelke	Green Synthesis of ZnO Nanoparticles Using Sugarcane Juice for LPG Sensing Applications	PDEA's, Annasaheb Waghire College, Otur, Tal: Junnar, Pune (Pune University)

	Ravindra Mene		
P-64	RoopaVishwanath Sangvikar	A Brief Review on Ethnomedicinal Plants used by Tribal Healers for the Maintenance of Primary Healthcare in India.	Department of Botany, Microbiology and Biotechnology, NES Science College, Nanded
P-65	Gajanan Patil, Subhash Pawar, Jalindar Bhosale, Prachi Patil, Pratik Patil	Air Ion Concentrations And Pollution Index For Irrigated And Non- Irrigated Vegetation Areas At Rural Station Khatav (16.57°n, 74.31°e)	Secondary school & Jr. College, Bhilawadi, Maharashtra, India
P-66	A. D. Kanwate, E. U. Masumdar	Morphological And Electrical Properties of spray deposited $CdSe_{0.3}Te_{0.7}$ thin film	Thin Films and Materials Science Research Laboratory, Department of Physics, Shahu College, Latur
P-67	Vishnu Kadam, Rajendra Salunkhe, Sanjay Gaikwad Sambhajirao Bhosale	Life Table and Intrinsic Rate of Increase in Lepidopteran Pest *Hypsa Producta*	Department of Zoology, Bharati Vidyapeeth's Matoshri Bayabai Shripatrao Kadam Kanya Mahavidyalaya, Kadegaon Dist. Sangli
P-68	Vishnu Kadam, Nilofar Shaikh, Sunil Londhe, Rajendra Salunkhe, Sanjay Gaikwad	Histopathology of Prostate Gland in Terrestrial Slug *Semperula Maculata* after Acute Exposure of Zinc Chloride	Department of Zoology, Bharati Vidyapeeth's Matoshri Bayabai Shripatrao Kadam Kanya College, Kadegaon Dist. Sangli
P-69	Rajendra Salunkhe, Sambhajirao Bhosale, Sanjay Gaikwad and Vishnu Kadam	Reproductive cycles in two geographically separated populations of the oyster *Saccostrea cucullata* from Sindhudurg district, Maharashtra State, India.	Department of Zoology, Arts, Science and Commerce College, Indapur, Dist-Pune
P-70	Sheema Kauser Venkatesha Babu K R	Synthesis, Characterization and Antimicrobial activity of Sm^{3+} doped TiO_2 Nanoparticles	Department of Microbiology, Nrupathunga University, Bangalore
P-71	Raju Murkute and Sanjay Gaikwad	Synthesis, Characterization and in Silico Prediction of Oxime and Thiosemicarbazone Derivatives of Halo Hydroxy Naphthoquinone As An Anti-Viral Agent Against SARS2 Corona Virus	Department of Chemistry, Fergusson College, Shivaji Nagar, Pune
P-72	Sadekar H. K.	Deposition and Characterization of CdSe Thin Film for Photovoltaic Applications	Department of Physics, Arts, Commerce and Science College, Sonai (MS)-India
P-73	Dinesh Gaikwad Sanjay Gaikwad	Insillico Prediction of Novel Halosubstituted Homoisoflavonoid Derivatives as an Anti-Inflammatory Agents.	Arts, Science and Commerce College, Wagholi, Pune
P-74	P.R. Babar D.H. Bobade Sohail Bagwan	Synthesis, Structural And Magnetic Characterization Of Mg-Ni-Zn Nanoferrite Synthesized By Using Sol-Gel Method	Ph.D. Research Scholar, Shri JJT University, Jhunjhunu, Rajasthan-333001
P-75	P.R. Babar D.H. Bobade Sohail Bagwan	Structural and magnetic properties of nanocrystalline MgNiZn spinel ferrite synthesized via sol–gel method.	Ph.D. Research Scholar, Shri JJT University, Jhunjhunu, Rajasthan-333001

Paper-1

Chemically Synthesized ZnO and Al, Ag and Cd Doped ZnO Nanoparticles at higher temperature 600^{0}C, study of Antibacterial Activity.

R.S.Shaikh.[1] L.S.Ravangave.[2]

1. Department of Physics S.G.B.S. College Purna (Jn.) Dist: Parbhani (M.S.) India.

2. Department of Physics S.S.G.M. College Loha Dist: Nanded (M.S.) India.

Abstract:. Sol-Gel chemical precipitation method has been implemented to synthesize ZnO nanoparticles at 600 ^{o}C. Wurtize hexagonal crystal structure of as prepared pure and Al ,Ag and Cd doped ZnO 600^{0}C nanoparticles have been confirmed by X-ray Diffraction (XRD) data. The crystalline size and have been estimated from XRD data. The chemical composition of as prepared ZnO and 5% Al, Ag and Cd doped ZnO at 600^{0}C samples nanoparticles has been investigated by analysis of Fourier transform infra red spectroscopy(FTIR). The direct band gap of nanoparticles has been estimated using Uv absorption spectra. The effect of calcintion temperature of Chemically prepared pure ZnO and 5% Al,Ag and Cd doped ZnO at 600^{0}C have been comparatively study using *Bacillus thuringiensis* NCIM2130 and *Pseudomonas cf. monteilii 9 culture.*

Keywords: Sol – Gel precipitation, ZnO nanoparticles, XRD, SEM, FTIR, UV, *Bacillus thuringiensis* NCIM2130 and *Pseudomonas cf. monteilii 9* Antibacterial activity.

Introduction: Zinc Oxide (ZnO) is one such important metal of multi dimension characteristics use. It has the unique optical and electrical properties which can be used in a variety of applications, such as high transmittance conductive oxide coatings for solar cells, gas sensors, UV photodetectors, and bulk acoustic wave resonators. It has direct bandgap energy of 3.37 eV, which makes it transparent in visible light and operates in the UV to blue wavelengths. The exciton binding energy is 60 meV for ZnO. The higher exciton binding energy enhances the luminescence efficiency of light emission [2, 3]. ZnO has exhibited better radiation resistance for possible devices used in space and nuclear applications [4]. Furthermore, ZnO is bio-safe and biocompatible, and may be used for biomedical applications [5].

ZnO has also been confirmed as a promising functional material in other nano devices such as field emitters and gas sensors. The synthesis of ZnO nanostructures is thus currently attracting intense worldwide interest. Other favorable aspects of ZnO include its broad chemistry leading to many opportunities for wet chemical etching, low power threshold for optical pumping, radiation hardness and biocompatibility. For a semiconductor to be useful, particularly in reference to optoelectronic devices; band gap engineering is a crucial step in device development. In the case of ZnO, alloying with MgO and CdO is an effective means of increasing or decreasing the energy band gap respectively.

The main advantage of zinc oxide nanostructures and is the wide band gap that can be utilized in various electronic and optoelectronic devices. Therefore we planned to synthesis of different type's morphology of pure and doped ZnO nanostructures and study their structural and spectroscopic properties. The antibacterial activity of pure and doped ZnO nanostructural have been studied.

(Fakhroueian *et al.,* 2013). Different methods have been used for the production of ZnO nanoparticles such as 1) Chemical synthesis 2) Hydrothermal method 3) Electrophoretic deposition 4) Co-precipitation 5) Mechanochemical-thermal synthesis 6) Chemical vapour depositions 7) Thermal decomposition 8) Sol-Gel method 9) Electrochemical depositions and 10) Anodization

The present study was aimed to i) Synthesis ZnO nanoparticle using simple Sol – Gel chemical precipitation method by utilizing Zinc acetate and sodium hydroxide in distilled water, ii) study the morphological changes after calcinations at 600^0C temperature and iii) detect the antibacterial activity of ZnO nanoparticles.

In order to study the antibacterial activity of doped ZnO nanoparticles against *Bacillus thuringiensis* NCIM2130 and *Pseudomonas cf. monteilii 9* cultures slightly modified Agar Well Diffusion method was used. The pure ZnO and Al doped ZnO, Ag doped ZnO, and Cd Doped ZnO nanopowder were calcined at 600 ^{o}C and used for antibacterial study.

Experimental method: Sol-Gel Chemical precipitation method for synthesized ZnO nanoparticles:

The chemicals used for this work were of analytical grade obtained from Merck (Mumbai).

A modified method of Fakhroueian *et al.*, 2013 was used where Zinc acetate and sodium hydroxide and distilled water used in the preparation of ZnO nanoparticles. Zinc acetate and sodium hydroxide was added slowly drop wise in a molar ratio of 1:2 under vigorous stirring, and stirring was continued for 4 hours. First Zinc acetate stirred for 2 hours and same time sodium hydroxide for 2 hours. Then the mixture of zinc acetate was slowly added drop wise in the solution of sodium hydroxide by continuous string for 2 hours. The precipitate obtained was filtered. The precipitate was dried in an oven at 100°C and ground to fine powder using agate mortar. The powder obtained from the above method was calcinated different temperatures such as prepared pure ZnO 600°C for 2 hours. Similarly method used for 5% doping Al,Ag and Cd in ZnO. The prepared pure sample ZnO 600^0C and doped ZnO(Al) 600^0C, ZnO(Ag)600^0C and ZnO(Cd) 600^0C was then characterized for physical and morphological changes by X – ray diffraction (XRD), UV absorption spectra, Scanning Electron Microscopy (SEM) and FTIR. **Results and Discussion:**

1.X - Ray Diffraction pattern study for prepared ZnO and doped ZnO(Al,Ag and Cd) 600^0C:

The X – ray diffraction (XRD) data were recorded by the intensity data collected over a 2θ range of 20-80 degrees. The particle size of samples was estimated with the help of Debye-Scherer's equation using the full width at half maximum of (100)(002) and (101) of the x-ray diffraction peaks (as shown in Figure 1).The particle crystalline size increases with increase in calcination temperature. A significant increase in crystalline size is observed for the sample calcination of as prepared ZnO600°C and doped ZnO(Al)600^0C,ZnO(Ag) 600°C, and ZnO(Cd)600°C.

$$\mathbf{D = 0.94\ \lambda / ß\ Cos\ \theta} \qquad \ldots\ldots\ldots\ldots\ldots\ldots\ (1)$$

Where **D** is size of crystalline nanoparticles(nm), **λ** is wavelength of incident X – ray (nm) **ß** is the full width at half maximum and **θ** is the diffraction angle.

X- ray diffraction studies confirmed that the synthesized ZnO all the diffraction peaks with the report (Origin 8.0 software) data and no charactertics were observed other than ZnO. The mean grain size of the particles was determined from the XRD line boarding measurement using Debye-Scherer equation. The diffraction peaks indicates that the synthesized material was in nanometer range. The particle size was found to be in the range

48.73nm depending on the calcination condition (as shown in Table 1). The lattice parameters calculated were also in agreed with report values. Similarly procedure used to calculate particle size doped ZnO(Al,Ag and Cd) (44.18,46.36 and 41.54nm).The reaction temperatures greatly influence the particles morphology of prepared ZnO nanoparticles. The size of ZnO nanoparticles increased as the temperature for the hydrothermal synthesis increases. This is due to the change of growth between the different crystalline planes.

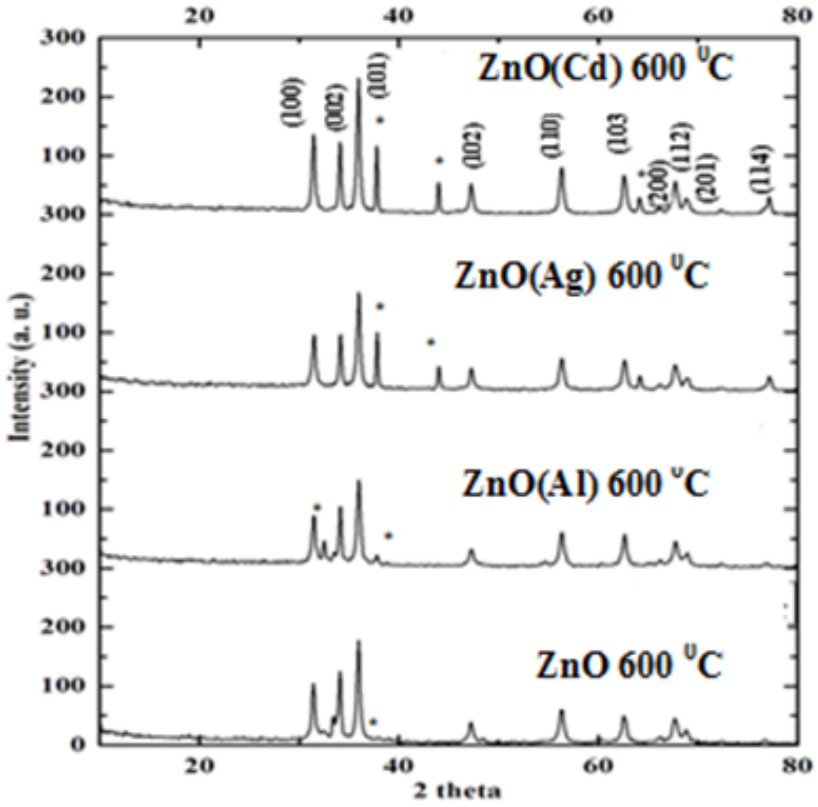

Figure 1: Shows XRD pattern of as prepared ZnO and doped ZnO(Al,Ag and Cd) at 600^{0}C

Table 1: FWHM, Particles Size, (h,k,l) Lattice constant of ZnO and Al, Ag and Cd Doped ZnO nanoparticles.

ZnO Sample	2 Theta 2θ	d (A^0)	h k l	FWHM (deg)	Particles Size D(nm)	Lattice Parameters	
						'a'	'c'
ZnO 600^OC	31.7942	2.8122	100	0.3446	48.73	3.24	5.205
	34.4443	2.6016	002	0.3078			
	36.2783	2.4742	101	0.3611			
	47.7489	1.90480	102	0.2952			
ZnO (Al) 600^0C	31.4975	2.84039	100	0.3149	44.18	3.181	5.250
	34.1553	2.62520	002	0.3149			
	35.9835	2.49591	102	0.3149			
ZnO (Ag) 600^0C	31.9616	2.80020	100	0.2952	46.36	3.284	5.255
	34.6379	2.58973	002	0.3936			
	36.4400	2.46568	101	0.3936			
	47.7176	1.90598	102	0.3936			
ZnO (Cd) 600^0C	31.5720	2.83385	100	0.4723	41.54	3.272	5.231
	34.3536	2.61789	002	0.3149			
	36.0813	2.48937	101	0.3149			
	47.3652	1.91933	102	0.3149			

2.Scanning Electron Microscopic Study (SEM):

The Scanning Electron Microscopic images (SEM) of the samples also shows that (Figure.2) the physical structure of ZnO was changed with calcinations temperature. The samples calcinate at 600°C. The SEM images of ZnO samples show that the agglomeration particles are much less in this method of preparation. High resolution SEM images of ZnO calcinate show the presence of nanoparticles grain size 52nm. The SEM images of Al doped ZnO-NPs were Shown in figure.2 exhibits distinct, inhomogeneous porous network with an average grain size 66 nm which is estimated form visualized data in micrographs. The wurzite hexagonal shaped nano rods of Ag attach on ZnO nanoparticles grain size 69nm. The small crystalline agglomerated to form nano fused clusters seen in the surface morphology of ZnO(Ag). The microstructure was observed changes to hexagonal nanorods at high temperature. The size of nanorods and nano grains are vary from 42 to 69nm which is visualized in SEM images. The increase in grain size as compared to obtained from XRD data is due to agglomeration of the grains together. ZnO(Cd) nanostructures exhibit significant varying morphology and may be used as antibacterial agent grain size 61nm.

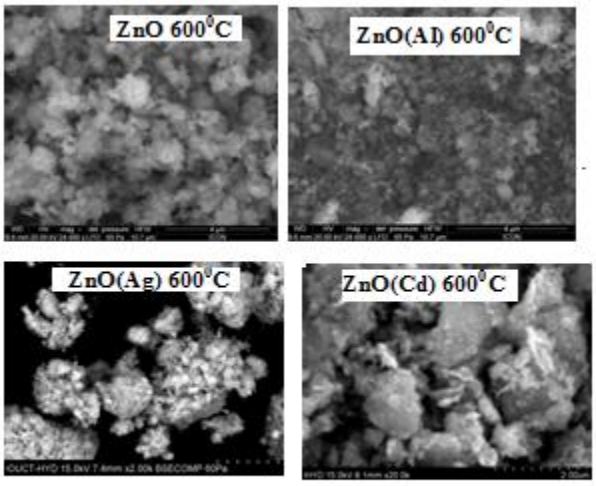

Figure2.SEM image shows morphology ZnO Nanoparticles and ZnO (Al,Ag and Cd) doped Nanoparticles at 600°C.

Tables No.2 Grain Size ZnO nanoparticles from SEM

ZnO and ZnO Doped Samples.	Grain Size from SEM (nm)
ZnO 600ºC	52
ZnO(Al) 600ºC	66
ZnO(Ag) 600ºC	69
ZnO9(Cd) 600ºC	61

3.FTIR Study of As-prepared Pure ZnO and calcined ZnO(Ag)

FTIR spectra of prepared and calcined ZnO were recorded at 600^0C temperature in the wave number range 399-4000 cm^{-1} and presented in figure 3. The modes of vibrations and their band assignment were shown in table 3. FTIR spectra of the ZnO nanopowder exhibit several characteristics bands with remarkable features. The absorption band assigned in the region 447 to 470 cm^{-1} attributed to characteristics stretching mode of ZnO and Al-O bonds [22, 23]. These absorption bands were broadly spread in the absorption region 464 to 497 cm^{-1} because of Al doping. On calcinations the band was observed shifted to higher wave number and become stronger. This shows that Ag is substituted at site of Zn ions by replacement of Zn ion or at interstitial sites. The absorption bands in the region 439 to 462 cm^{-1} associated vibration was not appearing in pure ZnO structure. The similar assignment has been reported in earlier literature [24]. The calcinations effect was also pronounced and bands were observed shifted to higher frequency region. The vibration band at 667 cm^{-1} in as-prepared Ag doped ZnO assigned to Cd-O-Zn stretching modes which was not appeared in the pure ZnO spectra. This band was fond shifted to higher wave number region on increasing the calcinations temperature. The absorption peak present at 1020 cm^{-1} is assigned to C-O-C bending vibrational mode [25]. The absorption band in the range 3425-3533 cm^{-1} was assigned to stretching mode O-H group. This reveals that small amount of water molecules absorbed by the ZnO nanopowder [26, 27].

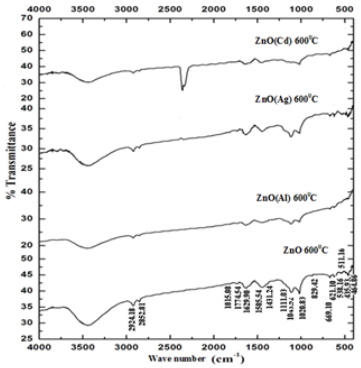

Figure3.FTIR spectra of ZnO Nanoparticles and Al,Ag and Cd doped ZnO Nanoparticles at 600^0C

Table No.3 FTIR Spectra Vibrational bond

Vibrational bond	Samples ZnO – 600^0C Freq.cm^{-1}	Samples ZnO Al 600^0C Freq.cm^{-1}	Samples ZnO Ag 600^0C Freq.cm^{-1}	Samples ZnO Cd 600^0C Freq.cm^{-1}
Zn-O	447	464	439	430
Zn-O	470	497	462	452
Zn-O	673	669.32	667	673
Zn-O	923	831	871	834
C=C	1022	1020	1020	1020
C=O	1408	1398.44	1408.08	1440.81
C=O	1600	1581.66	1580.11	1581.68
CO_2	2369.02	2346.61	2343.50	2359.02
C-H	2861.26	2852.81	2962.76	3026.41
O-H	3425.68	3434.60	3533.71	3425.69

4. UV-Visible Absorption Study for ZnOnanoparticles and Al,Ag and Cd doped ZnO.

The absorption spectrum of pure ZnO, as-prepared and calcined ZnO(Ag) nanopowder was shown in figure 4. All the samples represent significant absorption in ultraviolet and blue region of the absorption spectrum. The absorption intensity was decreased on 5% Ag doping in ZnO. As the calcinations temperature increased the peak height in the blue region decreased and peak shifted to longer wavelength. This concluded that major portion of the absorption spectrum (blue to visible region) can be actively utilized in the solar cell device applications. ZnO sample exhibit a strong absorption peak at about 362 nm. The significant red shift of 362 nm to 378 nm was observed for prepared Al doped ZnO samples. The band gap was calculated using equation **Eg=hc/λ**. The estimated band gap and near band edge wavelength is tabulated in table 4. On sintering at 600^0C temperature effectively tuned the band gap. Al though the grain size was smaller as compared to pure ZnO nanostructure as-prepared ZnO(Al) exhibit 3.34 eV band gap, which is significantly decreased. Further on increasing temperature of calcinations (600^oC) the absorption peak shifted to longer wavelength and band gap was found decreased. The decrease of band gap is related to presence of P-type conductivity of doped semiconductor [29]. The Cd doping in ZnO nanostructure with the impurity level in the energy band gap lead to the formation of P –type in the substance. It was reported that reduction in band gap 3.29eV led to enhance the efficiency of charge carrier and material is optoelectronically useful [29]. The Cd - doped ZnO nanostructure exhibiting acceptor impurity material may be used in optoelectronics, photoelectrochemical cells, and for biological applications[30, 31].

Table 4. Variation between band gap(Eg) and sintering Temperature		
Samples ZnO-Temperature	**Wavelength nm**	**Bandgap eV**
ZnO 600 ºC	**362**	**3.44**
ZnO (Al) 600ºC	**373**	**3.34**
ZnO(Ag) 600ºC	**376**	**3.31**
ZnO(Cd) 600ºC	**378**	**3.29**

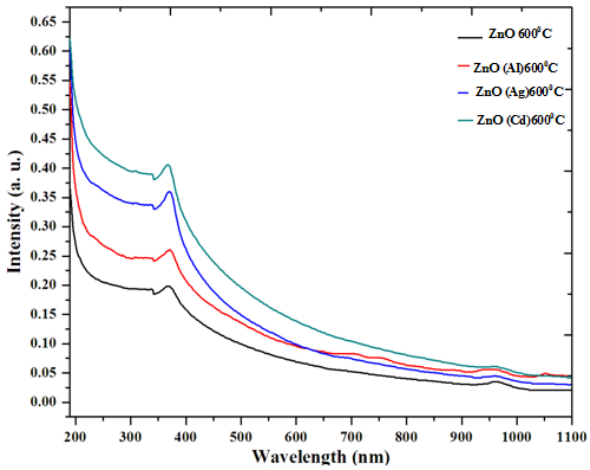

Figure 4.Uv- absorption spectra of ZnO nanoparticles and Al,Ag and Cd doped ZnO nanoparticles at 600^{0}C.

5. Material and Methods

The antimicrobial activity of doped compounds ZnO(Cd), ZnO(Ag) and ZnO(Al) (Calcinied at 600^{o}C) are tested in comparison with pure ZnO(calcinied at 600^{o}C) nanocompound and Chloramphenicol as known antibiotic agent against *Bacillus Thuringiensis* NCIM2130 and *Pseudomonas cf. monteilii* 9 by slightly modified agar well diffusion method (Perez,et.al,1990) [19] on Muller Hinton agar plates. The Bacillus thuringiensis NCIM2130 and Pseudomonas were grown separately in Nutrient broth at 37^{0}C for 24 hours on rotary shaker at 200 rpm. Muller Hinton agar plates were inoculated with (100 µl) 24 hours old culture of *Bacillus thuringiensis* NCIM2130 and *Pseudomonas cf.monteilii* 9 spread with sterile glass spreader. The well was made at the centre of inoculated agar plate with a sterile cork borer of 10 mm size. In each well 100µl (1µgms pure and doped nanocompounds), ZnO(Ag), ZnO(Al), ZnO(Cd) and pure ZnO was poured by using micropipette. The inoculated plates were allowed to stand for 30 minutes for diffusion of poured compounds. Then all these plates are incubated at 37^{0}C for 48 hours. After 48 hours the incubated plates were observed for the activity of tested compounds in terms of zone of inhibition. Zones of inhibition were measured and compared with inhibitory zone of pure ZnO600^{0}C, with Al,Ag and Cd doped ZnO compounds.

5.1 Results and Discussion

Incubated plates of tested doped compounds ZnO(Al), ZnO(Ag), ZnO(Cd), and pure ZnO and Antibiotic Chloramphenicol shows more or less Zones of Inhibition. As per the obtained results, known antibiotic Chloramphenicol shown more antimicrobial activity on both *Bacillus thuringiensis* NCIM2130 and *Pseudomonas cf.monteilii* 9 as compared to pure ZnO compounds. Chloramphenicol has 46 mm zone inhibition against *Bacillus thuringiensis* NCIM2130, 45 mm Zone of inhibition against *Pseudomonas cf.monteilii* 9 respectively.

In comparison with inhibition zone of Chloramphenicol, the inhibition zone of pure ZnO is smaller (16 mm) against *Bacillus thuringiensis* NCIM2130 but pure ZnO and doped ZnO never show antimicrobial activity against *Pseudomonas cf.monteilii* 9. While comparing inhibition zone of pure ZnO with respect to ZnO(Ag), ZnO(Al) and ZnO(Cd) against *Bacillus thuringiensis* NCIM2130 and *Pseudomonas cf.monteilii* 9, doped

compounds are more active than pure ZnO. The photo plates of Al doped ZnO, Ag doped ZnO and Cd doped ZnO nanostructures calcined at 600 ^{o}C have been shown in figures 5.1, 5.2 and 5.3 respectively. The diameters of inhibition zones for Al doped ZnO, Ag doped ZnO and Cd doped ZnO are tabulated in table 5. The zone of inhibition for doped ZnO(Cd) is 39 mm, for ZnO(Ag) is 32 mm and for ZnO(Al) is 26 mm .against ***Bacillus thuringiensis*** NCIM2130 where as for ZnO(Cd) is 0 mm, for ZnO(Ag) is 0 mm, and for ZnO (Al) is 0 mm zone of inhibition against *Pseudomonas cf.monteilii* 9 have been observed.

On the basis of obtained results pure ZnO has antimicrobial activity but modified doped ZnO compounds are more active than pure ZnO compound against *Bacillus thuringiensis* NCIM2130 where as pure ZnO and doped ZnO(Cd), ZnO(Ag) and ZnO(Al) compounds has no effect or less active against *Pseudomonas cf.monteilii* 9 have been observed. The effect of doping and calcinations of the material are essential factors for increase the antibacterial activity. The literature on ZnO reported that Ag doped ZnO and Al doped ZnO materials are bio safe material [3, 7, 10, 11]. The effect of doping decreased the grain size of nanoparticles for as-prepared doped ZnO nanostructure. The grain size of Al doped ZnO was 44.18 nm, that of Ag doped ZnO was 46.36 nm and of Cd doped ZnO was 41.54nm). The particle size estimated for pure ZnO is about 48.73 nm. The grain size is one of the important factor which helps to activate the material at particular site of the bacterial cell and prevent the growth. On calcinations the grain size was slightly increased due to aggregation of the particles however the microstructure of surface morphology of the ZnO and doped ZnO nano structures was modified which was described . The change in particle size and modification of surface morphology leads to increase the antibacterial activity of ZnO(Al), ZnO (Ag) and ZnO (Cd) nanostructures. The summarizing the figures 5.1, 5.2 and 5.3, table number 5 it is cleared that ZnO (Ag) and AnO (Cd) nanostructures are very effectively useful for antibacterial activity against ***Bacillus thuringiensis*** NCIM2130. Among pure ZnO, Al doped ZnO and Ag doped ZnO the Cd doped ZnO calcined at 600 ^{o}C showing good results. Therefore ZnO(Cd) nano sample can be used as antibiotic inhibiter against ***Bacillus thuringiensis*** NCIM2130. To increase the activity and stability the doping percentage of Cd should have to be increased.

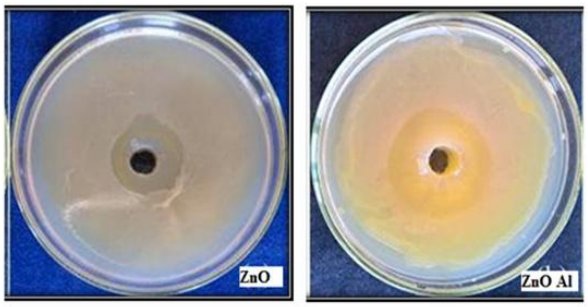

Figure 5.1 Photo plate shows Inhibition zone of *Bacillus Thuringiensis* NCIM 2130 ZnO(Al) in comparison with ZnO nanoparticles at 600^0C.

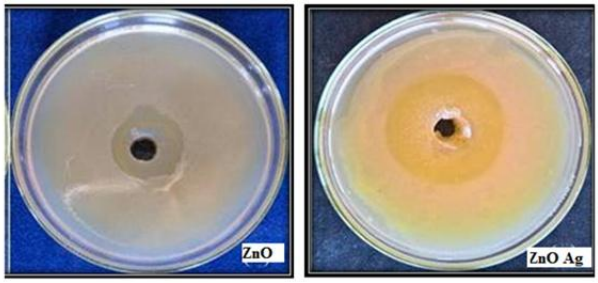

Figure 5.2 Photo plate shows Inhibition zone of *Bacillus Thuringiensis* NCIM 2130 ZnO(Ag) in comparison with ZnO nanoparticles at 600^0C.

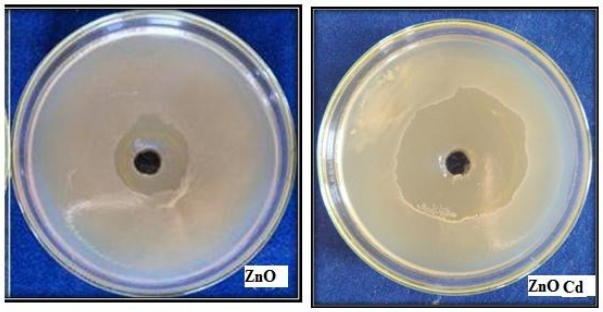

Figure 5.3 Photo plate shows Inhibition zone of *Bacillus Thuringiensis* NCIM 2130 ZnO(Cd) in comparison with ZnO nanoparticles at 600^0C

Table 5. Inhibition Zone (mm) Zones produced by ZnO nano particles at 600 ^{o}C calcinations Temperatures				
Bacterial Culture	Inhibition Zone (mm)			
	ZnO Cd 600^{0}C	**ZnO Ag 600^{0}C**	**ZnO Al 600^{0}C**	**ZnO Pure 600^{0}C**
***Bacillus thuringiensis* NCIM2130**	**39**	**32**	**26**	**16**
Pseudomonas cf. monteilii 9	**0**	**0**	**0**	**0**

Conclusion:

The prepared novel materials, Pure ZnO600^{0}C, Al doped ZnO, Ag doped ZnO and Cd doped ZnO 600^{0}C were tested against Bacillus *thuringiensis* NCIM2130 and *Pseudomonas cf. monteilii 9* for antibacterial activity. The entire samples show more or less inhibition activity against Bacillus *thuringiensis* NCIM2130 however no significant effect on *Pseudomonas cf.monteilii* 9 culture. The effect of calcinations temperature enhances the inhibition activity against *Bacillus thuringiensis* NCIM2130. In comparative study of pure and doped ZnO nanoparticles, Al doped ZnO , Ag and Cd doped ZnO nanostructures calcinated at 600^{o}C shows good results against ***Bacillus thuringiensis*** NCIM2130 However among pure ZnO, Al doped ZnO and Ag doped ZnO the Cd doped ZnO calcined at 600^{o}C showing versatile results. Therefore ZnO(Cd) nano sample can be used as antibiotic inhibiter against ***Bacillus thuringiensis*** NCIM2130.

The grain size is one of the important factor which helps to activate the material at particular site of the bacterial cell and prevent the growth. The effect of calcinations improved physical properties such as crystallity, band gap, surface morphology of the nanoparticles that change is responsible to activate the antimicrobial activity of doped ZnO nanoparticles. The doping of different element in ZnO shows varying antibacterial activity against *Bacillus thuringiensis* NCIM2130. In the present study Cd doped ZnO calcined at 600 ^{o}C temperature is significantly effective as microbial inhibiter against *Bacillus thuringiensis* NCIM2130.

References :

[1].Esmailzadeh H, Sang Poor P, Khaksar R, Farzaneh Sh. ***Food Sci and Nut.*** 2014;11(3): 21-28.

[2]. Emami Far A, Kadivar M, Shahedi M, Soleimanian Zad S, ***Iranian J of Food Industries.*** 2011; 6(1): 57-67.

[3]. Veissi Malekshahi Z, Afshar D, Ranjbar R, Shirazi MH,Rezaei F, Mahboobi R, ***J MDPI Tropical Med.,*** 2012; 17(59): 1-4.

[4].N. W. Emanetoglu, C. Gorla, Y. Liu, S. Liang and Y. Lu, **Materials Science in Semiconductor Processing,** 2, (3), 1999, 247-252. doi:10.1016/S1369-8001(9

[5].Y. Chen, D. Bagnall and T. Yao, ***Materials Science and Engineering***: *B*, 75(2-3) (2000), 190-198. doi:10.1016/S0921-5107(00)00372-X

[6].P. Mitra, A. P. Chatterjee and H. S. Maiti, ***Materials Letters***, 35 (1-2), (1998), 33-38. doi:10.1016/S0167-577X(97)00215-2

[7]. Chitra K, Annadurai G.. ***Int Food Res J,*** 20(1) (2013) 59-64.

[8].Khadije Rezaie Keikhaie , Mohsen Noori , Mehdi Hassanshahian , Saeide Saeidi, ***Advanced Herbal Medicine***, 3(4)(2017)33-37

[9].P. S. Bedi and Arshdeep Kaur, ***World Journal of Pharmacy and Pharmaceutical Sciences***, 4(12),(2015) 1177-1196

[10]. Sharma Neha, Kumar Jitender, Thakur Shaveta, Sharma Shruti, Shrivastava Vikas ***Drug Invention Today*** 5 (2 013)50 -54.

[11]. Navale Govinda R., Thripuranthaka M., Late Dattatray. J, and Shinde Sandip S, ***JSM Nanotechnology & Nanomedicine***, 3(1), (2015) 1033-39.

[12]. Haritha Meruvu, Meena Vangalapati, Seema Chaitanya Chippada and Srinivasa Rao Bammidi,***Rasayan Journal of Chem.*** 4(1) (2011), 217-222

[13]. Bauer, A. W., Kirby, W. M., Sherris, J. C., & Turck, M. ***American Journal of Clinical Pathology***, 45(4) (1966)., 493-496.

[14]. Zahra Fakhroueian, Faraz M. Harsini, Firoozeh Chalabian, Fatemeh Katouzian, Azizollah Shafiekhani, and Pegah Esmaeilzadeh, ***Advances in Nanoparticles,*** 2, (2013).247 – 258,

[15].J. I. Tariq Jan, M. Ismail, M. Zakaullah, S.H. Naqvi, N. Badshah,et.al, "Sn ***Int. J. Nanomed.*** 8(1)(2013).3679–3687

[16].N.G. Heatley, A method for the assay of penicillin**, *Biochem.J.***38(1944) 61–65.

[17].CLSI, Performance Standards for Antimicrobial Disk Susceptibility Tests, Approved Standard, 7th ed., ***CLSI document M02-A11***. Clinical and Laboratory Standards Institute, 950 West Valley Road, Suite 2500, Wayne, Pennsylvania 19087, USA, 2012. 19087-1898, USA, 2004.

[18].CLSI, Performance Standards for Antimicrobial Disk Susceptibility Tests, Approved Standard, 7th ed**., *CLSI document M02-A11***. Clinical and Laboratory Standards Institute, 950 West Valley Road, Suite 2500, Wayne, Pennsylvania 19087, USA, 2012.

[19]. Perez, C., Pauli, M.,Bazerque, P.,. ***Acta. Biol. Med. Exp***.15(1990)113-115

[20]. Monteiro, L., Mariano, R.D.L.R.,Souto-Maior, A.M., ***Brazilian Arch. Biol. Technol,*** 48 (2005)23-29.

[21]. Mounyr Balouiri, Moulay Sadiki, Saad Koraichi Ibnsouda ***A review. Journal of Pharmaceutical Analysis***. 6 (2016) 71-79.

[22].L. Jiang, F. Wang, F. Han, W. Prinyawiwatkul, H.K. No and B. Ge ***Journal of Applied Microbiology*** 114 (2012) 956 – 963.

Paper-2

Statistical Analysis of HDFC and ICICI Bank Stocks

Dr. Prakash Rajaram Chavan
Department of Statistics, Smt. Kasturbai Walchand College, Sangli
Affiliated to Shivaji University, Kolhapur, Maharashtra

ABSTRACT

Stocks are the financial securities that represent part ownership in one or more companies. Upon buying the company's stock, you become a shareholder of that company. You can buy stocks of single company or several companies. The definition of stock market is same as that of share market. Bank shares mean any ordinary shares of the bank. Distributable profits mean in respect of any fiscal year of the bank. Distribution means non-cumulative cash distribution payable for preferred security in accordance with terms thereof. Distribution periods shall have the meaning given to it in terms of preferred security. Fiscal years means the accounting year of the guarantee as set out in its by-laws. Group means the bank and its consolidated subsidiary. Holder means any holder from time to time of any preferred security; provided, however, that in determining whether the holders of the requisite percentage of preferred securities have given any request, notice, consent or waiver hereunder, holder shall not include the bank or any subsidiary.

Key Words:- Bank stock, Bank shares, Statistical Analysis.

1 Introduction

'Stocks 'and 'Shares' are the basic terms that the investor must understand before starting their stock market journey. However the terms often used interchangeably and many more people don't know that there is a subtle difference between bank stock and share. "Share are units of equity ownership interest of corporation that exists as a financial asset providing for an equal distribution in any residual profits, if any are declared, in the form of dividends. " A share is a smallest denomination of company's stock. So, each unit of stock is a share, and each share of stock is equal to piece of company's ownership. It enables investors to identify the intrinsic worth of security even before investing in it.

- It tries to find out activity of an instrument /sector/market in future.

- Investors and traders arrive at equity buying and selling decisions.
- Helps investors and traders to gain an edge in markets to make informed decision.

Problems Highlighted: -

1. Stock prices can plunge as well.
2. There is no assurance that the company stock you hold will grow and perform well.
3. Never invest more than you can afford to lose.
4. Stock price and company may fluctuate multiple times a day.

Here we have considered the shares of two leading banks HDFC and ICICI for statistical analysis. Further with help of the statistical tools we have analyzed which banks shares are good for future investments?

Share Market: - Share market is the place where all the financial securities are bought or sold by the investors or the traders.

2. Methodology

The paper is based on secondary data. The data is collected from various websites and data is derived from National Stock Exchange (NSE) of India. The shares have been studied from the standard websites of banks that are chosen for study.

Names of the websites: 1]. ticker.finology.in 2]. in.finance.yahoo.com

Variance:- In a statistics variance measure how far each number in a data set is from the mean and thus from every other number in set.

Standard deviation:- A standard deviation is a statistics that measures the dispersion of data set relative to its mean.

Correlation:- Correlation is any statistical relationship between two random variables or bivariate data

Regression:- Regression is statistical measurement that attempts to determine the strength of the relationship between one variable.

Multiple Correlations:- It is the statistical technique that predicts value of one variable on the basis of two or more variables.

Multiple regression: It is a statistical technique that can be used to analyse the relationship between a single dependant variable and several independent variables.

Terms related to share market: -

PE ratio:- The price-to-earnings ratio (P/E ratio) is the ratio for valuing a company that measures its current share price relative to its per-share earnings (EPS).

CASA:- CASA ratio is the ratio of deposits in current and savings accounts to the total deposits

Cost to income ratio:- Cost to income ratio is the measurement that is used in the company in order to evaluate its efficiency.

Earnings per share (EPS):- Earnings per share (EPS) are calculated as a company's profit divided by the outstanding shares of its common stock. The resulting number serves as an indicator of a company's profitability. ... The higher a company's EPS, the more profitable it is considered to be.

Capital adequacy ratio (CAR):- Capital adequacy ratio (CAR) is a measurement of a bank's available capital expressed as a percentage of a bank's risk-weighted credit exposures.

Return on equity (ROE):- Return on equity (ROE) is a measure of financial performance calculated by dividing net income by shareholders' equity. ROE is considered the return on net assets.

Return on capital employed (ROCE):- Return on capital employed (ROCE) is a financial ratio that can be used in assessing a company's profitability and capital efficiency. In other words, this ratio can help to understand how well a company is generating profits from its capital as it is put to use.

Profit growth:- Profit growth it shows the growth in net profit over fixed period of time. Higher the rates batter it is.

Return on assets (ROA):- Return on assets (ROA) is an indicator of how profitable a company is relative to its total assets.ROA is displayed as a percentage; the higher the ROA is, the better.

Net NPA:- Net NPA stands for Net Non-Performing Assets. Net NPA is a term used by commercial banks to indicate less allowance for poor and uncertain debts than the amount of non-performing loans.

Net interest margin or NIM:- Net interest margin or NIM denotes the difference between the interest income earned and the interest paid by a bank or financialinstitution relative to its interest-earning assets like cash. ... NIM measures the effectiveness of a company's investment decisions, particularly for financial institutions.

Liabilities:- *A liability, generally speaking, is* ***something that is owed to somebody else***

Eg-When a company sells its goods on credit, it becomes a liability for its customers.

BankLiabilities Is equal to its deposits

The PEG Ratio:- The PEG ratio is a company's Price/Earnings ratio divided by its earnings growth rate over a period of time Pe>earning growth it implies that the company is overvalued and vice versa Advances growth in the balance sheet of any company means the amount of money lent out as loans. The positive and sustainable growth rate is always viewed as a good sign for the company.

3. Statistical Analysis

Share price data of last 5 years of ICICI Bank: -

Date	Open	High	Low	Close	Mean Of Share rice
01-01-16	237.545456	239.6364	198	209.2273	221.1023
01-02-16	206.363632	206.6818	164.3182	172.7727	187.5341
01-03-16	177.5	219.4091	177.5	215.1364	197.3864
01-04-16	214.545456	234.3636	199.1818	215.4091	215.875

01-05-16	206.636368	226.3636	193.8182	222.4091	212.3068
01-06-16	221.727264	237.4545	201	218.6818	219.7159
01-07-16	219.727264	249.0909	217.7727	239	231.3977
01-08-16	232.636368	237.5455	215.1364	234.5455	229.9659
01-09-16	235.227264	257.9546	221.1818	229.2273	235.8977
01-10-16	228.181824	265.0909	217.3636	251.6818	240.5795
01-11-16	254.045456	271.2727	222.7273	241.4091	247.3636
01-12-16	242.045456	245.2727	224.2727	232.0909	235.9205
01-01-17	233	250.5455	225.5455	244.5	238.3977
01-02-17	241.681824	266.0909	238.9091	251.2273	249.4773
01-03-17	252.363632	262	240.4545	251.6818	251.625
01-04-17	253.454544	265.0909	241.0909	253.1818	253.2045
01-05-17	253.181824	297.6364	246.5909	296.7727	273.5455
01-06-17	295.909088	297.2727	283.45	290.15	291.6955
01-07-17	291.399994	314.45	288.5	302.6	299.2375
01-08-17	303.899994	305.2	261.55	298.05	292.175
01-09-17	299.700012	300	269.15	276.6	286.3625
01-10-17	276.600006	314.65	255	300.1	286.5875
01-11-17	303	332.35	302.4	307.55	311.325
01-12-17	309.700012	319.2	287	314	307.475
01-01-18	314	365.7	307.5	352.95	335.0375
01-02-18	347.549988	355.9	311.1	313.25	331.95
01-03-18	312.649994	314	273.55	278.35	294.6375
01-04-18	273	294.9	258.8	284.2	277.725
01-05-18	284.200012	317.5	275.55	285.8	290.7625
01-06-18	295	302.7	269.6	275.4	285.675
01-07-18	274	308.5	256.5	304.25	285.8125
01-08-18	302.600006	346.8	294.1	342.6	321.525
01-09-18	343.600006	344	300.05	305.55	323.3
01-10-18	306.299988	356.55	294.8	355	328.1625

01-11-18	357	375.3	347.65	355.15	358.775
01-12-18	358.899994	369.25	336	360.15	356.075
01-01-19	361.5	383.55	336.65	364.45	361.5375
01-02-19	364.5	364.9	336.15	350.15	353.925
01-03-19	352.049988	402.4	350.65	400.5	376.4
01-04-19	401.450012	411	385	407.5	401.2375
01-05-19	407.5	439.2	375.25	423.7	411.4125
01-06-19	426	443.9	407.9	437.1	428.725
01-07-19	439.5	442	401.7	424.6	426.95
01-08-19	423.25	427.9	385.8	409.65	411.65
01-09-19	409.649994	458.65	384.35	433.7	421.5875
01-10-19	436.950012	482	411.5	463.05	448.375
01-11-19	466.649994	520	460.5	512.6	489.9375
01-12-19	513.450012	552.2	504.65	538.9	527.3
01-01-20	539.900024	547.4	515	525.65	531.9875
01-02-20	524	550.7	492.2	497.25	516.0375
01-03-20	508.25	520.55	268.3	323.75	405.2125
01-04-20	319	392.95	281.5	380.15	343.4
01-05-20	380.149994	380.15	285.55	331.95	344.45
01-06-20	339	380	324.1	351.45	348.6375
01-07-20	354.25	395.65	340.4	346.8	359.275
01-08-20	346.799988	422	340.5	394.6	375.975
01-09-20	394.700012	399.65	333.75	354.75	370.7125
01-10-20	358.25	428.5	358.25	392.6	384.4
01-11-20	417	499	407	473.35	449.0875
01-12-20	479.700012	538.5	472.2	535.05	506.3625

Statistical measurements-	
Mean	330.002765
Median	322.412499
Mode	531.9875
Variance	7559.12694
Standard deviation	86.94324
Mean deviation	71.21117
Range of share price	187.534088 to 531.9875

Graphical Representation:

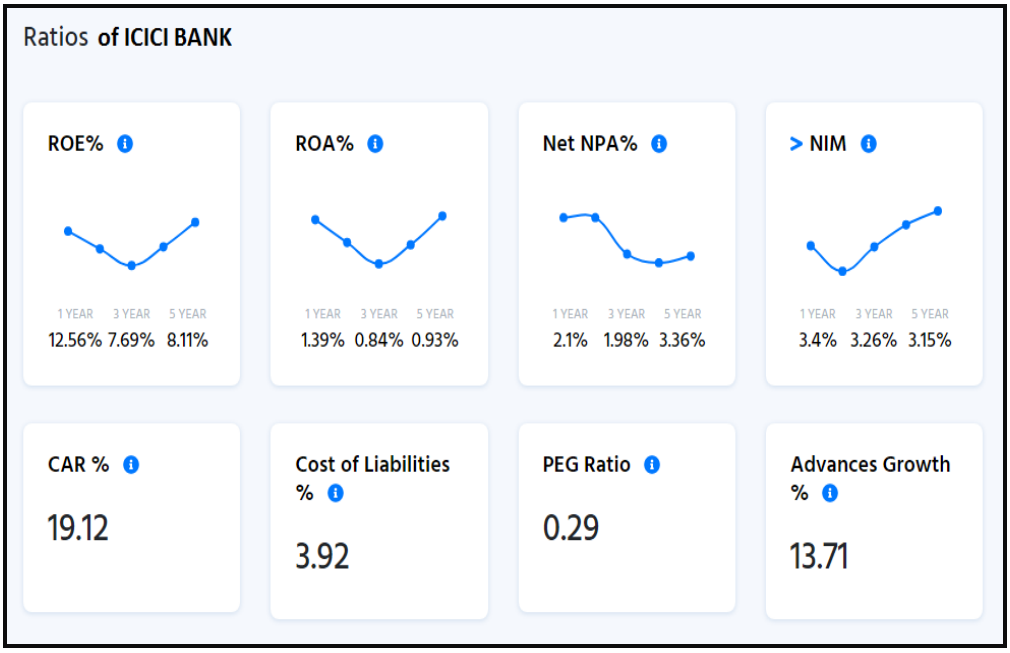

Analytical Report of ICICI Bank Stocks-

1. The company has been consistently maintaining a NIM of 3.15% since last 5 years.
2. CASA stands at 46.29% of total deposit.
3. Cost to Income ratio stands at 37.20 %
4. Good Capital Adequacy Ratio of 19.12%
5. Other Income is 23.97% of total income.
6. The company has delivered good Profit growth of 33.69% over the past 3 years.
7. Company has a low ROE of 8.11% over the last 5 years

Share Price Data of Last 5 Years of HDFC Bank-

Date	Open	High	Low	Close	MEAN SHARE PRICE
01-01-16	541.2	554	503.95	524.925	531.018753
01-02-16	529	533.5	464	485.925	503.106247
01-03-16	487.475	539.45	485.925	535.575	512.1062545

01-04-16	534.4	568.35	521.425	566.175	547.587494
01-05-16	563.875	597.5	556.575	590.95	577.225006
01-06-16	591.475	595.925	572.125	588.225	586.937485
01-07-16	590	625.625	580.45	623.1	604.793747
01-08-16	624.5	647.5	606.9	645.6	631.125
01-09-16	644	659.225	632.7	636.425	643.087494
01-10-16	640.5	650.025	612.075	629.525	633.031265
01-11-16	628	644.5	579	599.8	612.824997
01-12-16	601.15	606	581.8	603.1	598.012497
01-01-17	604.725	650	591.55	643.325	622.399994
01-02-17	643.1	727	640.25	695.05	676.349991
01-03-17	698.225	739.975	684.5	721.275	710.993744
01-04-17	723	786.975	712.525	773.25	748.9375
01-05-17	773.25	824	761.3	818.1	794.162491
01-06-17	819.5	858	810.275	826.025	828.450012
01-07-17	826.3	899.4	822.5	892.2	860.100006
01-08-17	890.925	904.575	865.575	888.225	887.324997
01-09-17	890.5	934	869	902.85	899.087494
01-10-17	902.85	939.8	878.925	904.25	906.456238
01-11-17	907.55	937.75	894	926.85	916.537491
01-12-17	927.45	951.55	899.5	936.2	928.675003
01-01-18	936.35	1006.75	925.25	1002.85	967.799988
01-02-18	1003	1007.5	918.15	942.1	967.6875
01-03-18	939.65	950	914.25	943.05	936.737503
01-04-18	945.25	989.5	930.15	972.15	959.262512
01-05-18	972.15	1080	972.15	1069.725	1023.506256
01-06-18	1058	1078.5	1004.55	1054.225	1048.818741
01-07-18	1054.175	1110	1031.625	1089.75	1071.387512
01-08-18	1081.4	1087.5	1029.125	1030.6	1057.15625
01-09-18	1034.7	1039.475	955.1	1003.025	1008.074982

01-10-18	1004.9	1026.1	942.5	955.875	982.34375
01-11-18	965	1068.775	948	1064.225	1011.5
01-12-18	1065.5	1079.7	1016	1060.85	1055.512482
01-01-19	1063.825	1083.25	1011	1039.975	1049.512482
01-02-19	1039.975	1077.5	1036.6	1038.775	1048.212494
01-03-19	1043.125	1164.025	1035	1159.45	1100.399994
01-04-19	1162.625	1166	1115.5	1158.725	1150.712494
01-05-19	1158.725	1232.5	1135.8	1212.675	1184.925019
01-06-19	1213.5	1247.25	1201.5	1221.875	1221.03125
01-07-19	1228	1251.65	1111.525	1125.825	1179.25
01-08-19	1114.55	1144.5	1069.8	1113.975	1110.706269
01-09-19	1113.975	1282.7	1084	1227.45	1177.03122
01-10-19	1231.5	1263.9	1181.15	1230.35	1226.725006
01-11-19	1239	1287	1227.6	1274.95	1257.137482
01-12-19	1273.95	1305.5	1234.2	1272.1	1271.43747
01-01-20	1276.1	1304.85	1211.75	1226.3	1254.75
01-02-20	1220	1259.9	1170.1	1177.65	1206.912506
01-03-20	1200.2	1201.15	738.75	861.9	1000.5
01-04-20	863.85	1019	810	1001.8	923.662491
01-05-20	1001.8	1001.8	826.1	951.65	945.337494
01-06-20	975	1082.6	928	1065.85	1012.862488
01-07-20	1065.85	1157.95	1020.05	1032.8	1069.162491
01-08-20	1025.95	1148.8	993	1115.85	1070.899994
01-09-20	1128	1145.95	1025	1078.6	1094.387482
01-10-20	1090.1	1251	1090.1	1183.55	1153.6875
01-11-20	1194.35	1464.4	1177.5	1440.85	1319.274994
01-12-20	1440.85	1449	1345	1436.3	1417.787506

Statistical Measurements-	
Mean	938.2737467
Median	975.071869
Mode	1417.787506
Variance	54512.69357
Standard deviation	233.4795356
Mean deviation	192.4795406
Range of share price	503.106247 to 1417.78750625

Graphical Representation:-

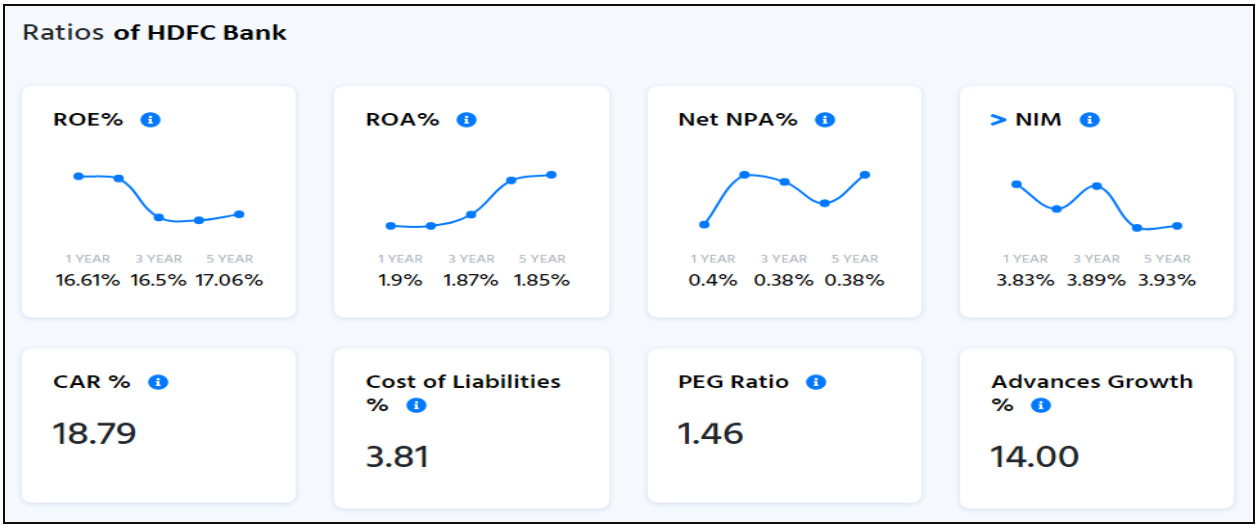

Analytical report of HDFC Bank Stocks

1. The CASA ratio of bank is 46.12% which gives the information about the deposited funds got by bank at low interest cost.
2. Net NPA% percentage of bank in last five years is 0.38% which is good sign and give idea of well distributed loan by the banks.

3. Cost of liabilities of bank is 3.81% means that bank gives average 3.81% interest to his depositors.
4. The advances growth of bank is 14% which is at moderate level.
5. CAR percentage of bank is 18.79% which is excellent for financial health of bank.
6. NIM of bank is 3.93% which tells us that bank get profit of Rs.3.93 for each Rs.100.
7. ROA% of bank is 1.83% which is positive sign and gives information that bank get profit of 1.83% on his assets.
8. Deposits of banks are granules and well diversified which make bank more stable.
9. The bank has been maintaining a healthy ROA of 1.87% since last 3 years.
10. The company is trading 4.04 times of its Book Value

CORRELATION AND REGRESSION ANALYSIS: -

The Correlation and Regression Analysis between Bank Nifty and Oil prises and Gold prices are as follows: -

Date	MEAN OF BANK NIFTY (Y)	OIL PRICES (X1)	GOLD PRISES (X2)
01-Dec-20	30398.9625	3589.35	136887.2
01-Nov-20	27073.775	3141.53	138605.9
01-Oct-20	23018.475	2931.66	139622.5
01-Sep-20	22487.5375	2984.05	141258.9
01-Aug-20	22890.55	3243.75	147001.4
01-Jul-20	21808.3375	3156.01	138521.8
01-Jun-20	20771.4125	2987.46	131144.1
01-May-20	19361.8625	2298.55	129825.5
01-Apr-20	19941.775	1603.02	128239.4
01-Mar-20	23688.1	2392.98	118306.2
01-Feb-20	29914.9625	3811.78	114110.6

01-Jan-20	31488.375	4395.91	111318.5
01-Dec-19	31944.8625	4509.77	105296.5
01-Nov-19	31078.2375	4314.32	105057.2
01-Oct-19	29319.1	4069.14	106209.1
01-Sep-19	28446.25	4282.87	107755.2
01-Aug-19	27867.1625	4102.97	106747.7
01-Jul-19	30086.1875	4230.22	97215.99
01-Jun-19	31121.1625	4149.67	94370.2
01-May-19	30346.0625	4664.02	89588.57
01-Apr-19	30101.8125	4761.33	89277.4
01-Mar-19	28698.9625	4432.04	90384.77
01-Feb-19	27082.975	4352.94	93999.48
01-Jan-19	27197.1125	4003.08	91392.22
01-Dec-18	26790.2875	3822.07	88567.77
01-Nov-18	26072.575	4476.09	87672.27
01-Oct-18	25063.1375	5648.69	89474.27
01-Sep-18	26550.1875	5448.55	86643.99
01-Aug-18	27865.7875	4942.53	83560.63
01-Jul-18	27015.725	4992.51	85032.02
01-Jun-18	26598.675	4879.75	86881.56
01-May-18	26299.2125	4959.75	88040.16
01-Apr-18	24861.925	4516.93	87643.83
01-Mar-18	24529.3375	4171.72	86116.81
01-Feb-18	26209.3625	4085.16	85664.2
01-Jan-18	26411.625	4215.16	84729.66
01-Dec-17	25336.55	3930.99	81231.2
01-Nov-17	25400.675	3887.81	83160.05
01-Oct-17	24579.6375	3574.53	83278.23
01-Sep-17	24289.6625	3413.19	84705.81
01-Aug-17	24623.0625	3194.46	82070.82

01-Jul-17	24164.1	3071.23	79702.45
01-Jun-17	23374.8875	2975.01	81206.16
01-May-17	22886.7125	3213.83	80267.72
01-Apr-17	21916.6625	3365.04	81731.26
01-Mar-17	21065.6	3355.09	81169.45
01-Feb-17	20160.7375	3647.03	82818.17
01-Jan-17	18785.95	3649.89	81191.05
01-Dec-16	18256.35	3572.84	78583.48
01-Nov-16	20200.25	3056.29	83622.54
01-Oct-16	0	3290.46	84551.36
01-Sep-16	0	3006.05	88540.4
01-Aug-16	0	3004.16	89707.71
01-Jul-16	19063.125	2966.28	89845.99
01-Jun-16	17806.8625	3208.66	85878.28
01-May-16	16805.75	3072.75	84340.04
01-Apr-16	16188.125	2708.63	82572.44
01-Mar-16	0	2503.95	83496.73
01-Feb-16	14412.45	2117.58	81857.57
01-Jan-16	15607.4625	2004	73882.06

Determinant of Correlation Matrix R

	Bank nifty	Oil prices	Gold prices
Bank nifty	1	0.572373381	0.195365504
Oil prices	0.572373381	1	-0.223871727
Gold prices	0.195365504	-0.223871727	1

Regression Statistics	
Multiple R	0.661655373
R Square	0.437787833
Adjusted R Square	0.41806109
Observations	60

	Coefficients
Intercept (a)	-10542.73301
OIL PRICES ($b_{12.3}$)	5.671660897
GOLD PRISES ($b_{13.2}$)	0.131123419

Regression Equation

$Y = a + b_{12.3} X_1 + b_{13.2} X_2$

$Y= (-105420733) +(5.6716) X_1+(0.1311) X_2$

4 Concluding Remarks-

- The correlation coefficient between bank nifty and oil prices is 0.5723 that means dependency of bank nifty on oil price is 57.23% approximately.
- Dependency of bank nifty on gold price is 19.53% approximately.
- We observe the negative correlation between oil prices and gold prices.
- The value of multiple correlation coefficient R is 0.4377 which shows that there is approximately 43% dependency of bank nifty on oil prices and gold prices.
- The equation of regression plane of bank nifty(Y) on oil prices(X_1) and gold prices(X_2) is

$Y= (-105420733) +(5.6716) X_1+(0.1311) X_2$

- **From above data we conclude that HDFC bank is better than ICICI bank for long term investment and for option treading also.**

5. References-

1. Reddy, I.P. (1995). Price behavior of agricultural commodities. Indian J. Mktg., 24(7): 25-30.

2. Surya Prakash, S., Venkataram, J.V. and Reammanna, R. (1979). An analysis of prices and arrivals of potato in Karnataka. Indian J. agric. Mktg, 11(5): 14-18.

3.Thaur, D.S. and Shandil, A.S.(1993). Steps to increase market arrivals and efficiency of regulated markets. Bihar J. agric. Mktg., 1(2): 155- 160.

4. Upender, M. and Manoharachary, S. (1996). An analysis of market arrivals and prices of paddy in regulated agricultural markets. Bihar J. agric. Mktg, 4(1) : 15-21.

5.Wadhwani, M.K. and Bhogal, T.S. (2002). An analysis of seasonality, trends, cycles and the factors influencing vegetable price. A case study of Western A.P. Bihar J. agric. Mktg., 10(3): 271-284.

Paper-3

ASSESSING THE SUITABILITY OF BEACH TOURISM AT ACHARA AND DEVBAUG AREA IN MALVAN TEHSIL, SINDHUDURG DISTRICT OF MAHARASHTRA, INDIA.

D.M.Markad[1] M.L.Muluk[2] D.D.Muluk[3] S.K. Ranyewale[4]

1. Assistant Professor
Dept of Geography
Hutatma Rajguru Mahavidyalaya
Rajgurunagar

2. Assistant Professor
Dept. Of Geography
Hutatma Rajguru Mahavidyalaya
Rajgurunagar

3. Associate Professor and Head
Dept of Geography
Hutatma Rajguru Mahavidyalaya, Rajgurunagar

4. Assistant Professor and Head
Dept of Geography
Arts, Commerce and Science college Dehane

Abstract:

Seacoast is the most dynamic part of the world, there are many accidental cases occurred every year on many beaches all over the world e.g. drowning. Beaches have potential to attract the tourist for recreation activity, so the safety and security of the tourists are also very important in the beach area. The present paper investigates the site suitability of beach tourism in the context of tourist safety and recreation. The suitability of the beach is assigned into four categories or classes from highly suitable (S1) to not suitable (NS). A specific weight is given to each parameter according to their total impact in the process of decision-making. The present study of beach suitability for tourism at Achara and Devbaug was assessed by using different models work in the coastal recreation research. Both Achara and Devbaug are beaches with creekside. Data obtained from field survey, observation, subject experts, interviews, and discussion with local people and service providers. Beach cross profiles were measured through the dumpy level- collimation method. Result of the analysis showed that the coastal area of Achara and Devbaug has the area in the class of Category S2 quite suitable. Both sites have the potential for tourism development due to their beautiful scenery but steep slope, current speed are an obstacle for beach tourism of swimming and recreation category.

Keywords: Assessing, Suitability, Recreation, Beach Tourism.

Introduction:

Sindhudurg district of Maharashtra has a 121 km coastline with clean and long beaches. Sindhudurg district is the only district declared as a "Tourism District" in India. Tourism is the leading economic activity of the district (Weerapon Thongma, 2011). Many coastal destinations attract tourists. Achara and Devbaug are two different beach and creek sides at Malvan tehsil in Sindhudurg district which is famous for its beautiful scenery over the past many years. Both Achara and Devbaug beach have the potential for tourism development but both are creek area and slope of the beach are comparatively steep which is quite unsuitable (unsafe) for recreation. Achara and Devbaug beach area have fine and white sand

with Scenic beauty of the surrounding attract tourists but the slope of the beaches and current speed are not perfectly suitable for swimming. Coast is the most dynamic part of the world and itself is the transaction area between sea and land ecosystem. Landside is influenced by coastal processes including wave, current, tide, ebb, etc.

Objective:

1. To assess the site suitability of beach tourism for recreation.

Study Area:

Malvan Tahsil is a coastal Tahsil located in the western part of the Sindhudurg district(Suryawanshi and Ranyewale 2018)(Sahoo 2014). The district is surrounded by the Devgad Tahsil on the north, Kankavli and Kudal Tahsil on the east, Kudal and Vengurla Tahsil on the south, and the Arabian Sea on the west. The geographical extent of Malvan tehsil is $16^{0}00$' north to $16^{0}05$' north latitude and $73^{0}25$' east to 73^{0} 30' east longitudes. Malvan Tahsil of Sindhudurg coast is reaching with beach and creek sites with clean and white sand. Beaches with creeks are very common features, clean and white sand with rich geodiversity are potential for tourism development in this area(Rajan, Varghese, and Anakkathil Purushothaman 2013)(Gole 1982). Physical landscapes play a significant role in the development of tourist activity(Benur and Bramwell 2015); basically, geomorphological features with beautiful scenarios are a key factor in recreation at this destination(Brandolini, Faccini, and Piccazzo 2006)(Chen and Teng 2016). Achara creek and beach are located in the northern part of the tehsil whereas Devbaug is the southern part of the tehsil.

Methods:

Coastal scenic assessment via checklist table provides benchmark measures regarding reliable/ non-reliable beach condition(Putra and Al Tanto 2017) which also classify site suitability (Anfuso et al. 2014) Topography (slope and aspect), the geological structure of the region, water availability, soil permeability, infrastructure, flora, and fauna are being important aspects in the assessment of site suitability of the coastal recreation (Abed et al. 2011). The initial stage of tourism development is an assessment of the elements or the entire area to priorities identification (Gormsen 1997) which will continue to be presented and economically valorized through specific activity and measures (Perch-Nielsen 2010) (Sahoo 2014) (Pawar 2016). This is possible to achieve with the help of different models of evolution with qualitative characteristics express quantitatively through this idea is to develop a universal model, which can apply to different areas in order to compare to each other, so decision-makers and planners knew exactly which an area has great potential to develop as a tourist destination (Obrenic et.al. 2015). For the analysis of site suitability of beach tourism, the parameters of beach type, water depth, current speed, beach slope, beach land coverage, dangerous biota, and the distance of freshwater supply are very useful (Sihasale 2013).

The present study of assessing beach suitability for tourism at Achara and Devbaug assessed by using different models work in the coastal recreation research. For this study research method is depend on the available data.10 parameters were selected for assessing site suitability based on Sihasale et.al. (2013), Anfuso et.al. (2014), Putra and Tanto (2017). Data were obtained from field surveys, observation, subject experts, interviews, and discussions with local people and service providers. Beach cross profiles were measured through the dumpy level- collimation method.

Table 1: The Matrix of Site Suitability Criteria of Beach Tourism for Recreation

Parameter	Wt	Category S1	Score	Category S2	Score	Category S3	Score	Category NS	Score
Water base Depth (Bathymetry)(m)	5	0-3	4	>3-6	3	>6-10	2	>10	1
Beach Type	5	White Sand	4	White Sand Few Rocks	3	Rocky Black Sand,	2	Mud, Rocky, Steep	1
Beach Slope (^{0})	5	<10	4	10-25	3	25-45	2	>45	1
Beach Width (m)	5	>15	4	10-15	3	3-<10	2	<3	1
Current Speed (m/second)	5	0-0.17	4	0.17 - 0.34	3	0.34-0.51	2	>0.51	1
Water Transparency (%)	3	>80 (Transparent)	4	50-80	3	20-50	2	<20 (Turbid)	1
Official Level of Protection	3	Best	4	Partially Protected	3	Partially Unprotected	2	No Protection	1
Beach Land Coverage	1	Coconut, Open land	4	Shurbs, Low Savanna	3	High Shurbs	2	Mangrove, Housing, Port	1
Dangerous Biota	1	-	4	Pig fur	3	Pig fur, rayfish	2	Pig fur, rayfish, shark	1
Freshwater Supply (distance/km)	1	<0.5	4	0.5-1	3	1-2	2	>2	1

Source: Sihasale et.al. (2013), Anfuso et.al. (2014), Putra and Tanto (2017) and modified by Author.

Notes:

The site suitability of beach tourism assigned into 4 categories

Maximum rate of suitability= 136

Category S1: Very Suitable with a rate 80-100%

Category S2: Quite Suitable with a rate 60-80%

Category S3: Suitable with Conditions with rate 40-60%

Category NS: Not Suitable with a rate of less than 40%

$$\text{Beach Suitability} = \frac{\sum \left[\text{Suitability Score Rate} \right]}{\text{Maximum Rate of Suitability}} \times 100$$

Result and Discussion:

Table 2: The Matrix of the Suitability of beach tourism for Recreation

Sr. No.	Parameters	Weight	Achara Beach		Devbaug Beach	
			Score	Rate	Score	Rate
1	Water base Depth (Bathymetry)(m)	5	2	10	2	10
2	Beach Type	5	4	20	4	20
3	Beach Slope (^{0})	5	2	10	3	15
4	Beach Width (m)	5	4	20	4	20
5	Current Speed (m/second)	5	2	10	2	10
6	Water Transparency (%)	3	3	9	3	9
7	Official level of Protection	3	1	3	2	6
8	Dangerous Biota	1	4	4	4	4
9	Freshwater Supply (distance/km)	1	2	2	3	3
10	Beach Land Coverage	1	2	2	3	3
	Total			90		100

Source: Compiled by author (2017)

The suitability of beach tourism for recreation is assessed by the site suitability index. For this purpose, ten (10) parameters in the matrix of suitability were selected. The parameters are Water base depth, Beach type, Beach slope, Beach width, Current speed, Water transparency; Official level of protection, Dangerous biota; Freshwater supply, and Beach land coverage were selected. The suitability of beaches has been measured by the following equation.

$$\text{Beach Suitability} = \frac{\sum \left[\text{Suitability Score Rate} \right]}{\text{Maximum Rate of Suitability}} \times 100$$

Suitability Score Rate (Achara) = 90

Suitability Score Rate (Devbaug) = 100

Maximum Rate of Suitability= 136

$$\textbf{Achara Beach} = \frac{\sum\left[10+20+10+20+10+9+3+4+2+2\right]}{136} \times 100$$

$$= \frac{90}{136}$$

$$= 66.17\%$$

$$\textbf{Devbaug Beach} = \frac{\sum\left[10+20+15+20+10+9+6+4+3+3\right]}{136} \times 100$$

$$= \frac{100}{136}$$

$$= 73.52\%$$

The result of the above calculation of Tourism Suitability Index rate in both Achara and Devbaug beach respectively obtained a score of 90 or 66.17% and 100 or 73.52%, therefore both beaches got score range between 60-80% under the category of S2- Quite Suitable. In the overall parameter, we found that both beaches are quite suitable for recreation. But in the context of the slope, both beaches are not secure for swimming and recreational purpose.

Achara Geomorphic Map with Beach Profiles:

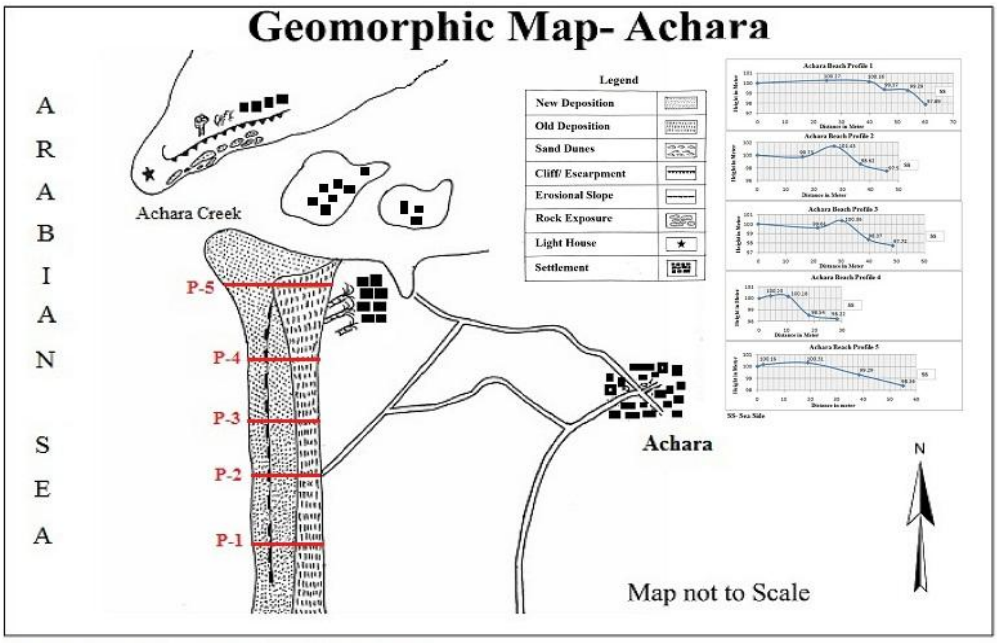

Source: Compiled by Author (Field Survey 2019)

Above map shows that beach profiles showing a clear picture of Achara beach, which shows that the first four profiles having a very steep slope of more than 45^0 whereas profile number 5 is nearly gentle to steep. In the context of the slope, the slope of all profiles was found 25^0-45^0 (Suitable with Conditions) to more than 45^0 criteria NS (Not Suitable). it means the beach is unsuitable for swimming or recreation.

Devbaug- Geomorphic Map with Beach Profiles:

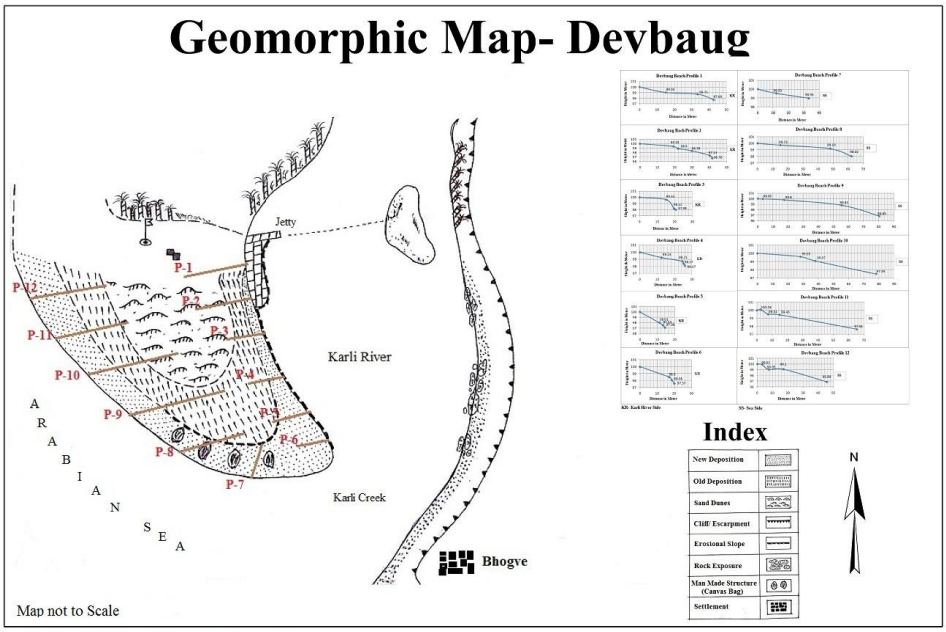

Source: Compiled by Author (Field Survey 2019)

The above geomorphic map and beach profiles show a clear picture of the slope of the beach. There were twelve beach cross profiles were collected, six from the Karli River (Creek) side and six from the sea side. Profiles no. 1 to 6 are from Karli Riverside steeper than profiles no. 7-12. Profiles no. 7 to 12 are collected from the seaward side which is relatively gentle to steep in slope. It means the river side (creek) slope is more dangerous than the seaward side for swimming and recreation. But the slope of the seaside is between 25^0 to 45^0 which falls in criteria S3 (Suitable with Conditions) whereas Karli River (creek) side slope is found more than 45^0 falls in category NS (Not Suitable).

Beach Profile:

Both Achara and Devbaug beach cross profiles were collected by Dumpy level survey-Collimation method during the field visit in 2019. 100-meter height is considered as base level height. Both beaches are located near the creek area having a great potential to attract visitors and both are famous for tourism. Both beaches having very steep slopes towards the creek side which is highly risky for swimming and recreation. Slope and current speed are the very crucial factor in the development of coastal recreation activity.

Conclusion:

It is concluded that both beach sites Achara and Devbaug are quite suitable for beach tourism but not suitable for recreation due to their steep slopes. About site suitability of beach tourism of Achara beach site registered a total score of 90 or 66.17% whereas Devbaug beach site registered 100 or 73.52% score which falls under the category of Category S2: Quite Suitable with rate 60-80% to beach tourism for recreation. Both beaches are famous tourist destinations and having great potential as a tourist spot in the context of scenic beauty but both are risky for swimming due to their steep slopes along the creekside.

References:

1. Abed, Mahsa Hakimi, Masoud Monavari, Abdolreza Karbasi, Parvin Farshchi, and Zahra Abedi. 2011. "Site Selection Using Analytical Process by GIS for Sustainable Coastal Tourism." *International Conference on Environmental and Agriculture Engineering IPCBEE* 15:120–24.
2. Anfuso, G., A. T. Williams, J. A. Cabrera Hernández, and E. Pranzini. 2014. "Coastal Scenic Assessment and Tourism Management in Western Cuba." *Tourism Management* 42:307–20. doi: 10.1016/j.tourman.2013.12.001.
3. Benur, Abdelati M., and Bill Bramwell. 2015. "Tourism Product Development and Product Diversification in Destinations." *Tourism Management* 50:213–24. doi: 10.1016/j.tourman.2015.02.005.
4. Brandolini, P., F. Faccini, and M. Piccazzo. 2006. "Geomorphological Hazard and Tourist Vulnerability along Portofino Park Trails (Italy)." *Natural Hazards and Earth System Science* 6(4):563–71. doi: 10.5194/nhess-6-563-2006.
5. Chen, Chung Ling, and Ning Teng. 2016. "Management Priorities and Carrying Capacity at a High-Use Beach from Tourists' Perspectives: A Way towards Sustainable Beach Tourism." *Marine Policy* 74(September):213–19. doi: 10.1016/j.marpol.2016.09.030.
6. Gole, Prakash. 1982. "Journal of Ecological Society." 1982.
7. Gormsen, Erdmann. 1997. "The Impact of Tourism on Coastal Areas." *GeoJournal* 42(1):39–54. doi: 10.1023/A:1006840622450.
8. Obrenic J., Bjeljac Z., Terzic A. (2015): Assessment Model of Nature-Based Touristic Motives in the Ovkar-Kablar Gorge (Serbia), *J. Geogr. Inst. Cvijic.*, 65(3), pp- 407-422.
9. Pawar, Priyanka R. 2016. "Sea Turtle Conservation and Allied Activities with Community Participation at Velas, Maharashtra, India." *Indian Ocean Turtle*

Newsletter (I).

10. Perch-Nielsen, Sabine L. 2010. “The Vulnerability of Beach Tourism to Climate Change-an Index Approach.” *Climatic Change* 100(3):579–606. doi: 10.1007/s10584-009-9692-1.
11. Putra, Aprizon, and Try Al Tanto. 2017. “The Suitability Ecotourism Beach Based Geopasial in Padang City, Indonesia.” *Sumatra Journal of Disaster, Geography and Geography Education* 1(1):83. doi: 10.24036/sjdgge.v1i1.40.
12. Rajan, Brilliant, Vincy Mary Varghese, and Pradeepkumar Anakkathil Purushothaman. 2013. “Beach Carrying Capacity Analysis for Sustainable Tourism Development in the South West Coast of India.” *Environmental Research, Engineering and Management* 63(1):67–73. doi: 10.5755/j01.erem.63.1.2648.
13. Sahoo, Debasis. 2014. “A Case Study On “ Beach-Tourism Potential Of Odisha.” 1(2).
14. Sihasale, Daniel Anthoni. 2013. “The Suitability of Coast Area for the Development of Beach Tourism of Recreation Category at Naku Village, South Leitimur Subdistrict, Ambon City, Indonesia.” *IOSR Journal of Engineering* 3(7):07–14. doi: 10.9790/3021-03740714.
15. Suryawanshi, Rajendra S., and Siddharth K. Ranyewale. 2018. “Tourism Potential of Geomorphosites: A Comparative Assessment of Selected Beach Sites in Malvan Tahsil, Sindhudurg Coast of Maharashtra (India).” *Transactions of the Institute of Indian Geographers* 40(2):285–92.
16. Weerapon Thongma, W. L.-T. (2011). Tourists’ satisfaction towards tourism activities management of maesa community, pongyang sub-district, Maerim district, Chiang Mai province, Thailand. *International Journal of Asian Tourism Management , 2* (1), 86-94.

Paper-4

Growth and Characterizations of Single Crystals of Pure and L-Alanine Doped Zinc Tris-Thiourea Sulphate

M. A. Patil[1], S. G. Thube[1], V. M. Nikale[1], Y. A. Pathak[2]

1. Dada Patil Mahavidyalaya, Karjat Dist- Ahmednagar [MS.].

2. Karmaveer Bhaurao Patil Mahavidyalaya, Pandharpur (Autonomous) [MS.].

Abstract:

The Pure Zinc Tris-Thiourea Sulphate and L-alanine doped ZTS single crystal grown at temperature 37℃ and 24℃ temperature by employing slow evaporation technique and further have been analyzed by various characterization techniques. The good transparency is achieved by slow evaporation method. The crystals were confirmed by single crystal X-ray diffraction analysis using Bruker D8-Advanced Diffractometer. From that structure of crystal and lattice parameter and also observed the change in particle size. Band gap is calculated using UV-Visible absorption spectra recorded by double beam UV-Visible spectrophotometer (Systronics-AU-2701) in the wavelength range 200-1000 nm .The functional groups were identified by using FT-IR Spectrophotometer with ATR (Shimatzu Japan- ISWL) in the wave number range 500-4500 cm^{-1}. The uniform distribution of particles confirmed from SEM study which reveals the cubical morphology.

Keywords: *slow evaporation, Zinc Tris-Thiourea sulphate, X-ray diffraction,*

Introduction:

Recent years thiourea molecules are an appealing chemical matrix modifier as having large dipole moment and capability to form an network of hydrogen bonds.[1-4] The bis zinc chloride,), potassium thiourea bromide, tris-zinc sulphate (ZTS) and bis (thiourea) cadmium chloride (BTCC possesses nonlinear optical properties have focus major attention in the last few years since organic and inorganic both components in Thiourea contribute in particular to the process of second harmonic generation. The combination of centrosymmetric thiourea with inorganic salt gives non centrosymmetric complexes, which shows the nonlinear optical properties.[5-6] For second harmonic generation Zinc thiourea sulphate (ZTS) will acts as superior nonlinear optical semi organic material. It has low angular sensitivity,at higher frequency low dielectric constant, high laser damage threshold and extensive range of transparency. The X-ray structural determination shows a zinc ion terahedrally coordinating

three planar thiourea molecules and one oxygen from a sulfate .There is also extensive inter- and intramolecular hydrogen bonding between N-H's and the sulphate O's and this feature most likely gives rise to the noncentrosymmetry, which is an essential property for second harmonic generation.[7-19]

Experimental Work:

Preparation of Zinc Tris-thiourea Sulphate Salt:

The ZTS Salt has been synthesized from Zinc sulphate heptahydrate and Thiourea taking in the 1:3 molar ratios. Take 1 mole means 28.756 gm Zinc sulphate heptahydrate and 3 mole means 22.836gm Thiourea. Prepare the solution in 100 ml distilled water by continuously adding 28.756 gm Zinc sulphate heptahydrate and when it dissolves completely then add 22.836gm Thiourea. The solution of Zinc sulphate heptahydrate and thiourea in molar ratio 1:3 are reacting under continuous stirring at room temperature (~36^0c) .To avoid precipitation of other phases the mixture is stir vigorously.

The reaction is takes place as:

$$ZnSO_4.7H_2O + 3CS(NH_2)_2 \longrightarrow Zn[CS(NH_2)_2]_3SO4+7H_2O$$

According to above reaction we get the resultant precipitate of Zinc Tris-Thiourea Sulphate. On filtering and drying the solution we get precipitate of ZTS .In this way we get the salt of ZTS.

Preparation of saturated solution of Zinc Tris-Thiourea Sulphate:

Take 100 ml double distilled water as a solvent and stir it. Simultaneously add ZTS salt until equilibrium condition occurs. Then filter the solution using watmann filter .We get clear, transparent, saturated solution of ZTS. Keep this solution at room temperature for slow evaporation process after 4 to 6 days and the nucleation is takes place .there is formation of seed crystal.After 25 to 27 days we get transparent, colorless, grown ZTS crystal. Crystal size of grown crystal is 0.9×0.5×0.2mm

Preparation of L-Alanine Doped ZTS Single Crystal

Take 1 mole % L-Alanine for the doping in ZTS solution. For the synthesis of L-Alanine doped ZTS crystal Take 50 ml double distilled water. Add 2.25 gm L-Alanine in the solution of ZTS Separately. The solution was stirred thoroughly for 3 hours. Filter the solution

using watmann filter paper. Keep this solution at room temperature upto 6 to 8 days for slow evaporation process. By the nucleation there is formation of crystal. And after 30 to 35 days we get transparent, colorless, grown ZTS crystal. We observed crystal size of grown crystal is 0.9×0.6×0.3mm.

Result and Conclusion:

Characterization:

The grown crystals were subjected to different characterization viz. Powder XRD, FT-IR analysis, UV-visible spectral studies and dielectric constant measurement by transmission line wave guide method.

a) Powder X- ray Diffraction Analysis

Single crystal X-ray diffraction analysis for the grown crystal has been carried out to identify the cell parameters by using Bruker D8-Advanced Diffractometer in the 2 θ range of 20-80 degree which was operated at 40 KV and 30 mA. with CuKα radiation (λ=1.5406 Å) and The XRD patterns ZTS are shown in Fig.(a),Fig (b) and Fig (c). It is confirmed that, each crystal posses orthorhombic structure and have definite cell parameters. The XRD Data used to estimate the particle size of the grown sample . It is found that the grown crystal belongs to orthorhombic crystal system with space group Pca21 and the lattice parameters of Pure ZTS at Temp 37℃ *a* = 7.797Å, b= 11.144Å and c= 15.512 Pure ZTS at Temp 24℃*a* =7.795 Å, b=11.147 7Å and c= 15 Å . L- Alanine doped ZTS at Temp 37℃ *a* =7.799 Å, b= 11.141Å and c=15.471 Å

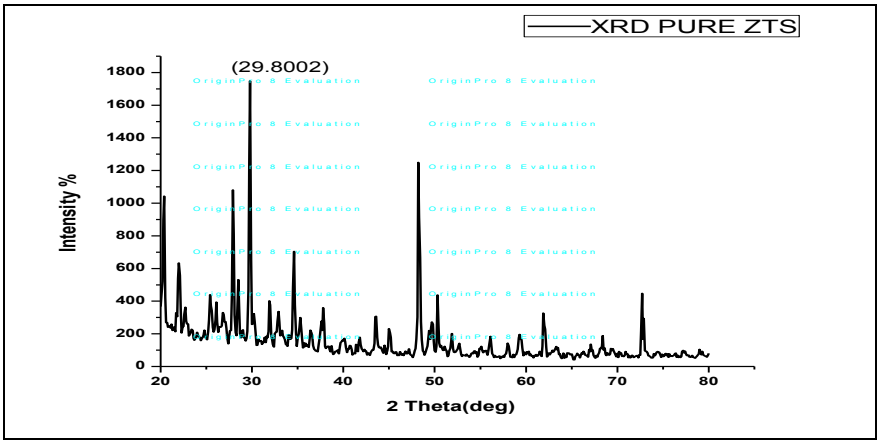

Fig (a): XRD Pattarn of Pure Zinc Tris-Thiourea Sulphate at Temperature 37℃

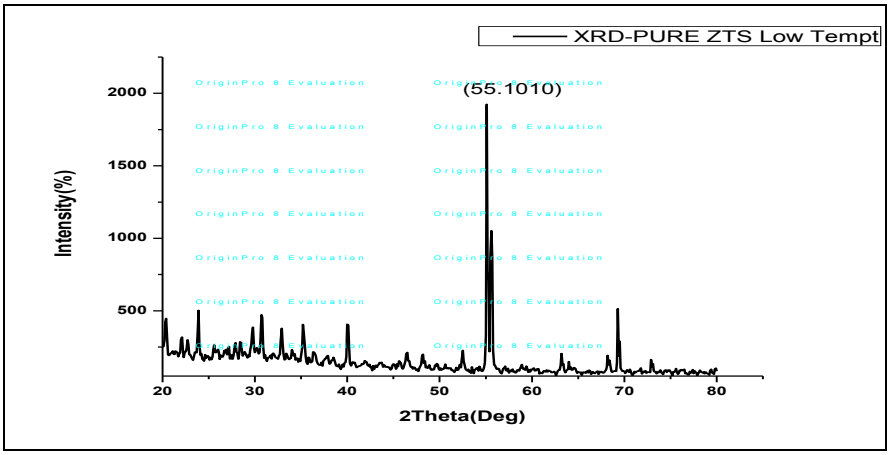

Fig(b): XRD of Pure Zinc Tris-Thiourea Sulphate At Temperature 24℃

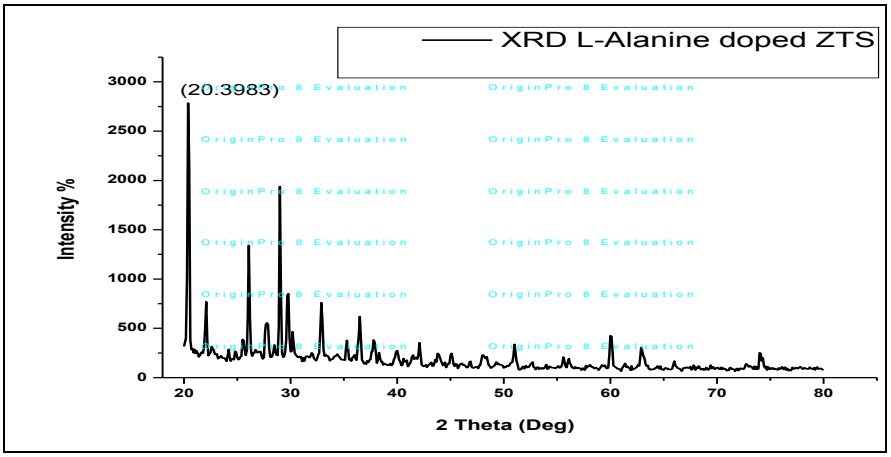

Fig(c): XRD pattern of 0.5 mole% L-Alanine doped Zinc Tris Thiourea Sulphate

b) UV-Visible Spectroscopy:

UV-Visible absorption spectra of Pure Zinc Tris-Thiourea Sulphate At Temperature 37℃ and 24℃ were recorded by double beam UV-Visible Spectrophotometer (Systronics-AU-2701) in the wavelength range 200-1000 nm. The UV-visible absorbance spectra of Pure ZTS At Temp 37℃ and Pure ZTS at temperature 24℃ are shown in following fig. The absorption spectra reveal that these two crystals have lower cut off wavelengths at around 280 nm. The wide transmission in the entire visible region (200nm- 1000nm) enables it be a potential candidate for optoelectronics applications.

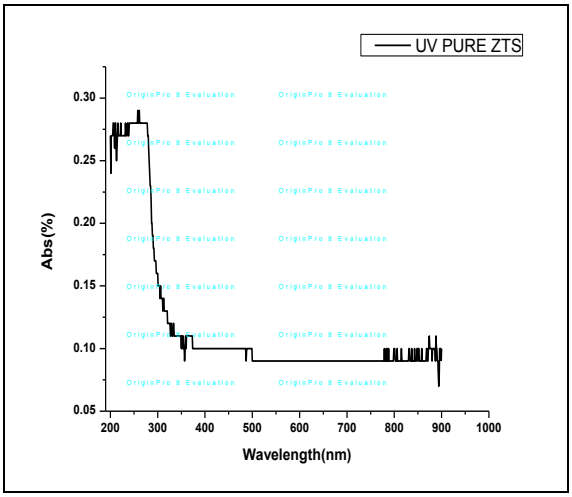

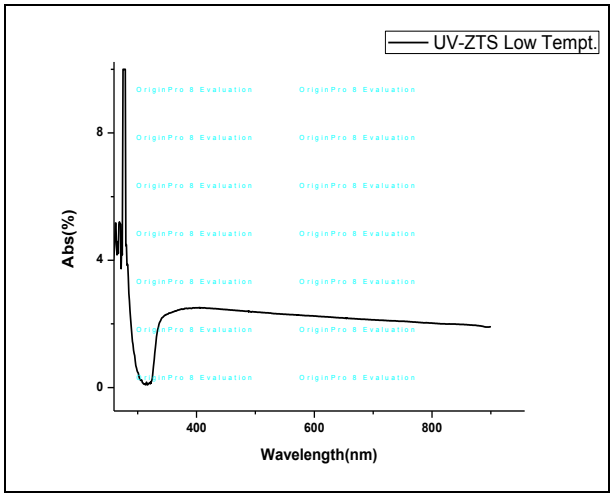

Table : The Band Gap of Given crystal sample

Sample	Cut of Wavelength (nm)	Bandgap (eV)
Pure ZTS	278 nm	4.4 eV
Tempt. Change ZTS	279 nm	4.4eV

c) Fourier Transform Infrared Spectral Analysis:

FTIR transmission spectra of Pure Zinc Tris-Thiourea Sulphate At Temperature 37℃ and 24℃ were recorded by FT-IR Spectrophotometer with ATR (Shimatzu Japan- ISWL) in the wavenumber range 500-4500 cm^{-1}. FTIR used to find the functional group, internal structure of the molecule and the nature of chemical bond of the compound which are present in crystal.[20] Fourier transform infrared spectral analysis is one of the most prominent and broadly used spectroscopic method for the analyzing the structure of the unknown components.

The FTIR analysis of zinc-tris thiourea sulphate was carried out to investigate the presence of functional groups and their vibrational modes. The spectrum was recorded between the frequencies 600 and 4000 cm-1 using spectrum RXI spectrometer, the sample was prepared by using pellet technique with mixture of KBr as shown in the figure 5.12. In between the higher energy region 3789 to 2109 cm^{-1}, the (NH2) asymmetric stretching mode is observed at

3371 cm^{-1}. The (NH) stretching modes are observed at3260 & 3162 cm^{-1}. The (NH2) symmetric stretching mode is observed at 2852 cm^{-1}. The(N-H) bending vibrational mode ,(-N=N-) Streching mode .The (NH2) asymmetric bending mode is observed at 1514 cm^{-1}.The (CN) asymmetric stretching mode is observed at 1440cm^{-1}.The (CS) asymmetric stretching mode is observed at 1402 cm^{-1}.The (CN) symmetric stretching mode is observed at1085cm^{-1}.The (CS) symmetric stretching mode is observed at 715 cm^{-1}.[21]

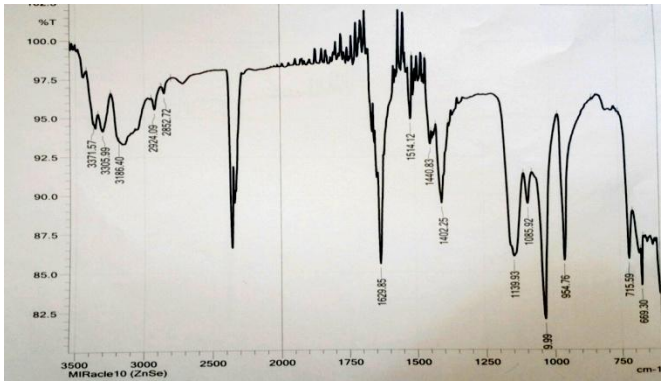

Fig. FTIR Spectra for Pure Zinc Tris Thiourea Sulphate At Temperature 37℃

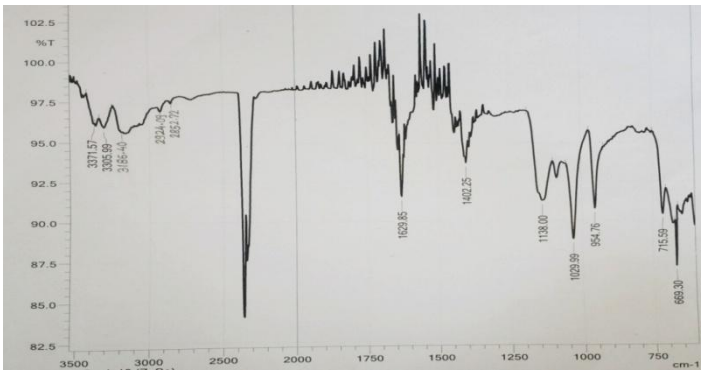

Fig. FTIR Spectra for Pure Zinc Tris Thiourea Sulphate At Temperature 24℃

d) Dielectric constant:

The dielectric behavior of pure ZTS crystal were carried at room temperature using the Gwin stek LCR-819 cube meter with varying frequency range of 10 Hz to 100 kHz. The dielectric constant is calculated using the relation, $\varepsilon=Cd/\varepsilon_0 A$where, C is the capacitance, d is the thickness; A is the area of the sample. The frequency response of dielectric constant for

pure and doped ZTS crystal is shown in fig.d. It shows that the dielectric constant has high values in the lower frequency region and decreases with the applied frequency. The high values of dielectric constant at lower frequencies may be due to the presence of polarizations mechanism namely orientation, space charge, electronic and ionic polarization. The low values of dielectric constant at high frequencies indicate high crystal perfection and low space charge polarization.

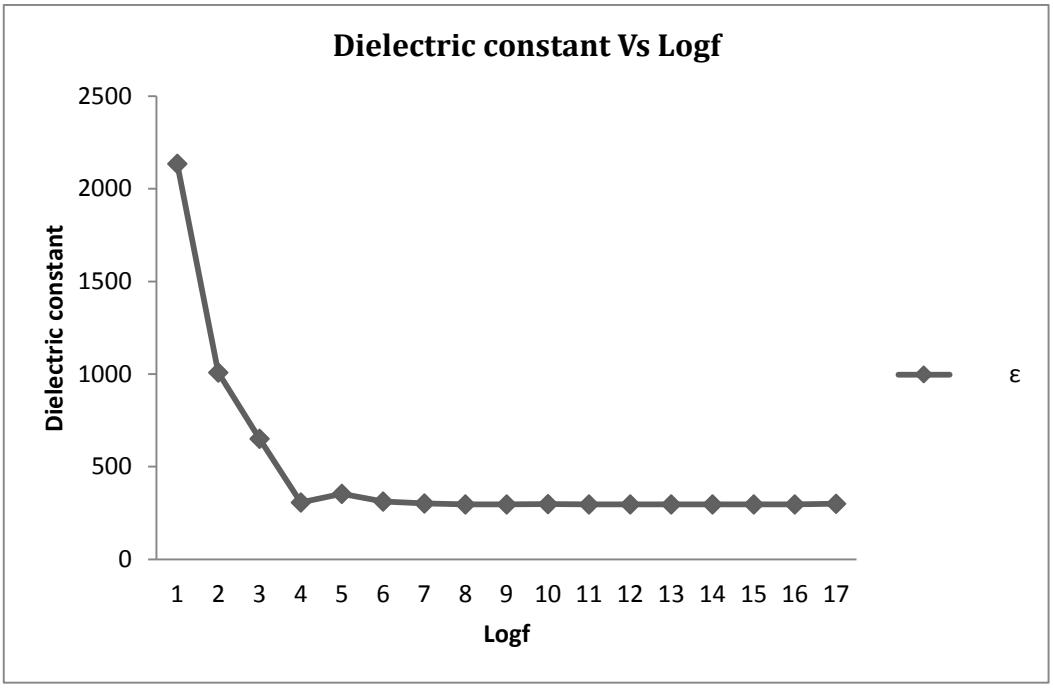

Fig.d. Frequency response of dielectric constant for pure and doped ZTS crystal.

E) SEM Results:

The morphology of Zinc Tris Thiourea Sulphate single crystal particles was determined by SEM spectra. The spectra obtained with SEM of Zinc Tris Thiourea Sulphate synthesized for various magnifications are shown below:

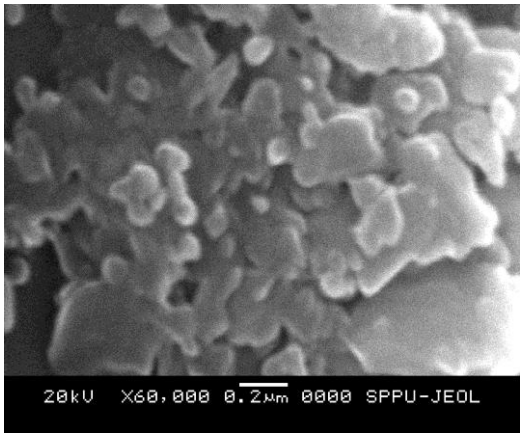

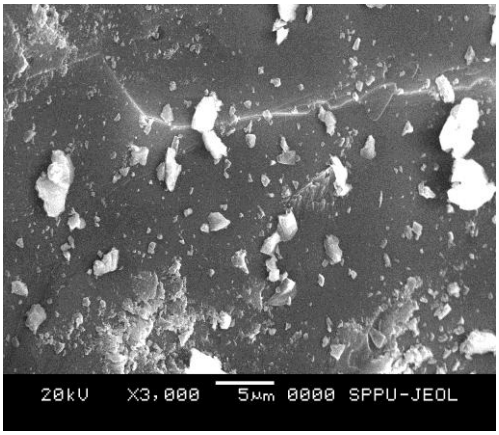

Conclusion :

The analysis of single crystals grown at 37℃ of pure Zinc Tris-Thiourea Sulphate and L-alanine doped ZTS at 24℃ has been carried out by different characterization techniques. Crystal is confirmed by single crystal X-ray diffraction. Single crystal ZTS is suitably grown by slow evaporation technique. As compare to other technique crystal grown by slow evaporation method shows good transferency. Also we get the structure of crystal and lattice parameter, and it is observed that the change in particle size .UV-Visible absorption spectra were recorded by double beam UV-Visible spectrophotometer (Systronics-AU-2701) in the wavelength range 200-1000 nm. From this by using cut off wavelength we calculate the band gap of given crystal sample. The functional groups were identified by using FT-IR spectrophotometer with ATR (Shimatzu Japan- ISWL) in the wave number range 500-4500 cm^{-1}. SEM shows the cubical morphology. It confirms the uniform distribution of particles.

References:

1. A Subashini , K Rajarajan and S Sagadevan 2017 Mater. Res. Express 4 026202
2. Angelimary PA and Dhanuskodi S 2001 Cryst. Res. Technol. 11 1231–7
3. Anie Roshan S, JosephC and Ittyachen MA 2001 J. Mater. Lett. 49 299–302
4. Selvakumar S, Packiam JJ, Rajasekar SA, RamanandA and Sagayaraj P 2005 Mater. Chem. Phys. 93 356–60.

5. R. Muraleedharan, J. Ramajothi and M. Basheer Ahamed Indian Journal of Science and Technology, *Vol 8(S7), 165–170, April 2015 ISSN (Print) : 0974-6846 ISSN (Online) : 0974-5645.*
6. M. Lawrence1, J. Felicita ISSN Journal of Engineering Science and 3. Innovative Technology (IJESIT) Volume 4, Issue 2, March 2015 208 : 2319-5967.
7. K. Senthil Kannan, S.Gunasekaran1 Seethalakshmi, International Journal of Scientific & Engineering Research Volume 4, Issue 2, February-2013.
8. Nikale VM, Thube SG, Patil MA and Pathak YA. Int. Res. Journal of Science & Engineering, January 2018, Special Issue A4 : 103-106.
9. K. Kirubavathi, K. Selvaraju, R. Valluvan, N. Vijayan, S. Kumararaman, Spectrochim. Acta A, 69 (2008) 1283.
10. C. Krishnan, P. Selvarajan, T.H. Freeda, C.K. Mahadevan, Physica B: Condensed Matter, Volume 404, Issue 2, 28 February 2009, Pages 289-294.
11. S.Anie Roshan, C.Joseph, M.A. Ittachen, Matter.Lett.49 (2001) 299.
12. P.M. Ushasree, R. Muralidharan, R. Jayavel, P. Ramasamy, J. Cryst. Growth 210 (2000) 741.
13. Venkataramanan V. Subramanian CK. Bhat HL. J. Appl. Phys. 1995; 77: 6049-51.
14. Sumil Verma, Singh MK.Wadhawan VK.Suresh CH. Pramana J Phys 2000; 54: 879-88.
15. M. Iyanar, C. Muthamizhchelvan, J. Thomas Joseph Prakash, S. Stephen Rajkumar Inbanathan, S. Ponnusamy, Spectrochimica Acta Part A 94 (2012) 265-270.
16. C. Krishnan, P. Selvarajan, T.H. Freeda. Journal of Crystal Growth, Volume 311, Issue 1, 15 December 2008, Pages 141-146.
17. Reena Ittyachan, P.Sahauaraj, J.Crystal Growth 249 (2003) 557.
18. K. Selvaraju, R. Valluvan, K. Kirubavathi, S. Kumararaman, Opt. Comm. 269 (2007) 230.
19. N.R. Dhumane, S.S. Hussaini, V.V. Nawakhele, M.D. Shirsat, Cryst. Res. Technol. 41 (2006) 897.
20. Rosi Oktiani, Risti Ragadhita, Asep Bayu Dani Nandiyanto Indonesian Journal of Science and technology 4 (1) 2019 97-118.
21. N.Balasundari, P.Selvarajan, S.Lincy Mary Ponmani and D.Jencylin International Journal of Current Research and Review Vol. 04 issue 17 September 2012

Paper-5

Design and Development of low cost Spin Coating system for thin film development

Rohit R. Motkar[1], Nitin. D. Sali[2]
[1] Department of Physics, Ahmednagar College, Ahmednagar
[2]P.V. P. College Pravaranagar

Abstract

A low cost technique is applicable for the creation of a spin coater device using reasonable low cost mechanical constituents and an active source of innovation. A newly designed and advanced spin coater is used for producing thin film. It can be represented having knowledge of branches including physics, mechanics, dynamics (kinematics and kinetics) and electronic science. Spin coater can convert a liquid into a substrate by spreading it uniformly. Generally, spin coater is used in nanotechnology as it authorizes the deposition of smooth and uniform layer of polymer. It is made using a well-designed electric circuit containing DC motor to spin the substrate. In our model the speed is controlled manually by a potentiometer. In this device the speed is increase from 500 rpm up to 7000 rpm. Further, in this work, for fabricating spin coater we have used cheaper mechanical and electronic parts as compare to the commercial spin coater.

Keywords: Spin coater, thin films, Low cost design etc.

Introduction

In the advanced scientific industry, a day of thin film research and technology began to play a major part. The first aim was to meet the demand of the integrated circuit industry for the advancement of thin film technology. But daily demand for high-speed smaller and smaller devices is growing, making advanced materials and latest processing technologies suitable for integration technology needed to produce smaller and smaller higher-speed devices, particularly in new generations of integrated circuits. Small film technology can play a crucial role in achieving that objective, as it can fulfil these specifications. In the last four decades thin films are being industrialized for application purposes. Thin films are extremely significant as a two-dimensional structure in many real-world issues. The costs of their products are very modest, whereas the prices of the corresponding bulky content are strong and work and, in reference with the surface processes, often much better [1]. In case, to build up innovative solutions that are suitable for potential uses, knowledge and determination on the structure, roles and new features of thin films should also be used. Thin film layers range from nanometer

fractions to many micrometers [2]. Thin film deposition primarily consists of three principal techniques such as the deposition of solid, liquid and gas. Chemical deposition of vapor and physical deposition of vapor are methods of gas deposition. These are comparatively costly processes. Pyrolysis spray is another common way of filming. Although there are certain drawbacks, such as uncontrollable surface thickness, uncracked, time to process, etc. Temperature regulation is very important in thin film deposition, but temperature control is very complicated in Pyrolysis mist. Compare yourself with others Spin coating is a quick and easy way to make thin, uniform films. The spin-coating equipment is known as spin-coater or a spinner. In brief, the amount of a solvent is more than needed, then rotates and the rotation speed rises and is rotated constantly at high speed for centrifugal force to expand the fluid. Initially, a bunch of authors [3,4] have clarified this mechanism by many simplifications. Repeatability in the spinning coating is one of the most important considerations. Various techniques for the cultivation of inorganic half-conductors leads an important role in the progress of new technology. Regulation of the film properties is crucial to obtain the efficiency of thin film-based systems.

The process of spin coating is very particular due to the value of comfort, reproducibility, usage of low-cost equipment and quick operating speed. Due to their enormous advantages, they can also be used within many industries: photolithography using polymer photo resistance, dielectric solar gel films, planners for diverse optical applications and microelectronic industries for manufacturing integrated circuits [6]. The prototype built and produced is highly economical than the spin-coating device available on the market. The selling price for the spin coater varies from 50 dollars and 4000 dollars, whereby the. This spinning layer is time-free and can easily be cleaned after any activity.

Construction of spin coating system

Figure.1 and 2 demonstrate the photograph of the fabricated in-house spin coating device with spinning intensity varying from 500 to 7000 rpm and thin films deposited using developed spin coater respectively. The fabricated device is used to coat sample on substrates such as glass, metal and silicon wafers. DC controlled variable power supply is used to adjust the spinning rate of the system using potentiometer which is attached to the output of power supply. The potentiometer output is provided to the DC motor to vary the spinning rate of the motor. The substrate holder is made on the spinning disc that installed on the axle of the DC motor. As the DC motor rotates, the rotating disc often rotates along with the substrate holder. Transparent chuck is made up of plastic foil and is used to enclose the rotating disc to prevent sprinkling of

the experimental solution. A tiny opening on the top of the chuck is to inject a syringe with the solvent to cover on the substrate. The core of the sheet and the chuck align to avoid inhomogeneous coating. The centrifuge power of any solution decreases on the substratum in the centre, decreasing particle size and the even distribution of solution around the substratum.

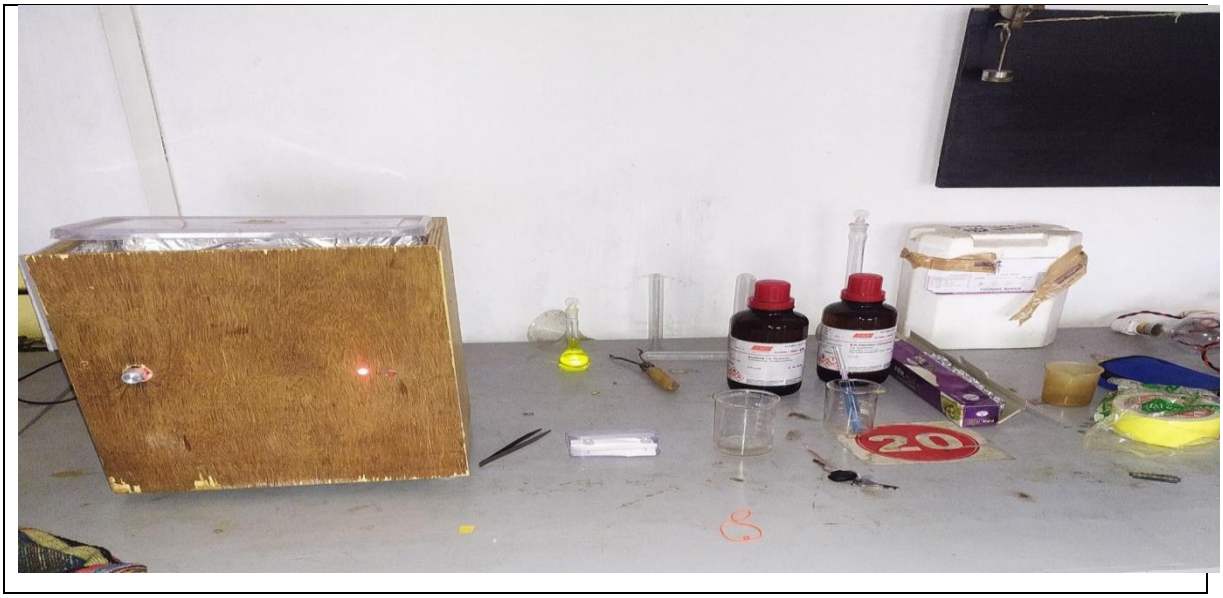

Fig 1: Spin coating machine

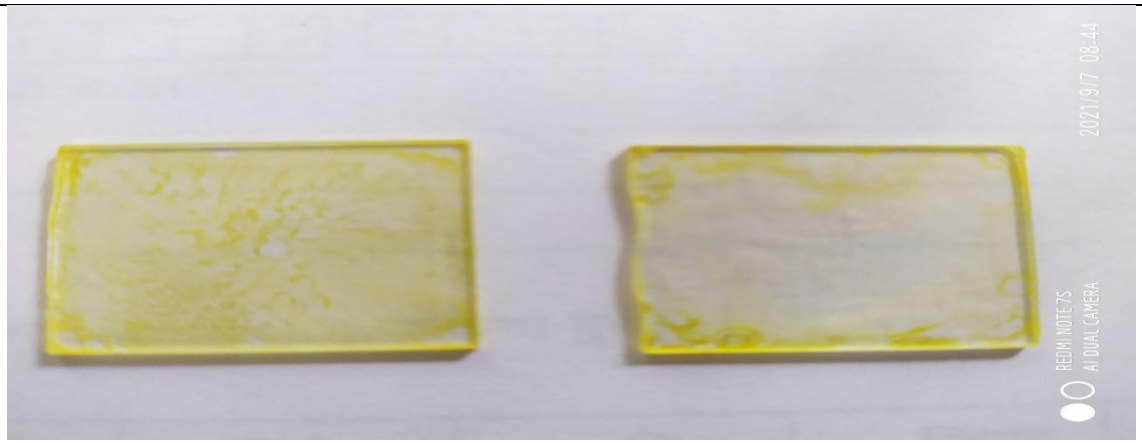

Fig 2: Deposited thin films

Proposed design consists of several components such as DC motor which is used to rotate the substrate. In order to monitor the rotations per minute of system tachometer is installed in design. It will facilitate the measurement of rmp. Which results in thickness control of developed thin layers. Potentiometer is used to control the current as well as voltage given to DC motor. This results in regulation of rpm of DC motor up to desired value. 12V DC Power supply is used to drive DC motor. Spinning disk is used to mount the substrates as shown in figure 3. The spinning disc of the device is made up of plastic sheet with thickness of 4mm and the substrate holder is grooved at the middle of the spinning disc with a lock on the top side.

The substrate of the same size inserts at the groove and the lock is used to take the substrate as forceps. The whole structure is enclosed with cubic chuck to prevent the sample from dust and sprinkling of the solution. The rotating disc is related to the axis of DC motor.

Fig 3: Top view of design

Conclusion

We have designed and developed spin coater successfully. We documented the development of a spin coater being built for utilizing the same, open source, control device. Furthermore, we have demonstrated the possibility to build low cost, high quality research instruments by using readily accessible mechanical parts and open-source tools.

References

[1] Aguilar, R.G., J.O. López, 2011. Low-cost instrumentation for spin-coating deposition of thin films in an undergraduate laboratory. Lat. Am. J. Phys. Educ., 5(2): 369-373.

[2] Smirnov, M., A.P. Rambu, C. Baban, G.I. Rusu, 2010. Electronic Transport Properties in Polycrystalline ZnO Thin Films.Journal of Advanced Research in Physics, 1(2): 021011.

[3] Emslie, Dudley F. Hart, M.D. Edin, J.R. Golding, B.M. Oxon, Denis Burley and M.B. Lond, 1958. Triamcinolone. The Lancet, 272(7045): 495-498.

[4] Meyerhofer, D., 1978. Spin Coating Process. J. Appl. Phys., 49(7): 3993.

[5] Hussein, H.F., G.M. Shabeeb, S. Sh. Hashim, 2011. Preparation ZnO Thin Film by using Sol-gelprocessed and determination of thickness and study optical properties.J. Mater. Environ. Sci., 2(4): 423- 426.

[6] Panigrahi1, S., S. Waugh, S.K. Rout, A.K. Hassan, A.K. Ray, 2004. Study of Spin Coated Organic Thin Film Under Spectrophotometer. Indian Journal of Physics, 78(8): 823-826.

[7] Hu, Y., Y. Xie, M. Qu, L. Wang, H. Xu, 2010. Studying on the Preparation and Characteristics of Al2O3- Based Textured ZnO Thin Films. 2010 Symposium on Photonics and Optoelectronics, 1-4. Doi: 10.1109/SOPO. 2010.5504410.

[8] Znaidi, L., T. Touam, D. Vrel, N. Souded, Yahia, S. Ben, O. Brinza, (n.d.)., 2012. ZnO Thin Films Synthesized by Sol-Gel Process for Photonic Applications, 121: 165-168.

[9] D. B. Hall, P. Underhill, and J. M. Torkelson, Polym. Eng. Sci. 38, 2039 (1998).

[10] J. Puetz and M. Aegerter, in Sol-Gel Technologies for Glass Producers and Users, edited by M. Aegerter and M. Mennig (Springer US, 2004) pp. 37–48.

[11] F.H. Ali ,2020. Building a spin coater device for thin-film preparation .Materials Science and Engineering 757 (2020) 012050 IOP Publishing doi:10.1088/1757-899X/757/1/012050

Paper-6

Electro-optical properties of Cu-doped ZnS thin film used as window layer in solar cell

Arun S Garde and Jitendra A Borse

Department of Physics, S P H Arts, Science and Commerce College Nampur India.

Department of Physics, Late Pushpadevi Patil Arts & Science College Risod., India.

Abstract: The simplified 2-electrode Electrochemical deposition method was carried out to prepare pure and Cu doped ZnS thin films on Fluorine doped tin oxide (FTO) glass and stainless steel substrate using an aqueous solution of 0.1M Zinc sulfate ($ZnSO_4$), 0.1M Sodium thiosulphate ($Na_2S_2O_3$). The 0.1M copper sulfate ($CuSO_4$) was used as a dopant. The Cyclic voltammetry method was used to investigate the deposing potential of Zn, S, and Cu ions. The Cu-doping in ZnS thin film was achieved by adding different amounts of 0.1M CuSO4 solution in the main electrolyte bath. The XRD pattern of all film samples have seen a Zincblende cubic structure. The lattice constant and crystallite size decreases by increasing Cu in ZnS thin film. The Field Emission Scanning electron microscopy (FE-SEM) micrograph images showed some samples are composed of big grains with 135-375 nm dimension embedded in the matrix of nanoflakes. The average thickness of the nanoflakes was found to be 65.37 to 219.50 nm when copper doping was increased by 0-2% and decreased to 219.50-102.78 nm after increasing from 2-3%. The UV-Visible spectroscopy confirmed the energy band gap of Cu-doped ZnS thin film varied from 3.97- 2.11 eV. The electrical resistivity of ZnS thin film decreases with increasing Cu-doping. The hall coefficient values of the film samples showed the all deposited films are n-type electrical conductivity. **Keywords:** Electrochemical deposition**,** Cu-doped ZnS thin film, Optical properties, electrical properties

1. Introduction

Zinc sulfide is an important society II-VI chalcogenide semiconductor material with a wide energy band gap which has application in solar cell, light-emitting diode, and photocatalysis [1]. The band gap of ZnS is about 3.95 eV. The optical band gap of ZnS makes it a potential material to replace CdS in heterojunction of CdS/CdTe solar cell [1]. The zinc sulfide is used as a window layer due to its suitable band gap. It allowed and delivered high- energy photons to absorbing material which improves the short circuit current in a solar cell. ZnS can be deposited by various techniques such as electrochemical deposition [2, 3], chemical bath deposition [4,], Chemical vapor deposition [5],

physical vapor deposition, sputtering [6], atomic layer epitaxy, and SILAR method [7]. ZnS can be an n-type or p-type semiconductor in electrical conduction depending on the composition of Zn and S ions. The electrical conduction is important to the fabrication of solar cells [8]. The electrical conduction can be varied by various dopants [8]. The n-type ZnS as a window layer in ZnS/CdTe solar cell gives 12% efficiency [9]. The n-type or p-type electrical conductivity of ZnS can be achieved by varying the Zn/S ratio or suitable doping. The ZnS thin films with various dopants have been grown by many researchers by using different techniques. ZnS has a refractive index of 2.40. ZnS can be used as a reflector in optics because of its high reflective index [10]. ZnS can be used to manufacturing light-emitting diodes because of its wide energy bandgap [10]. The optical property of chalcogenide semiconductors depends on the size of their nanoparticles due to quantum confinement effect [11]. ZnS has two allotropic structures one is cubic sphalerite and another is wurtzite hexagonal structure [12]. Doping is the one method to tailor the energy bandgap. It influences optical, structural, and electrical properties. The transition metals such as Cu^{2+}, Ag^{2+}, Mn^{2+}, and Pb^{2+} can be dope in ZnS to achieve tunability of energy band gap [13]. It has been investigated by various techniques to reveal the effect of doping on the energy bandgap. The electro-optical properties of n-type ZnS thin films were analyzed by various atomic percentages of Cu-doped in ZnS material [14]. In this paper, the electrical parameters such as resistivity, mobility, hall coefficient, and carrier concentration have been investigated of Cu-doped ZnS thin films.

2. Experimental Details

2.1 Film Preparation

The Pure and Cu-doped ZnS thin film deposition was carried out by using a 2-electrode electrodeposition method consisting of stainless steel/FTO glass as working electrode, high purity graphite as counter electrode immersed in an electrolyte which is made up of pure distilled water. The aqueous electrolyte bath containing 0.1M $ZnSO_4$ (AR grade), 0.1M $Na_2S_2O_3$ (AR grade), and 0.1M $CuSO_4$ (AR Grade) were used as precursors for Zn, S, and Cu ions respectively [15]. 0.1M Triethanolamine was added to the electrolyte as a complexing agent [16]. The main electrolyte bath of 100 ml prepared by a mixed solution of 0.1M $ZnSO_4$ and 0.1M $Na_2S_2O_3$. The adding different amounts such as 1%, 2% and 3% correspond to 1 ml, 2 ml, and 3 ml of 0.1 M $CuSO_4$ as Cu-dopant added in the main electrolyte bath. The stainless steel (316 L) and FTO glass substrates

are used for deposition. The stainless steel substrates were cleaned with double distilled water. The growth of ZnS and Cu was estimated by the cyclic voltammetry technique. **Figure.1** shows a 2-electrode simple electrochemical deposition setup.

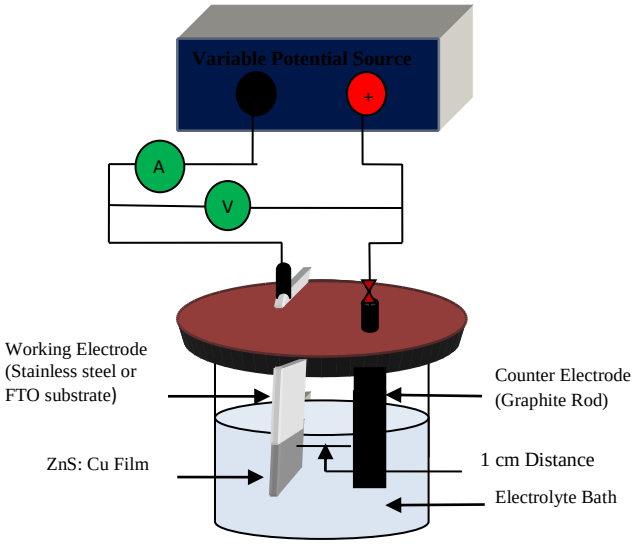

Fig.1. Schematic diagram of 2-electrode electrochemical deposition set up

The material is grown at fixed voltage by the electrochemical deposition method. 0.1M $CuSO_4$ of 1-3% of total electrolyte bath volume was added in the main electrolyte bath to achieve Cu-doping level in ZnS film. The deposition parameters are shown in **Table.1**. The resulting Pure and Cu-doped ZnS thin film samples were investigated by using X-ray diffraction (XRD), Field emission scanning electron microscope (FESEM), UV-visible spectrophotometer, and Hall Effect measuring system by Vander Pauw method for structural, surface morphology, optical properties, and electrical behavior respectively.

Table.1: Parameters of electrodeposition method for preparation of Cu-doped ZnS thin film

Sr. No.	Parameter	Value
1	Total quantity of electrolyte bath	100 ml
2	Bath composition	0.1 M $ZnSO_4$, 0.1 M $Na_2S_2O_3$, 0.1 M $CuSO_4$ & 0.1 M Triethanolamine (TEA)
3	Potential range applied	– 0.45 V to -1.0 V /Ag/AgCl (3-electrode set up) 1720 mv (2-electrode set up)

4	Deposition temperature	27^0C
5	pH	3.5
6	Substrate	Stainless steel, FTO glass

2.2 Film characterization

The X-ray diffraction pattern and identification of phase were obtained by X-ray diffractometer with Cu-Kα excitation wavelength of 1.54056 A^0. The average crystallite size was estimated by using Debye-Scherer's formula [17]. The optical bandgap of Pure and Cu-doped ZnS films were estimated by absorption spectra of films deposited on FTO glass and were measured using Carry 100 UV-Visible spectrophotometer in the range 100-800 nm [18]. The surface morphology of the film was observed using a field emission scanning electron microscope of model JEOL JSM-7600F. The resistivity, mobility, carrier concentration, and hall coefficient of Pure and Cu-doped ZnS thin film have been investigated by the Hall Effect measuring system of Vander Pauw method of ECOPIA model [19].

3. Result and Discussion

3.1 Cyclic Voltammetry

Figure.2 shows cyclic voltammetry of 0.1 M $CuSO_4$ solution. During forwarding scanning of potential, the two anodic peaks are found A1 and A2. The complete oxidation of Cu takes place at two anodic peaks.

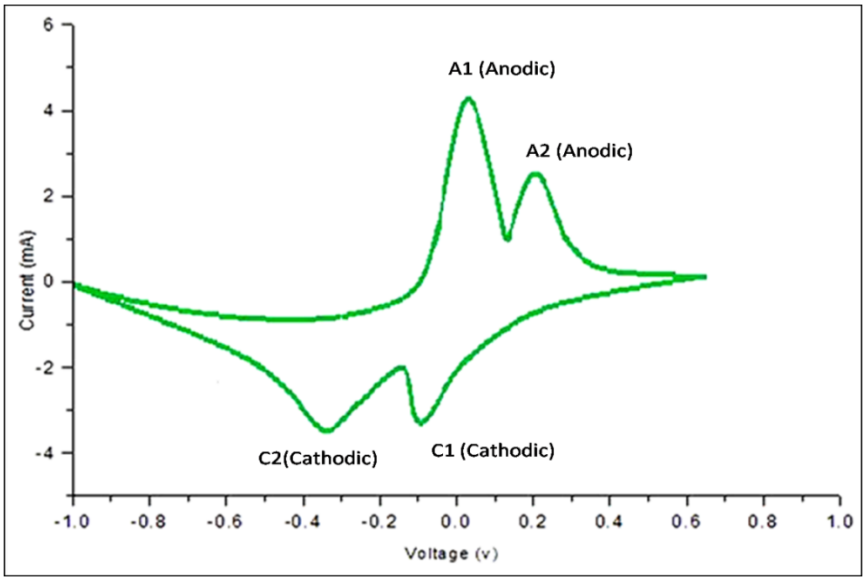

Fig.2. Cyclic Voltammograms of 0.1 M $CuSO_4$ solution

The oxidation reaction corresponds to peak A1 and A2 are given below.

$$A1: Cu \longrightarrow Cu^{1+} + e$$

$$A2: Cu^{1+} \longrightarrow Cu^{2+} + e$$

The anodic potential for oxidation of Cu was found at +0.2 V causes to the dissolution of Cu ion in an electrolyte bath. During reverse scanning, two cathodic potential peaks (C1 and C2) are found at -0.1 V and -0.35 V against Ag/AgCl (Reference Electrode) showed the reduction of copper ions. The reduction reactions correspond to peaks C1 and C2 are given below.

$$C1: Cu^{2+} + e \longrightarrow Cu^{1}$$

$$C2: Cu^{1} + e \longrightarrow Cu$$

The copper deposited at the cathodic potential in the range -0.1 V to -0.4 V against the Reference electrode (Ag/AgCl). The complete oxidation and reduction of copper ions are obtained in two successive steps. Figure.3 shows cyclic voltammetry for 0.1M $ZnSO_4$ and 0.1M $Na_2S_2O_3$ aqueous solution at scan speed 50 mv/sec to deposit ZnS. When the two solutions are mixed, the ZnS film growth voltage is estimated by the cyclic voltammetry technique. It indicates the variation of voltage with a current to estimate the appropriate deposing potential of ZnS thin film. The anodic peak was found in the range +0.5 V-+1.0 V at scan speed 50 mV/sec. The cathodic potential was reached at -0.75 V against Ag/AgCl (Reference Electrode). The appearance of a new reduction peak at -0.45 V due to the presence of Cu in the electrolyte.

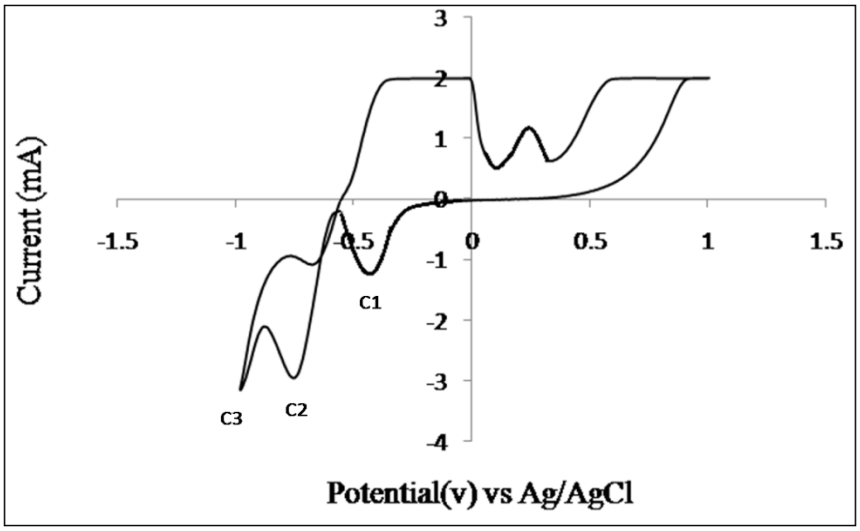

Fig.3. Cyclic Voltammograms of mixed bath of 0.1M $CuSO_4$, 0.1M $ZnSO_4$, and 0.1M $Na_2S_2O_3$ at scan rate 50mV/s.

It has been found that the deposing potential of ZnS with Cu content was observed at -0.75 V to -0.9 V. After investigating the electrochemical behavior of Zn, S, and Cu ions by using the cyclic voltammetry technique the deposition of Cu-doped ZnS thin film was carried out by a simple two-electrode electrodeposition technique. The area 2.25 cm^2 of substrate was selected for deposition of film.

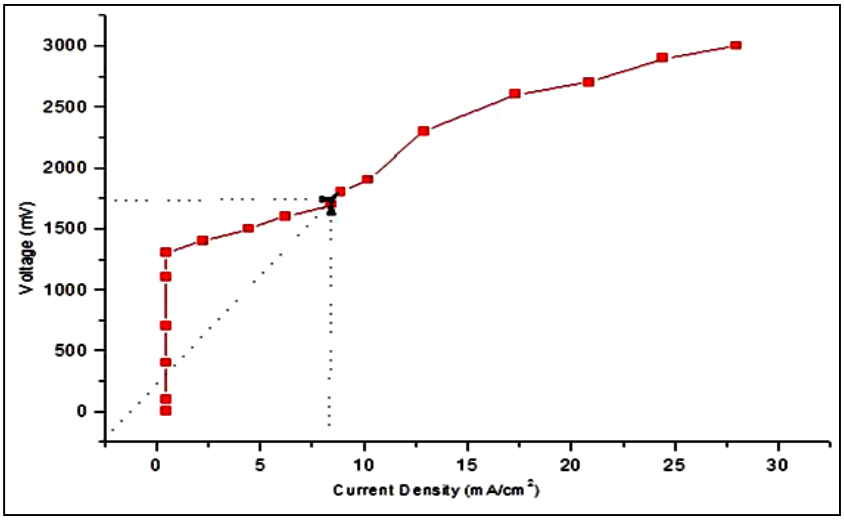

Fig.4. Polarization curve of mixed bath of 0.1M $ZnSO_4$ and 0.1M $Na_2S_2O_3$ for optimizing deposing potential in 2-electrode system

As per **Figure.4**, The potential 1720 mV was optimized corresponding current density 8.40 mA/cm^2 by plotting polarization curve of voltage versus current density for deposition of Cu-doped ZnS thin film in a 2-electrode system. The current density increases with increasing potential. The current density is current per unit deposited area of film.

3.2 Energy dispersive analysis by x-ray spectroscopy (EDAX)

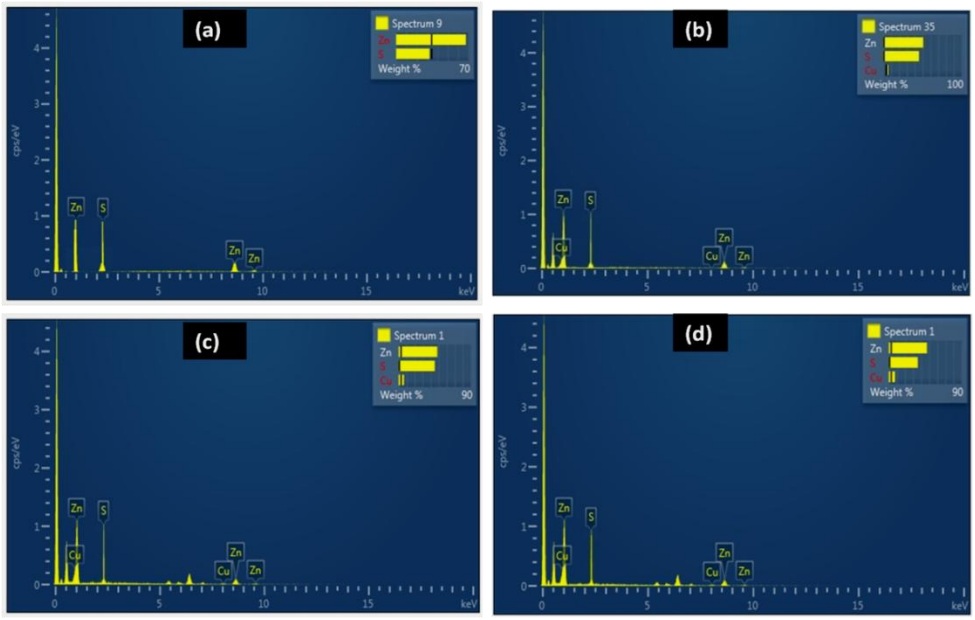

Fig.5. EDS spectrum of a) Pure ZnS b) ZnS: Cu (1%) c) ZnS: Cu (2%) d) ZnS: Cu (3%)

Figure.5 showed EDS spectrum of Un and Cu-doped ZnS thin film samples. As seen from spectrum the Cu- composition in deposited samples of undoped, ZnS: Cu (1%), ZnS: Cu (2%), and ZnS: Cu (3%) were observed about 0 at%, 0.6 at%, 6.32 at %, and 9.86 at% respectively. It has been confirmed the incorporation of increasing Cu ions in ZnS thin film without any impurity. The detailed composition of Zn, S, and Cu are listed in Table.2.

Table.2: Elemental composition of as prepared thin films samples

Samples	Zn (at %)	S (at %)	Cu (at %)	Total
a) Undoped ZnS	50.51	49.49	0	100
b) ZnS: Cu (1%)	50.00	49.40	0.60	100
c) ZnS: Cu (2%)	50.10	43.58	6.32	100
d) ZnS: Cu (3%)	50.14	40.00	9.86	100

3.3 X-ray Diffraction Analysis

Figure.6 shows the XRD pattern of Pure and Cu-doped ZnS thin films. After the XRD pattern is analyzed the peaks are observed at the orientation of plane (200), (220), (311), (222) and (400) are matched to the standard database (JCPDS data No.05-0566). It was confirmed the deposited ZnS film exhibit a Zincblende cubic structure without the founding secondary phase of CuS.

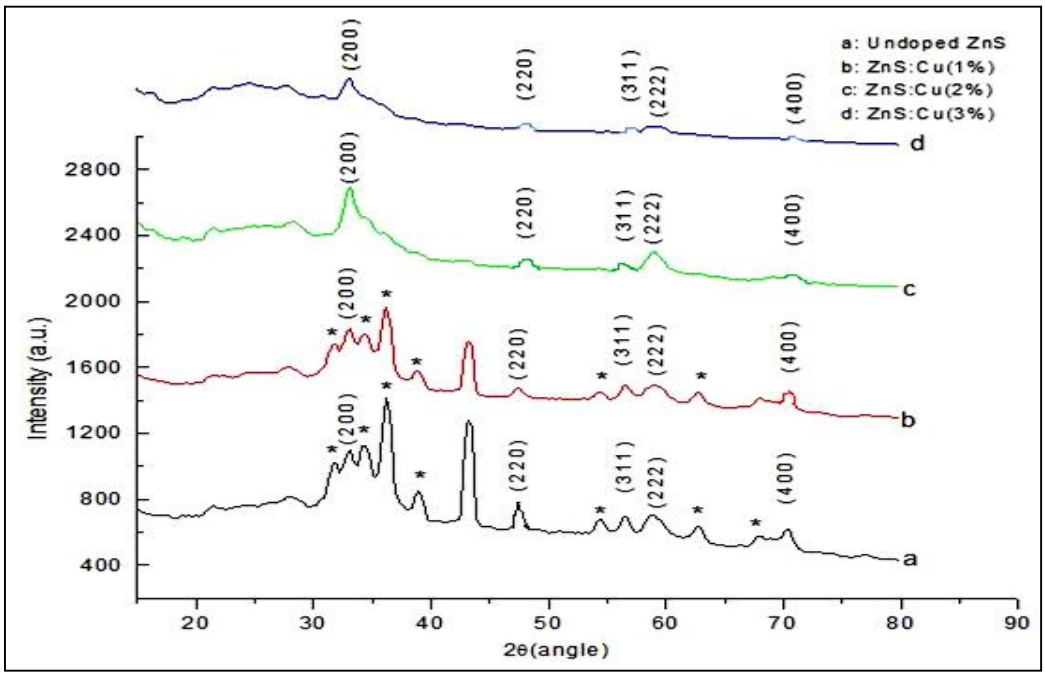

Fig. 6. XRD pattern of (a) Pure ZnS thin film (b) ZnS: Cu (1%) (c) ZnS: Cu (2%) (d) ZnS: Cu (3%)

The peaks denoted by * are matched to the standard database (JCPDS data No.33-0397) of stainless steel. It is confirmed * peaks indicate stainless steel substrate. As per the XRD pattern sample a of Pure ZnS exhibits high crystallinity than other Cu-doped ZnS samples [20, 21]. The intensity of peaks reduced with the incorporation of Cu ions in ZnS [22]. This is due to electronic density or point defect in lattice position and change in scattering factor. The crystallite size Pure and Cu-doped ZnS samples were estimated by using the Debye-Scherrer equation

$$D=\frac{0.9\lambda}{\beta cos\theta} \qquad (1)$$

Where 'D' is the crystallite size, λ=1.5405 Å, 'β' is the full width at half maximum and 'θ' is the angle of diffraction. The crystallite size of Pure ZnS, ZnS: Cu (1%), ZnS: Cu (2%), and ZnS: Cu (3%) thin films for a plane (200) were estimated by using equation (1) about 34.46 nm, 24.41 nm, 20.72 nm, and 18.02 nm respectively. Consequently the crystallite size decreases and peak

broadening and increases dislocation density and microstrain [23, 24]. The lattice constant was also affected by Cu-doping in ZnS and it was estimated by using the following equation.

$$a = d\sqrt{h^2 + k^2 + l^2} \qquad (2)$$

Where d is interplanar spacing and (h k l) is the diffraction plane. The lattice constant for undoped ZnS thin film was found 5.452 A^0. Therefore, the lattice constant of ZnS: Cu (1%), ZnS: Cu (2%) and ZnS: Cu (3%) was found about 5.443 Å, 5.433 Å, and 5.424 Å respectively. The lattice constant is found to decreases with increasing Cu-doping in ZnS due to increasing microstrain and dislocation density upon Cu-doping. This is due to the ionic radius of Cu is less than Zn. So Cu ions are incorporated in the interstitial site of Zn. Hence lattice constant is affected by the ionic radius of the dopant. The dislocation density (δ) of deposited films was estimated by using the Williamson Smallman equation given below.

$$\delta = \frac{1}{D^2} \qquad (3)$$

Where D is crystallite size. It is observed that the dislocation density increased by increasing Cu-doping in ZnS thin film. Subsequently, crystallite size decreases. The microstrain (ϵ) was estimated by using the following equation.

$$\epsilon = \frac{\beta}{4\tan\theta} \qquad (4)$$

Where, β is full width at half maximum, the peak broadening with increasing Cu-doping. The broad peak indicates the lower intensity and large FWHM. The crystallite size is decreased by increasing Cu-doping this is due to lattice distortion or microstrain. Consequently, the sample ZnS: Cu (3%) shows a large lattice plane as compared to other samples. As per table.3 the microstrain is increased with increasing Cu-doping in ZnS nanostructure. The dislocation density and microstrain are observed maximum value in 3% Copper doped ZnS. The estimated values are listed in Table.3.

Table.3: Shows estimated values of average crystallite size, dislocation density and microstrain of a) undoped ZnS thin film b) ZnS:Cu (1%), c) ZnS:Cu (2%) and d) ZnS:Cu (3%) thin films.

Thin film Samples	2θ for plane (200)	FWHM	d-spacing	Lattice constant a(A^0)	Average Crystallite Size (nm)	Dislocation density(δ)x 10^{-3}(nm^{-2})	Microstrain (ϵ)x10^{-3}
Undoped ZnS	32.823	0.251	2.7264	5.452	34.46	0.8421	211.35
ZnS: Cu (1%)	32.883	0.357	2.7216	5.443	24.41	1.6782	276.40
ZnS: Cu (2%)	32.942	0.428	2.7168	5.433	20.72	2.3292	282.47
ZnS: Cu (3%)	33.02	0.501	2.7120	5.424	18.02	3.0795	290.87

3.4 UV-Visible Spectroscopy Analysis:

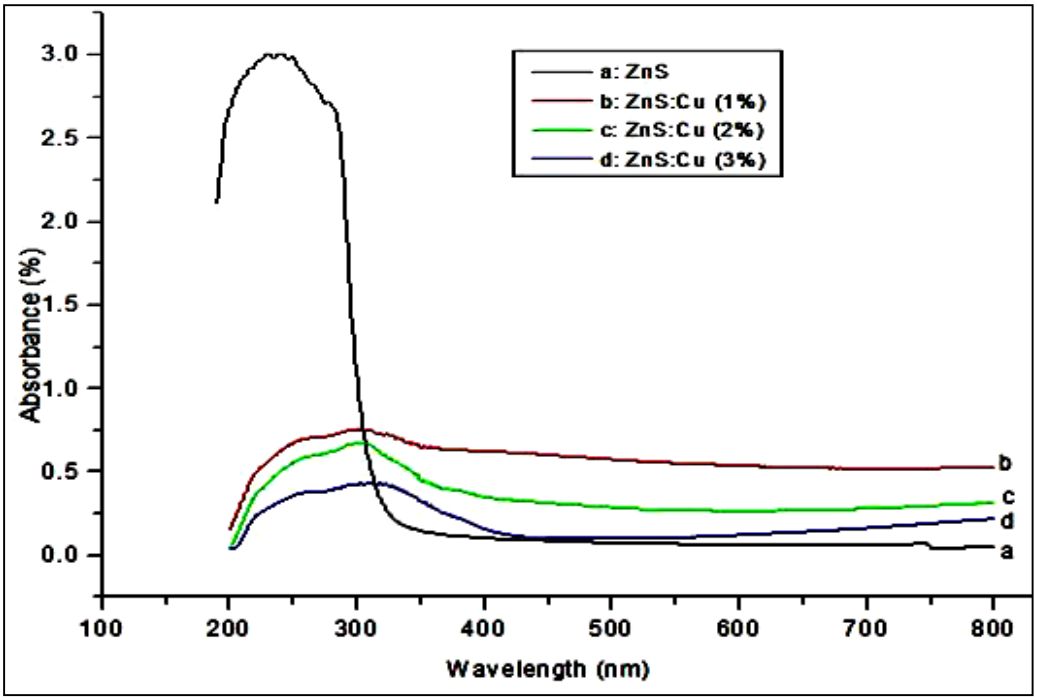

Fig.7. Optical Absorbance spectra of a) Pure ZnS b) ZnS: Cu (1%) c) ZnS: Cu (2%) d) ZnS: Cu (3%)

Figure.7 shows the UV-Visible absorption spectra of Pure and Cu-doped ZnS film thin films. The optical properties of films were investigated by a UV-Visible spectrophotometer with a wavelength range of 200-800 nm [25]. According to absorption spectra, the absorption edges are shifted to a higher wavelength 319 -412 nm with enhancing Cu-doping from 1-3% in ZnS thin film. This is a fundamental absorption edge. As a result, absorption increases with increasing Cu-doping percentage in ZnS. The energy band gap of Pure and Cu-doped ZnS thin film was estimated by tauc plotting of $(\alpha h\nu)^2$ versus hν by using the below equation.

$$\alpha h\nu = (h\nu - Eg)^n \qquad (5)$$

Where α is absorption coefficient, h is Planck's constant, ν is photon energy, E_g is optical bandgap and n is equal to ½ for direct band gap material. n is equal to 2 for allowed indirect, n is equal to 3/2 for non-radiative direct, n is equal to 3 for non-radiative indirect.

From **Figure 8**, the bandgap can be determined by the intercept of straight-line portion of $(\alpha h\nu)^2$ versus hν on hν axis [26]. It is observed that the energy band gap of Pure ZnS, ZnS: Cu (1%), ZnS: Cu (2%) and ZnS: Cu (3%) was found 3.97 eV, 3.07eV, 2.45eV, and 2.11 eV respectively. The estimated energy band gaps are listed in Table.4. As per Table.4 the bandgap energy decreases upon increasing Cu-doping due to increases in the specific surface area of ZnS nanostructure.

Table.4: Illustrate the estimated energy band gap values of Pure ZnS and Cu-doped ZnS thin films

Thin film Samples	Zn (at %)	S (at %)	Cu (at %)	Film thickness (nm)	Band gap energy (eV)
Undoped ZnS	50.51	49.49	0	954	3.97
ZnS: Cu (1%)	50.00	49.40	0.60	961	3.07
ZnS: Cu (2%)	50.10	43.58	6.32	960	2.45
ZnS: Cu (3%)	50.14	40.00	9.86	963	2.11

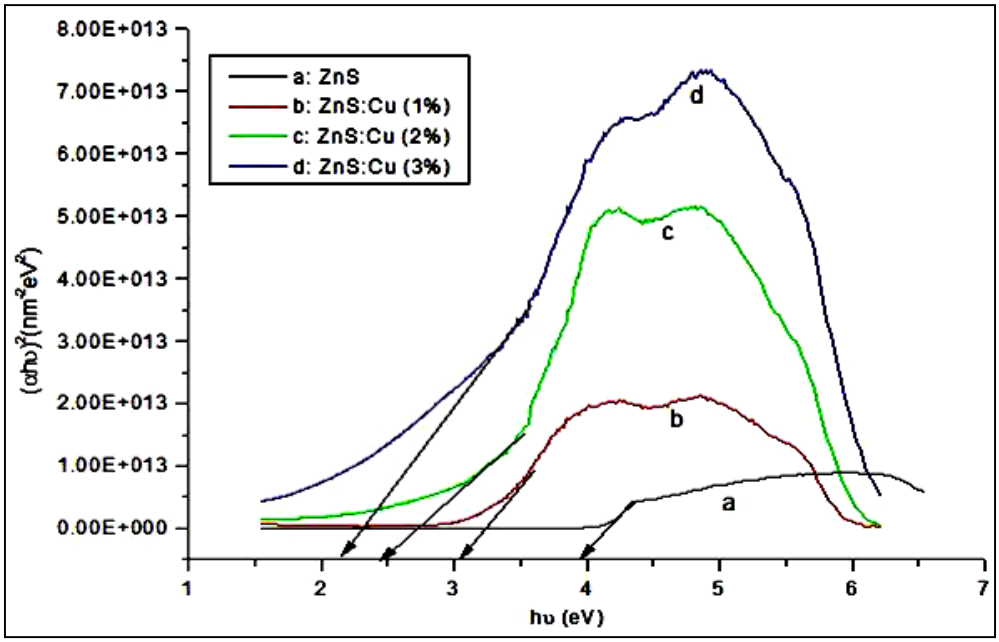

Fig.8. Energy Band Gap of a) Pure ZnS b) ZnS: Cu (1%) c) ZnS: Cu (2%) d) ZnS: Cu (3%)

Figure 8 shows the refractive index of Pure and Cu-doped ZnS thin film. The refractive index of Pure and Cu-doped ZnS thin films was estimated by using the following equation

$$n = \frac{1}{TS} + \sqrt{\frac{1}{Ts-1}} \qquad (6)$$

Where n is the refractive index, Ts is percent transmittance. The percent transmittance (Ts) was determined by using the following equation

$$Ts = 10^{(-A)}X100 \qquad (7)$$

Where A is the absorbance

From **Figure 9,** It has been observed that for all Pure and Cu-doped ZnS thin film samples, the refractive index (n) reduced with increasing wavelength. The Pure ZnS thin film has a high refractive index in the visible region. But the effects of Cu-doping the ZnS thin film are allowed to pass light of longer wavelength. The thin film samples Pure ZnS, ZnS: Cu (1%), ZnS: Cu (2%), and ZnS: Cu (3%) have greater transparency due to low refractive index for the wavelength 326 nm, 627 nm,718 nm, and 456 nm respectively. The thin film of ZnS: Cu (2%) has the highest transparency due to the low refractive index to wavelength 718 nm in the visible region. This allows employing this film layer as an optical window or buffer layer in the solar cell.

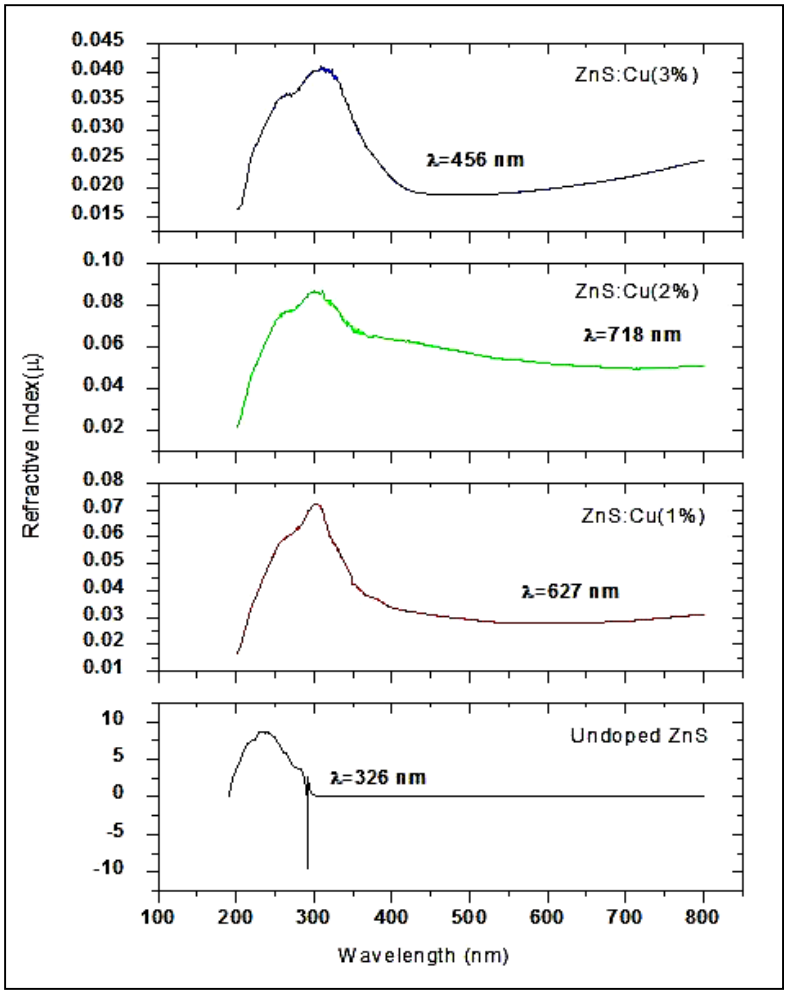

Fig.9. Illustrate the refractive index of Pure and Cu-doped ZnS thin film

3.5 Scanning Electron Microscopy (SEM) Analysis

Figure 10 illustrates the scanning electron micrograph (SEM) of ZnS films samples a, b, c, and d with different percentages of Cu content in ZnS thin films. As per FESEM micrograph images, all thin-film samples exhibit the same morphology. They showed some big grains with 135 to 375 nm dimensions composed in the matrix of nanoflakes of ZnS: Cu (2%) and ZnS: Cu (3%) thin films respectively. The average thickness of nanoflakes of sample Pure ZnS, ZnS: Cu (1%), ZnS: Cu (2%), and ZnS: Cu (3%) were observed about 65.37 nm, 88.74 nm, 219.50 nm, and 102.78 respectively. The sample 3% Copper doped ZnS shows hexagonal grain morphology. It is confirmed that the stress effect of Cu-doping on ZnS nanostructure [27].

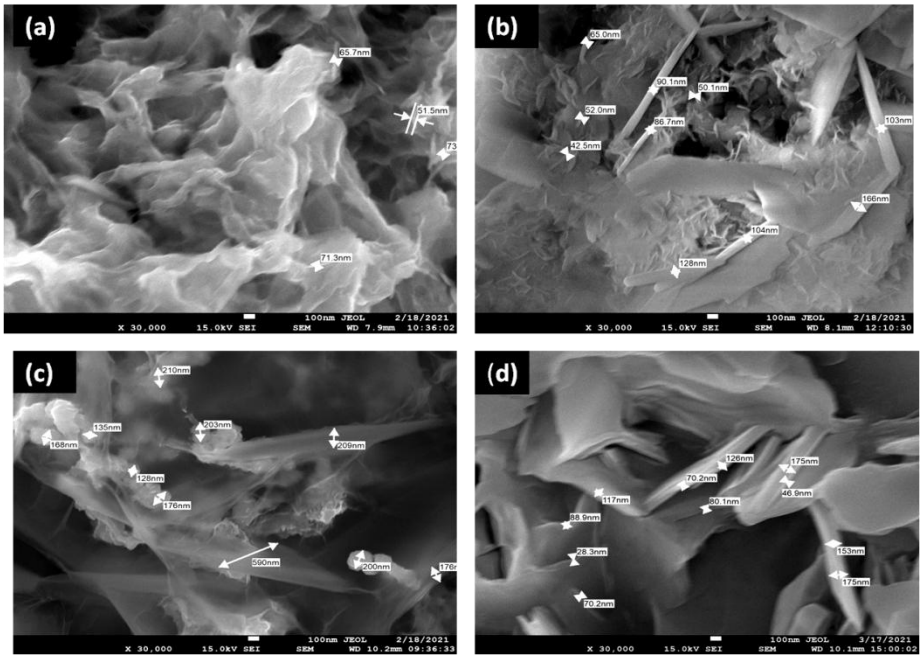

Fig.10 FESEM micrograph images of a) Pure ZnS thin film b) ZnS: Cu (1%) c) ZnS: Cu (2%) d) ZnS: Cu (3%)

3.6 Electrical properties by four probes Van Der Pauw method

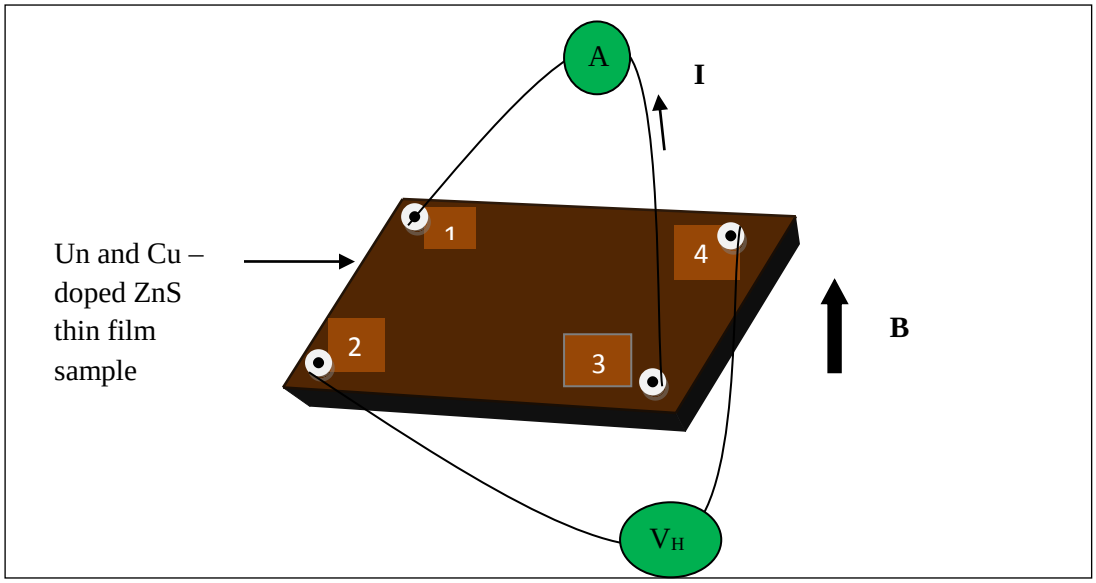

Fig.11 Schematic diagram of Vander Pauw method measuring system

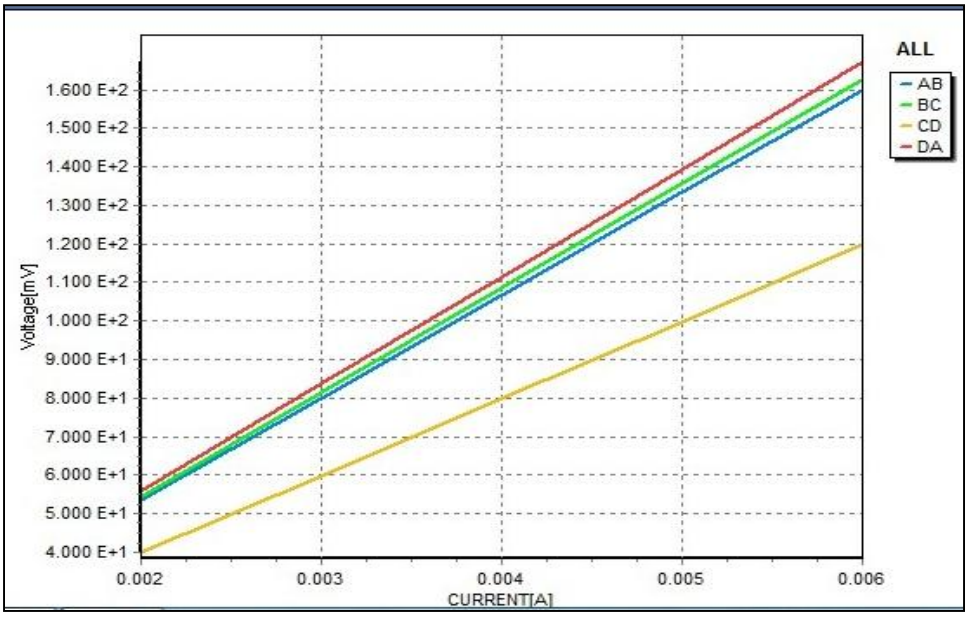

Fig.12 (a) Current- Voltage sweep of standard FTO glass by Vander pauw method

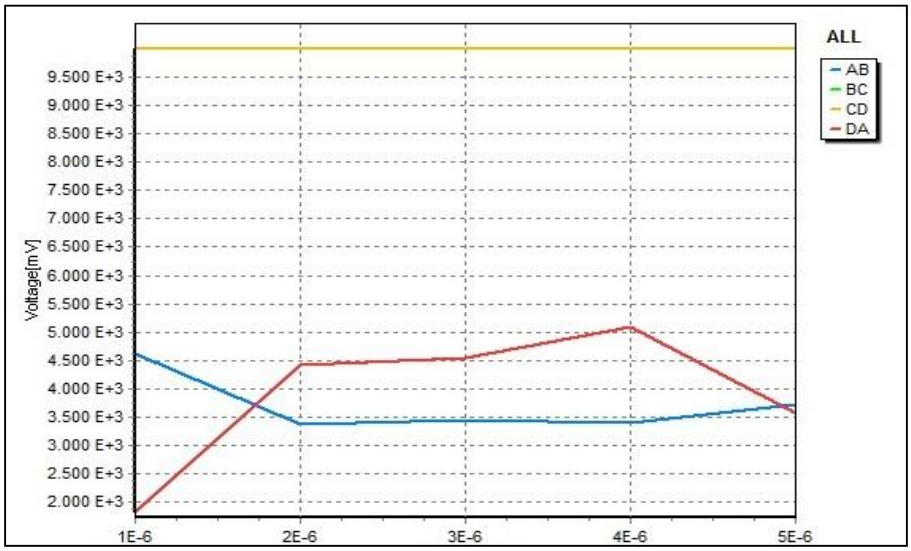

Fig.12 (b) Current-Voltage sweep of ZnS thin film on FTO glass by vander pauw method

The electrical properties such as resistivity, conductivity, mobility, hall coefficient, and carrier concentration of deposited films are directly estimated by the Hall Effect measuring system by the Vander Pauw method [28]. **Figure 11** shows the four-probe Vander Pauw method.

Fig.12 (c) Current-Voltage sweep of ZnS: Cu (1%) thin film on FTO glass by vander pauw method

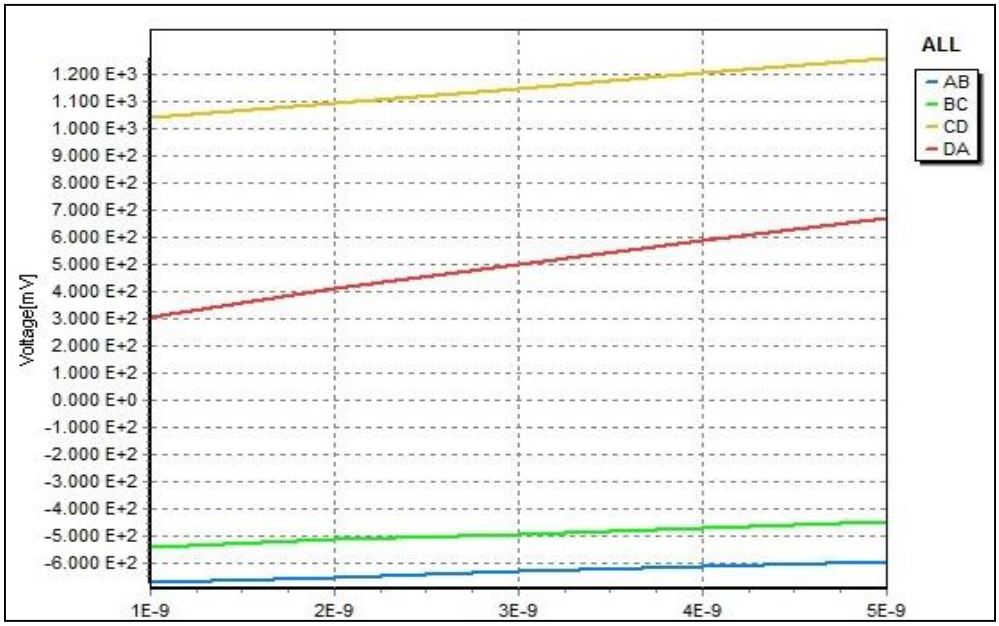

Fig.12 (d) Current-Voltage sweep of ZnS: Cu (2%) thin film on FTO glass by vander pauw method

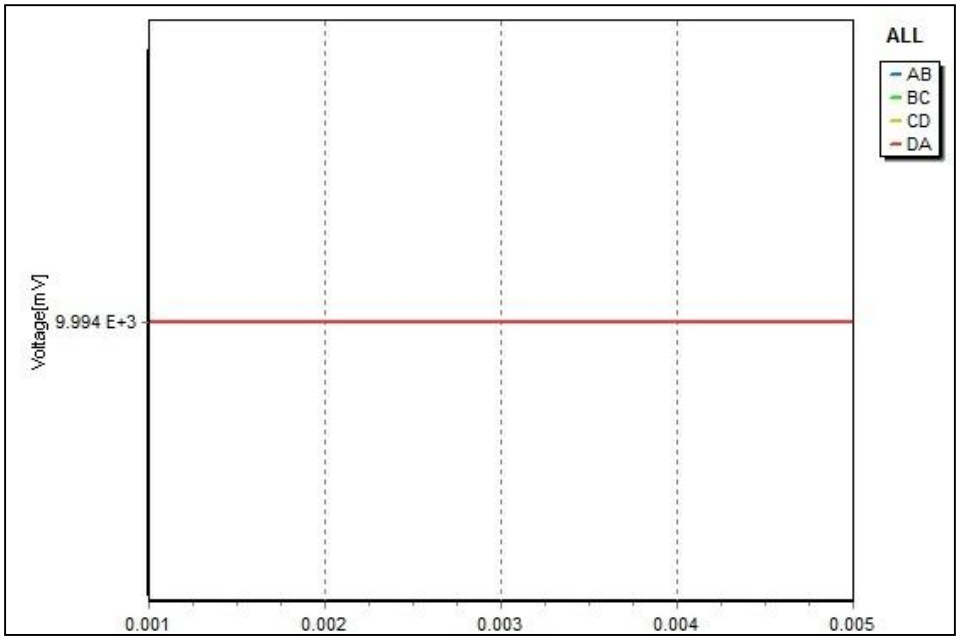

Fig.12(e) Current-Voltage sweep of ZnS: Cu (3%) thin film on FTO glass by vander pauw method

From **Figure 12** (a), (b), (c), (d), and (e) the resistivity of Pure ZnS, ZnS: Cu(1%), ZnS: Cu(2%), and ZnS: Cu(3%) film samples were observed about 1.782 x 10^6 Ω/cm, 1.081x10^6 Ω/cm, 2.789x10^4 Ω/cm and 2.235x10^3 Ω/cm respectively. The resistivity of films reduced in the range of 10^6 -10^3 Ω/cm with enhancing Cu-doping in ZnS thin film [29]. This is due to the concentration of electrons increases. The Cu ions can be incorporated on Zn sites acts as acceptor impurity and on interstitial sites acts as a donor impurity. Here is confirmed the Cu ions incorporated on interstitial sites. So the concentration of electrons increases. The carrier concentration of films Undoped ZnS and ZnS: Cu (1%), ZnS: Cu (2%) and ZnS: Cu (3%) were estimated about -1.7815x10^{11} /cm^3, -2.5867x10^{11} /cm^3, -1.6412x10^{12} /cm^3 and -2.9519x10^{12}/cm^3 respectively. The carrier concentration was observed highest value at Cu (3%) in ZnS due to ZnS play donor type impurity. The mobility of Pure ZnS and ZnS: Cu (1%), ZnS: Cu (2%) and ZnS: Cu (3%) were observed about 0.1234x10^2 cm^2/vs, 2.6843x10^2 cm^2/vs, 6.2178x10^3 cm^2/vs and 9.4612x10^3 cm^2/vs respectively. The mobility was also found highest at Cu (3%) in ZnS due to low resistivity and high electron concentration. The average hall coefficient of deposited thin film samples was found -2.0785x$10^6$$cm^3$/c. It is confirmed the negative value indicates the film exhibit n-type electrical conductivity. The electrical and optical parameters are listed in Table.5

Table.5: Electro-optical properties of Un and Cu-doped ZnS thin films

Electro-Optical Properties	Undoped ZnS	ZnS: Cu (1%)	ZnS: Cu (2%)	ZnS: Cu (3%)
Resistivity(Ω/cm)	*1.782x10^6*	1.081x10^6	2.789x10^4	2.235x10^3
Carrier concentration(/cm^3)	-1.781x10^{11}	-7.586x10^{11}	-1.641x10^{12}	-2.951x10^{13}
Mobility(cm^2/vs)	0.1234x10^2	2.6843x10^2	6.2178x10^3	9.4612x10^3
Hall coefficient(cm^3/c)	-1.5362x10^6	-1.6812x10^6	- 2.1146x10^6	-2.9821x10^6
Energy band gap(eV)	3.97	3.07	2.45	2.11

4. Conclusion:

The Pure and Cu-doped ZnS thin film successfully deposited on stainless steel and FTO substrates by simplified 2-electrode electrodeposition method. The electrochemical behavior of Zn, S, and Cu was investigated by the cyclic voltammetry technique for good deposition carried out by the 2-electrode method. The XRD pattern of doped film samples have seen a Zincblende cubic structure. The lattice constant of ZnS thin films decreases in the range 5.452- 5.424 A^0 by increasing Cu-doping in ZnS due to lattice microstrain and Cu ions incorporated in the interstitial site of Zn. The crystallite size of ZnS thin films decreases with increasing copper (range 34.46- 18.02 nm). Also peak intensity of ZnS thin films have been seen reduced. The XRD pattern of 3% Copper doped ZnS film showed maximum value of dislocation density and microstrain of films. SEM micrograph showed the hexagonal grain morphology in 3% copper doped ZnS film sample. The energy band gap was decreased by enhancing Copper in ZnS thin film. 2% copper doped ZnS film sample showed the highest transparency due to a low refractive index up to wavelength 718 nm. They can be used as a window layer or buffer layer in the modified solar cell. The electrical resistivity of copper doped ZnS film samples varied in the range 1.782 x 10^6 to 2.235x10^{3}Ω/cm. The highest carrier concentration and mobility were found at about -2.951x10^{13}/cm^3, 9.4612 x 10^{3}cm^2/Vs respectively in samples of 3% copper doped ZnS. The average value of hall coefficient of all deposited films was found to -2.0785 x 10^{6}cm^3/c. From this, 2% copper doped ZnS thin film sample may be used as a window or buffer layer in a thin-film heterojunction solar cell device.

Acknowledgment:

The authors are thankful to the Research Center in Physics, Mahatma Gandhi Vidyamandir's Panchavati Nashik for conducting research work. Also thankful to SAIF- IIT Bombay, SAIF-IIT Kanpur, and CIF Chandigarh University Punjab for sample characterization.

Compliance with ethical standards:

Conflict of interest Authors declares no conflict of interest.

References:

[1] Alireza Goudarzi, Ghaffar Motedayen Aval, Reza Sahraei, Hiva Ahmadpoor, Ammonia-free chemical bath deposition of nanocrystalline ZnS thin film buffer layer for solar cells, Thin Solid Films. 2008, 516, P-4953-4957. https://doi.org/10.1016/j.tsf.2007.09.051

[2] Naglaa Fathy, Masaya Ichimura, Photoelectrical properties of ZnS thin films deposited from aqueous solution using pulsed electrochemical deposition, Solar Energy Materials and Solar Cells, 2005,87, P-747-756. https://doi.org/10.1016/j.solmat.2004.07.048

[3] H.M.M.N. Hennayaka, Ho Seong Lee, Structural and optical properties of ZnS thin film grown by pulsed electrodeposition, Thin Solid Films, 2013, 548, P-86-90. https://doi.org/10.1016/j.tsf.2013.09.011

[4] Poulomi Roy, Jyoti R.Ota, Suneel Kumar Srivastava, Crystalline ZnS thin films by chemical bath deposition method and its characterization, Thin Solid Films, 2006, 515, P- 1912-1917. https://doi.org/10.1016/j.tsf.2006.07.035

[5] J.Wang,T.Li, Q.Wang,W.Wang, R.Shi, N.Wang, A.Amini, C.Cheng, Controlled growth of atomically thin transition metal dichalcogenides via chemical vapor deposition method, Material todays advances, 2020, 8, P-100098. https://doi.org/10.1016/j.mtadv.2020.100098

[6] J.M.Blackmore, A.G.Cullis, The structure of ZnS thin films deposited by r.f. sputtering, Thin Solid Films, 1991, 199, P-321-334 https://doi.org/10.1016/0040-6090(91)90014-O

[7] EdwinJose, M.C.Santhosh Kumar, Room temperature deposition of highly crystalline Cu-Zn-S thin films for solar cell applications using SILAR method, Journal of Alloys and Compounds, 2017, 712, P-649-656. https://doi.org/10.1016/j.jallcom.2017.04.097

[8] Tayfur Kucukomeroglu, Emin Bacaksiz, CabirTerzioglu, AhmetVarilci, Influence of fluorine doping on structural, electrical and optical properties of spray pyrolysis ZnS films, Thin Solid Films, 2008,516, P-2913-2916 https://doi.org/10.1016/j.tsf.2007.05.075

[9] G Contreras-Puente, OVigil, MOrtega-López, AMorales-Acevedo, JVidal, M.LAlbor-Aguilera, New window materials used as heterojunction partners on CdTe solar cells, Thin Solid Films, 2000, 361–362, P- 378-382. https://doi.org/10.1016/S0040-6090(99)00806-8

[10]Hyun JooLee, Soo IlLee, Deposition and optical properties of nanocrystalline ZnS thin films by a chemical method, Current Applied Physics, 2007, 7, P-193-197. https://doi.org/10.1016/j.cap.2006.03.005

[11] S.KMandal, SChaudhuri, A.K Pal, Optical properties of nanocrystalline ZnS films prepared by high pressure magnetron sputtering, Thin Solid Films, 1999, 350, P-209-213 https://doi.org/10.1016/S0040-6090(99)00236-9

[12] Z.Z.Zhang, D.Z.Shen, J.Y.Zhang, C.X.Shan, Y.M.Lu, Y.C.Liu, B.H.Li, D.X.Zhao, B.Yao, X.W.Fan, The growth of single cubic phase ZnS thin films on silica glass by plasma-assisted metalorganic chemical vapor deposition, Thin Solid Films. 2006, 513, P-114-117. https://doi.org/10.1016/j.tsf.2006.01.054

[13] Sema Ebrahimi, Benyamin Yarmand, Nima Naderi, Enhanced Optoelectrical properties of Mn-doped ZnS films deposited by spray pyrolysis for ultraviolet detection applications, Thin Solid Films. 2019, 676, P-31-41. https://doi.org/10.1016/j.tsf.2019.02.046

[14] T.Vdovenkova, A.Vdovenkov, R.Tornqvist, ZnS wide band gap semiconductor thin film electronic structure sensitivity to Mn impurity, Thin Solid Films.1999,343–344, P-332-334. https://doi.org/10.1016/S0040-6090(98)01596-X

[15] M.A.Hernández-Fenollosa, M.C.López, V.Donderis, M.González, B.Marí, J.R.Ramos-Barrado, Role of precursors on morphology and optical properties of ZnS thin films prepared by chemical spray pyrolysis, Thin Solid Films. 2008, 516, P-1622-1625. https://doi.org/10.1016/j.tsf.2007.05.031

[16]JunLiuAixiangWei, YuZhao, Effect of different complexing agents on the properties of chemical-bath-deposited ZnS thin films, Journal of Alloys and Compounds. 2014, 588, P- 228-234. https://doi.org/10.1016/j.jallcom.2013.11.042

[17] M.Shobana, S.R.Meher, Effect of cobalt doping on the structural, optical and magnetic properties of sol-gel derived ZnS nanocrystalline thin films and ab initio studies, Thin solid films. 2019, 683, P- 97-110. https://doi.org/10.1016/j.tsf.2019.05.037

[18] X.D.Gao, X.M.Li, W.D.Yu, Morphology and optical properties of amorphous ZnS films deposited by ultrasonic-assisted successive ionic layer adsorption and reaction method, Thin Solid Films. 2004, 468, P-43-47. https://doi.org/10.1016/j.tsf.2004.04.005

[19] Evren Turan, Muhsin Zor, A. Senol Aybek, Metin Kul, Electrical properties of ZnO/Au/ZnS/Au films deposited by ultrasonic spray pyrolysis, Thin Solid Films. 2007, 515, P-8752-8755. https://doi.org/10.1016/j.tsf.2007.04.001

[20] Taisuke Iwashita, Shizutoshi Ando, Preparation and characterization of ZnS thin films by the chemical bath deposition method, Thin Solid Films. 2012, 520, P-7076-7082 https://doi.org/10.1016/j.tsf.2012.07.129

[21] T.Kryshtab, V.S.Khomchenko, J.A.Andraca-Adame, L.V.Zavyalova, N.N.Roshchina, V.E.Rodionov, V.B.Khachatryan, Preparation and properties of thin ZnS:Cu films phosphors, Thin Solid Films.2006, 515, P-513-516. https://doi.org/10.1016/j.tsf.2005.12.284

[22] V.S.Ganesha Krishna, M.G.Mahesha, Characterization of transparent p-type Cu:ZnS thin films grown by spray pyrolysis technique, Journal of Alloys and Compounds.2020, 848, P-156568. https://doi.org/10.1016/j.jallcom.2020.156568

[23] M.E Rincón, M.W Martínez, M Miranda-Hernández, Nano structured vs. polycrystalline CdS/ZnS thin films for photocatalytic applications ,Thin Solid Films. 2003, 425, P-127-134. https://doi.org/10.1016/S0040-6090(02)01301-9

[24] H.H.Afifi , S.A.Mahmoud, A.A shour, Structural study of ZnS thin films prepared by spray pyrolysis, Thin Solid Films. 1995, 263, P-248-251. https://doi.org/10.1016/0040-6090(95)06565-2

[25] G.Leftheriotis, P.Yianoulis, D.Patrikios, Deposition and optical properties of optimized ZnS/Ag/ZnS thin films for energy saving applications, Thin Solid Films. 1997, 306, P-92-99. https://doi.org/10.1016/S0040-6090(97)00250-2

[26]J.Díaz-Reyes, R.S.Castillo-Ojeda, R.Sánchez-Espíndola, M.Galván-Arellano, O.Zaca-Morán, Structural and optical characterization of wurtzite type ZnS, Current Applied Physics. (2015),15, P-103-109. https://doi.org/10.1016/j.cap.2014.11.012

[27] Mingyue Sun,JunchengLiu, BeipingDong, Effects of Sb doping on the structure and properties of SnO_2 films, Current Applied Physics. 2020, 20, P-462-469. https://doi.org/10.1016/j.cap.2020.01.009

[28] K.Nagamani,N.Revathi, P.Prathap, Y.Lingappa, K.T. Ramakrishna Reddy, Al-doped ZnS layers synthesized by solution growth method, Current Applied Physics. 2012, 12, P-380-384. https://doi.org/10.1016/j.cap.2011.07.031

[29] John L.Davis Bland B.Houston, Antonio Martinez, Preparation and properties of epitaxial films of indium-doped lead tin telluride, Thin Solid Films. 1984, 122, P-217-229. https://doi.org/10.1016/0040-6090(84)90049-X

Paper-7

Interpretation of Viscometric, Thermodynamic and Acoustic properties of sodium fluoride in aqueous solutions of Dextrose at different molarities and temperatures.

[1]Raghunath K.Sonawane, [1]Kailas. H. Kapadnis, [2]Arun B. Nikumbh, [3]Vishnu A. Adole and [1]Kailaspati K.Jadhav

[1]Research centre in Chemistry, M.G. Vidyamandir's L.V.H. College Nashik-,

[2]A. A. College, Manchar (Pune), Maharashtra, India.

[3]Arts Commerce and Science College Manmad

Affiliated to S. P. Pune University, Pune

Abstract:-In the present work interpretations of viscosity, density and ultrasonic velocity of sodium fluoride in aqueous solutions of Dextrose at different molarities and temperatures are summarised. The nature and magnitudes of solute- solute and solute- solvent have been taken into account byreporting the data of apparent molar volume (ϕ_v),slope (S_v)and coefficientsof Jones-Dole and modified Jones-Dole equation, adiabatic compressibility(β_{ad}),limiting apparent molarcompressibility (ϕ^0_k), apparent molar compressibility (ϕ_k), specific acoustic impedance(Z), relative association (RA). The plots also support the interpreted results.

Key words:-Solute-solute, solute-solvent interactions, alkyl halide solution, dextrose, Jones-Dole equation.

Introduction:-The physico-chemical behavior between non-ionic solutes and ionic solvent is clearly disclosed by interactive forces between them [1].Being a multidimensional use of carbohydrates, its study becomes a point of immense interest in various fields like foods, pharmaceutical and chemical industries [2-4]. Fluoride has been playing a significant role in improvement of oral and dental health during the past five decades. Our knowledge of dental caries and its mechanism, and the role of fluoride in this process have evolved during recent years. The use of fluoride mouthwash was recommended for children receiving orthodontics or radiotherapy [9-12]. It is well known that most of the biochemical processes take place in aqueous medium consequently investigation on thermodynamic and acoustic properties of sodium fluoride in ternary system seems to be very crucial for the interpretation of ion-ion, ion-solvent, and solute-solvent interaction in mixed solvent system. Being of a great practical

importance in many industrial process, density, viscosity and ultrasonic velocity and some derived parameters of aqueous sodium fluoride with dextrose with different molarities at temperatures 298.15 301.15, 304.15 and 304.15K have been taken into account. As far as physiological processes are concerned, the study of dextrose and lactose is very significant. They play the role in the configuration of biological molecules [13-14].

Materials and Methods:-

Sodium fluoride (Sigma Chemicals with 99.9 % purity) used was vacuum dried. Dextrose (99.5%purity) was also obtained from Sigma Chemicals. All chemicals were used as received from manufacturer without further purification. The solutions of different molarities of dextrose were prepared by dissolving accurately weighed dextrose in (0.1M, 0.2M, 0.4M and 0.6M) aqueous solutions of sodium fluoride.

Double armed pycknometer having capacity ~18 cm^3 was used to determine the densities of all solutions. Calibration of pycknometer was carried out by using triply distilled water at temperatures 298.15K, 303.15K, 308.15K and 313.15K with densities0.9970, 0.9956, 0.9940 and 0.9922$g.cm^{-3}$ respectively [5].The pycknometer filled with air bubble free experimental liquids was kept in a transparent walled water bath of thermal stability $\pm$0.01K for 10-15 minutes to obtain thermal equilibrium. The liquid levels in the two arms were recorded with the help of a travelling microscope that could be read to $\pm$0.1mm.The estimated accuracy of density measurements of solutions was $\pm$0.00005 $g.cm^{-3}$.

The viscosity measurements were made using a commercial Ubbelohde viscometer. Lee et al. [6-7] and Nikam et.al. [8] have made use of this type of viscometer earlier. Viscometer was calibrated with triply distilled water with 0.890, 0.797, 0.719, and 0.652mPa.s. as its viscosities at 298.15K, 303.15K, 308.15K and 313.15K respectively [5]. A thoroughly cleaned and perfectly dried viscometer filled with experimental liquid was placed vertically in a thermostat. After attaining thermal equilibrium, the efflux times of flow of liquids were recorded with a digital stop watch correct to $\pm$ 0.01s.Since all flow times were greater than 300 s, the kinetic energy corrections were not applied. To evaluate viscometer constants, the length of the capillary of the viscometer (l) term is to be corrected as l'= l + 0.5r, r being the radius of the viscometer capillary. Since l is much larger (50-60mm) as compared to r (0.5mm), l=l' and hence end effects in viscometer are negligible. The reproducibility in the measurement of viscosity was $\pm$ 0.001mPa.s.

The ultrasonic velocity in the prepared solutions was measured using ultrasonic interferometer (Mittal-F-05), a variable path-fixed frequency type (2MHz).The accuracy of sound velocity is $\pm$ 0.1ms^{-1}.

Results and Discussion:-

All recorded statistical data is reported in tabular form. Table-1, 2 and 3 disclose the values of densities, viscosities and ultrasonic velocities of dextrose in aqueous sodium fluoride. The concentration range selected for dextrose was 0.0249, 0.0499, 0.0999, 0.1999 and 0.3999M, while that of sodium fluoride 0.1, 0.2, 0.4 and 0.6M. It is observed that the values of densities and viscosities increases with increase in concentration of both dextrose and sodium fluoride, but the values decrease with increase in temperature. Density is a measure of solvent-solvent and ion-solvent interactions. Increase in density with concentration reveals the increase in solvent-solvent and ion-solvent interactions. It might be due to shrinkage in the volume in presence of solute molecules. Alternatively, it can also be disclosed in term of structure maker of the solvent due to the added solute [15]. It has been observed that the values of ultrasonic velocity show in increment with concentration and temperature suggesting that disruption in water structure is enhanced with the addition of solvent (aqueous NaF solution) and the solute (dextrose). The reason behind this behaviour is disclosed in the form cohesion brought about the ionic hydration.

The evaluated parameters like limiting apparent molar volume (ϕ^0_v), its associated constant (S_v) and apparent molar volume (ϕ_v) which are calculates by Messon equation and are tabulated in table number 4 and 5.

$$\phi_v = \phi^0_v + S_v\sqrt{C} \qquad \ldots\ldots\ldots\ldots \qquad (1)$$

It is observed that the values of apparent molar volume (ϕ_v) are found to be increases with increase in molar concentration of solute (dextrose) but the same parameters found to be decreases with increase in molar concentration of solvent (aqueous NaF).The values of limiting apparent molar volume (ϕ^0_v)are positive and decreasing with increase in molar concentration of solute (dextrose) and content of solvent (aqueous NaF).For dextrose in all aqueous NaF solutions, the values of slope (S_v) are reported to be positive at all temperatures. According to Debye-Huckel theory, positive values of S_v show that dextrose undergoes notably association

in presence of ions. As S_v relates with solute-solute interactions, disclosing the presence of such type of interactions [16, 17, 18]. As far as viscosity is considered, the values go on increasing with increase in concentration of both solute and solvent, but decreases with increase in temperature [19, 20, 21].Values of η_r-1/√C for dextrose solutions in aqueous NaF at different temperatures are presented in table number – 6, while values of η_r are listed in table number - 7 at different temperatures. For η_r-1/√C values, Jones -Dole equation is employed,

$$\eta_r - 1/\sqrt{C} = A + BC^{1/2} \qquad \ldots\ldots\ldots (2)$$

Modified Jones -Dole equation is employed to calculate the values of β.

$$\eta_r = 1 + \beta C \qquad \ldots\ldots\ldots (3)$$

The values of coefficient 'A' are positive suggests strong ion-ion interactions present in the system and it is listed in table number – 8, [22]. 'B' coefficient gives the information of the order or disorder introduced by solute with solvent molecules. The values of 'B' coefficient are positive stating the existence of strong ion – solvent interaction. Perhaps, positive nature of 'β' coefficient may interpret increase in ion- solvent interactions due to structure making tendency of dextrose molecule. These values are listed in Table number -9.

The various acoustical parameters of dextrose in aqueous NaF have been calculated using following relations.

$$\phi_K = \phi^o_K + S_K\sqrt{C} \qquad \ldots\ldots\ldots (4)$$

Where S_K and ϕ^o_K are the slope and intercepts derived from Bacham's equation.

$$\beta_{ad} = \frac{1}{U^2 \times \varrho} \qquad \ldots\ldots\ldots\ldots (5)$$

$$\phi_k = \frac{1000(\varrho_0\beta_{ad} - \varrho\,\beta^0_{ad})}{C \times \varrho_0} + \frac{\beta^0_{ad} \times M^2}{\varrho_0} \qquad \ldots\ldots\ldots\ldots (6)$$

$$Z = U \times \varrho \qquad \ldots\ldots\ldots\ldots (7)$$

$$R_A = \frac{\varrho}{\varrho_0}\left(\frac{U_0}{U}\right)^{1/3} \qquad \ldots\ldots\ldots\ldots (8)$$

Where β_{ad}, ϕ^0_k, ϕ_k, Z and RA represent adiabatic compressibility, limiting apparent molar compressibility, apparent molar compressibility, specific acoustic impedance and relative association respectively.

The ultrasonic velocity increases with increase in concentration of NaF and the content of dextrose as well as with rise in temperature. It might be due to disruption of water structure with the addition of solvent (aqueous NaF) and the solutes (dextrose). Apparent molar

compressibility (ϕk), limiting apparent molar compressibility (ϕ^0_k) and its related constant(S_K) are tabulated in table number 10 and 11. The values of apparent molar compressibility (ϕk), limiting apparent molar compressibility (ϕ^0_k) are negative and increases with increasing concentration of NaF and dextrose as well as temperature. The negative values ofϕ_k suggest the existence of hydrophilic interactions in the system. Limiting apparent molar compressibility (ϕ^0_k) provides information regarding ion-solvent interactions and its related constant (S_K) ion–ion interactions in the solution.

Here β_{ad} declines with inclination of concentration and temperature some exceptions which is listed in table 12-15. This trend suggests that solute-solvent interactions through dipole- dipole interactions of OH groups of dextrose with the aqueous solution of NaF. The credit of declination in values of β_{ad} goes to increase in electrostriction compression of solvent around the molecules which results in large decrease in compressibility of solutions [23]. The values of acoustic impedance (z) increase with increase in concentration of NaF and sugar as well as temperature. This trend discloses the effective solute-solvent interactions [24]. The factor relative association (RA) shows an increment with increase in concentration of NaF and dextrose as well as temperatures which reveals the significant ion – solvent interactions [24].

Table 1: density, ρ / (g.cm^{-3}) and Viscosity, η (mPa.s) for dextrose in aqueous NaF.

Molarity (M) of dextrose	ρ (g.cm^{-3})				η (mPa.s)			
	298.15K	301.15K	304.15K	307.15K	298.15K	301.15K	304.15K	307.15K
	Dextrose in 0.1M NaF							
0.0249	1.0021	1.0014	1.0004	1.0000	0.974	0.899	0.841	0.783
0.0499	1.0039	1.0033	1.0025	1.0025	1.013	0.931	0.868	0.805
0.0999	1.0072	1.0069	1.0064	1.0074	1.078	0.986	0.914	0.847
0.1999	1.0131	1.0132	1.0133	1.0162	1.192	1.086	0.997	0.924
0.3999	1.0221	1.0229	1.0245	1.0312	1.388	1.266	1.147	1.064
	Dextrose in 0.2M NaF							
0.0249	1.0073	1.0063	1.0056	1.0051	1.007	0.930	0.867	0.804
0.0499	1.0094	1.0085	1.0080	1.0079	1.050	0.967	0.899	0.829
0.0999	1.0132	1.0125	1.0123	1.0132	1.122	1.028	0.954	0.875
0.1999	1.0198	1.0196	1.0201	1.0229	1.248	1.137	1.050	0.959
0.3999	1.0308	1.0313	1.0332	1.0394	1.464	1.327	1.227	1.118
	Dextrose in 0.4M NaF							
0.0249	1.0171	1.0154	1.0144	1.0137	1.064	0.977	0.908	0.840

0.0499	1.0194	1.0178	1.0170	1.0167	1.116	1.020	0.945	0.872
0.0999	1.0237	1.0222	1.0218	1.0224	1.201	1.093	1.008	0.925
0.1999	1.0314	1.0303	1.0304	1.0328	1.339	1.215	1.116	1.018
0.3999	1.0436	1.0432	1.0453	1.0509	1.588	1.434	1.310	1.191
	Dextrose in 0.6M NaF							
0.0249	1.0267	1.0238	1.0229	1.0223	1.130	1.027	0.956	0.883
0.0499	1.0292	1.0265	1.0257	1.0256	1.190	1.079	1.000	0.920
0.0999	1.0341	1.0316	1.0311	1.0319	1.288	1.163	1.073	0.983
0.1999	1.0426	1.0407	1.0410	1.0434	1.448	1.302	1.195	1.089
0.3999	1.0567	1.0561	1.0577	1.0635	1.722	1.545	1.411	1.280

Table 3: Ultrasonic velocity, U/ (m/sec) for dextrose in aqueous NaF.

Molarity (M) of dextrose	U (m/sec)							
	298.15K	301.15K	304.15K	307.15K	298.15K	301.15K	304.15K	307.15K
	Dextrose in 0.1M NaF				**Dextrose in 0.2M NaF**			
0.0249	1508	1516	1522	1528	1517	1524	1531	1537
0.0499	1510	1518	1524	1530	1519	1526	1533	1539
0.0999	1514	1522	1528	1534	1523	1530	1536	1542
0.1999	1521	1529	1534	1540	1529	1535	1542	1548
0.3999	1530	1538	1544	1549	1537	1544	1550	1556
	Dextrose in 0.4M NaF				**Dextrose in 0.6M NaF**			
0.0249	1534	1541	1547	1554	1551	1557	1564	1571
0.0499	1536	1543	1549	1556	1553	1558	1565	1572
0.0999	1539	1546	1552	1559	1555	1561	1568	1575
0.1999	1544	1551	1557	1564	1560	1566	1572	1579
0.3999	1552	1558	1564	1570	1567	1572	1578	1585

Table 4: Values of apparent molar compressibility (ϕ_K) for dextrose solutions in aqueous NaF at different temperatures.

√C	0.1M NaF	0.2M NaF	0.4M NaF	0.6M NaF	0.1M NaF	0.2M NaF	0.4M NaF	0.6M NaF
	298.15 K				301.15 K			
0.1578	160.42	147.08	134.55	118.16	157.38	144.64	129.83	112.97
0.2236	167.48	155.00	141.44	126.02	163.60	150.16	135.35	119.14
0.3162	176.35	164.48	150.83	135.78	172.02	158.39	144.12	128.35
0.4471	190.22	178.41	166.26	151.49	185.08	171.32	158.38	142.53
0.6324	209.97	199.26	189.30	174.02	203.49	191.86	179.68	164.47
	304.15 K				307.15 K			
0.1578	147.89	134.17	120.04	102.47	128.20	116.28	102.93	86.94

0.2236	153.31	141.04	127.41	110.89	136.96	123.83	110.29	95.31
0.3162	162.85	150.64	137.24	121.66	147.36	134.18	121.83	107.08
0.4471	177.99	165.94	153.19	137.73	162.47	151.53	138.95	125.81
0.6324	199.65	187.94	177.04	162.33	184.16	175.28	164.45	150.87

Table 5: The limiting apparent molar volume ϕ^0_v and S_v for dextrose in aqueous NaF at different temperatures.

Temp. K	ϕ^0_v ($cm^3.L^{1/2}$ $Mol^{3/2}$)	S_v (cm^3 mol^{-1})	ϕ^0_v ($cm^3.L^{1/2}$ $Mol^{3/2}$)	S_v (cm^3 mol^{-1})	ϕ^0_v ($cm^3.L^{1/2}$ $Mol^{3/2}$)	S_v (cm^3 mol^{-1})	ϕ^0_v ($cm^3.L^{1/2}$ $Mol^{3/2}$)	S_v (cm^3 mol^{-1})
	Dextrose in 0.1M NaF		Dextrose in 0.2M NaF		Dextrose in 0.4M NaF		Dextrose in 0.6M NaF	
298.15	92.141	51.832	81.877	52.898	70.552	55.346	58.047	59.308
301.15	87.763	52.267	77.982	52.485	66.778	56.261	55.380	54.625
304.15	79.747	54.366	70.987	52.828	61.698	52.642	49.765	53.150
307.15	60.908	54.103	51.895	54.334	43.338	54.716	31.791	55.703

Table 6: Values of η_r-$1/\sqrt{C}$ for dextrose solutions in aqueous NaF at different temperatures.

$\sqrt{C}$	0.1M NaF	0.2M NaF	0.4M NaF	0.6M NaF	0.1M NaF	0.2M NaF	0.4M NaF	0.6M NaF
	298.15 K				301.15 K			
0.1578	0.4578	0.5364	0.6197	0.7188	0.3712	0.4706	0.5492	0.6408
0.2236	0.5192	0.5903	0.6778	0.7726	0.4300	0.5210	0.6046	0.7025
0.3162	0.5908	0.6610	0.7559	0.8522	0.5110	0.5914	0.6835	0.7810
0.4471	0.7000	0.7714	0.8548	0.9546	0.6244	0.7004	0.7851	0.8855
0.6324	0.8365	0.9128	1.0104	1.1009	0.7760	0.8410	0.9408	1.0380
	304.15 K				307.15 K			
0.1578	0.3146	0.4050	0.4678	0.5650	0.2600	0.3291	0.4035	0.5220
0.2236	0.3721	0.4610	0.5257	0.6240	0.3160	0.3827	0.4628	0.5688
0.3162	0.4474	0.5400	0.6040	0.7020	0.4013	0.4586	0.5408	0.6467
0.4471	0.5470	0.6460	0.7151	0.8071	0.5104	0.5720	0.6457	0.7484
0.6324	0.6840	0.7989	0.8681	0.9600	0.6570	0.7331	0.8018	0.9001

Table 7: Relative viscosities η_r for dextrose solutions in aqueous NaF at different temperatures.

C	0.1M NaF	0.2M NaF	0.4M NaF	0.6M NaF	0.1M NaF	0.2M NaF	0.4M NaF	0.6M NaF
	298.15 K				301.15 K			
0.0249	1.0722	1.0846	1.0978	1.1134	1.0586	1.0743	1.0867	1.1011
0.0499	1.1160	1.1319	1.1514	1.1726	1.0961	1.1164	1.1351	1.1569
0.0999	1.1867	1.2089	1.2389	1.2694	1.1615	1.1869	1.2160	1.2469
0.1999	1.3130	1.3449	1.3822	1.4268	1.2792	1.3132	1.3510	1.3959
0.3999	1.5290	1.5772	1.6390	1.6962	1.4907	1.5318	1.5949	1.6564
	304.15 K				307.15 K			
0.0249	1.0496	1.0639	1.0738	1.0892	1.0410	1.0519	1.0637	1.0824
0.0499	1.0831	1.1030	1.1174	1.1394	1.0706	1.0855	1.1034	1.1271
0.0999	1.1414	1.1707	1.1909	1.2219	1.1268	1.1449	1.1709	1.2044
0.1999	1.2446	1.2888	1.3197	1.3609	1.2282	1.2557	1.2887	1.3346
0.3999	1.4325	1.5052	1.5490	1.6071	1.4155	1.4636	1.5070	1.5692

Table 8: Jones-Dole parameters for dextrose solutions in aqueous NaF at different temperatures.

Temp. K	A ($dm^{3/2}$ $mol^{-1/2}$)	B (dm^3 mol^{-1})	A ($dm^{3/2}$ $mol^{-1/2}$)	B (dm^3 mol^{-1})	A ($dm^{3/2}$ $mol^{-1/2}$)	B (dm^3 mol^{-1})	A ($dm^{3/2}$ $mol^{-1/2}$)	B (dm^3 mol^{-1})
	Dextrose in 0.1M NaF		Dextrose in 0.2M NaF		Dextrose in 0.4M NaF		Dextrose in 0.6M NaF	
298.15	0.3383	0.7950	0.4118	0.7952	0.4938	0.8159	0.5940	0.8044
301.15	0.2394	0.8531	0.3461	0.7845	0.4208	0.8211	0.5146	0.8302
304.15	0.1978	0.7744	0.2759	0.8281	0.3368	0.8425	0.4375	0.8276
307.15	0.1310	0.8384	0.1921	0.8526	0.2747	0.8337	0.3931	0.7995

Table 9: Modified Jones-Dole parameter β for dextrose solutions in aqueous NaF at

different temperatures.

Temperature K	β / (dm^3 mol^{-1})			
	Dextrose in 0.1M NaF	Dextrose in 0.2M NaF	Dextrose in 0.4M NaF	Dextrose in 0.6M NaF
298.15	1.2026	1.2968	1.4193	1.5278
301.15	1.1420	1.2068	1.3358	1.4563
304.15	1.0110	1.1641	1.2522	1.3607
307.15	0.9929	1.0902	1.1686	1.2819

Table 10: Apparent molar compressibility (ϕ_K) for dextrose solutions in aqueous NaF at different temperatures.

√C	0.1M NaF	0.2M NaF	0.4M NaF	0.6M NaF	0.1M NaF	0.2M NaF	0.4M NaF	0.6M NaF
	298.15 K, ϕ_K (cm^2/dyne)				301.15 K, ϕ_K (cm^2/dyne)			
0.1578	-63.00	-57.74	-53.25	-47.97	-60.73	-55.43	-51.16	-46.24
0.2236	-59.70	-54.83	-50.14	-45.35	-57.61	-52.84	-48.84	-43.75
0.3162	-55.10	-50.58	-45.98	-41.51	-53.70	-49.28	-45.08	-40.09
0.4471	-49.07	-44.83	-40.43	-36.07	-48.22	-44.06	-39.56	-34.67
0.6324	-40.70	-36.51	-32.61	-28.79	-39.85	-35.47	-31.58	-27.17
	304.15 K, ϕ_K (cm^2/dyne)				307.15 K, ϕ_K (cm^2/dyne)			
0.1578	-59.59	-54.55	-50.26	-45.08	-56.64	-52.81	-48.07	-42.49
0.2236	-56.49	-51.74	-47.70	-42.55	-53.67	-50.04	-45.49	-40.36
0.3162	-52.28	-47.71	-43.78	-38.96	-50.03	-46.48	-41.98	-37.05
0.4471	-46.77	-42.72	-38.13	-33.57	-44.92	-41.48	-37.21	-32.57
0.6324	-38.81	-34.51	-30.61	-26.11	-37.51	-34.11	-29.76	-25.24

Table 11: Limiting apparent molar compressibility (ϕ^0_K), S_k for dextrose solutions in aqueous NaF at different temperatures.

Temp. K	ϕ^0_K(cm^3/mol)	S_k	ϕ^0_K (cm^3/mol)	S_k	ϕ^0_K (cm^3/mol)	S_k	ϕ^0_K (cm^3/mol)	S_k
	Dextrose in 0.1M NaF		Dextrose in 0.2M NaF		Dextrose in 0.4M NaF		Dextrose in 0.6M NaF	
298.15	-70.1714	46.8792	-64.7853	44.7090	-59.8712	43.3023	-54.3487	40.5562
301.15	-67.5189	43.6144	-62.2781	41.8279	-58.0007	41.5227	-52.7154	40.3321
304.15	-66.2706	43.5699	-61.1326	41.8931	-56.9077	41.6739	-51.4969	40.0796
307.15	-62.7652	39.9884	-58.8973	39.1542	-54.1296	38.3465	-48.4330	36.2794

Table 12: Adiabatic compressibility β_{ad}/(cm^2/dyne), acoustical impedance (Z), relative

association (RA) at different temperaturues.

Molarity (M) of dextrose	β_{ad} x 10^{12}	z x 10^{-5}	RA	β_{ad} x 10^{12}	z x 10^{-5}	RA	β_{ad} x 10^{12}	z x 10^{-5}	RA	β_{ad} x 10^{12}	z x 10^{-5}	RA
	Dextrose in 0.1 M NaF			Dextrose in 0.2 M NaF			Dextrose in 0.4 M NaF			Dextrose in 0.6 M NaF		
	298.15 K											
0.0249	44.066	1.511	1.002	43.762	1.528	1.005	43.219	1.560	1.011	42.685	1.592	1.017
0.0499	44.029	1.515	1.003	43.737	1.533	1.006	43.215	1.564	1.013	42.701	1.598	1.019
0.0999	43.942	1.524	1.005	43.698	1.543	1.009	43.216	1.575	1.016	42.741	1.608	1.023
0.1999	43.789	1.540	1.010	43.647	1.559	1.015	43.241	1.592	1.023	42.833	1.626	1.030
0.3999	43.662	1.563	1.017	43.628	1.584	1.024	43.328	1.619	1.033	43.041	1.655	1.043
	301.15 K											
0.0249	43.554	1.518	1.002	43.321	1.533	1.005	42.759	1.565	1.011	42.244	1.594	1.016
0.0499	43.519	1.523	1.004	43.305	1.539	1.007	42.761	1.570	1.013	42.268	1.599	1.018
0.0999	43.458	1.532	1.006	43.281	1.549	1.010	42.772	1.580	1.017	42.324	1.610	1.023
0.1999	43.359	1.549	1.011	43.250	1.565	1.016	42.818	1.598	1.023	42.450	1.630	1.031
0.3999	43.235	1.573	1.019	43.283	1.592	1.026	42.951	1.625	1.035	42.742	1.663	1.044
	304.15 K											
0.0249	43.171	1.523	1.002	42.896	1.540	1.006	42.390	1.569	1.011	41.830	1.600	1.016
0.0499	43.146	1.528	1.004	42.892	1.545	1.008	42.401	1.575	1.013	41.862	1.605	1.018
0.0999	43.109	1.538	1.007	42.889	1.555	1.011	42.433	1.586	1.017	41.934	1.617	1.023
0.1999	43.049	1.554	1.013	42.898	1.573	1.018	42.515	1.604	1.025	42.100	1.636	1.032
0.3999	42.997	1.582	1.022	42.998	1.601	1.029	42.737	1.635	1.038	42.459	1.669	1.047
	307.15 K											
0.0249	41.005	1.562	0.996	42.543	1.545	1.006	42.543	1.545	1.006	41.441	1.606	1.016
0.0499	41.032	1.567	0.998	42.561	1.551	1.009	42.561	1.551	1.009	41.494	1.612	1.019
0.0999	41.089	1.578	1.002	42.603	1.562	1.013	42.603	1.562	1.013	41.607	1.625	1.025
0.1999	41.196	1.596	1.010	42.701	1.583	1.022	42.701	1.583	1.022	41.836	1.648	1.035
0.3999	41.404	1.627	1.023	42.932	1.617	1.036	42.932	1.617	1.036	42.340	1.686	1.054

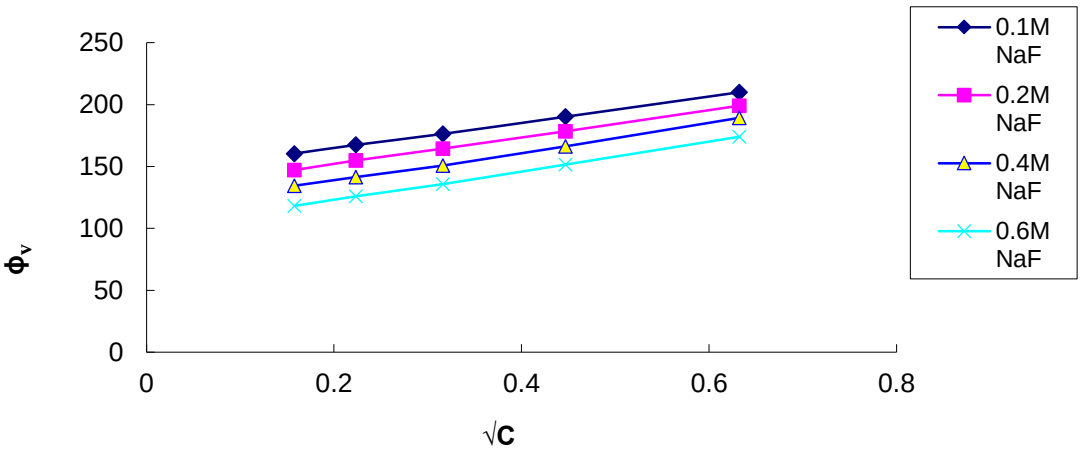

Fig 1. Plot of ϕv Vs √C of Dextrose in aqueosu NaF at 298.15K

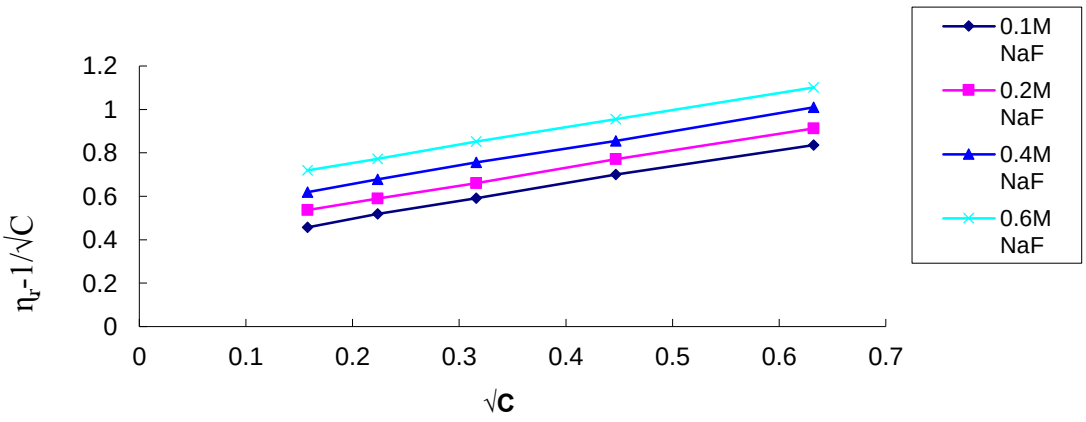

Fig 2. Plot of ηr-1/√C Vs √C of Dextrose in aqueous NaF at 298.15K

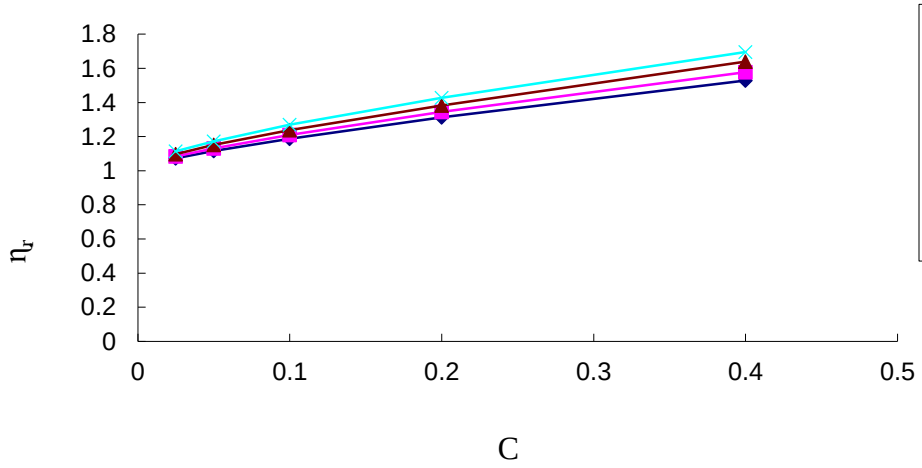

Fig 3.Ploat of ηr Vs C of Dextrose in aqueous NaF at 298.15K

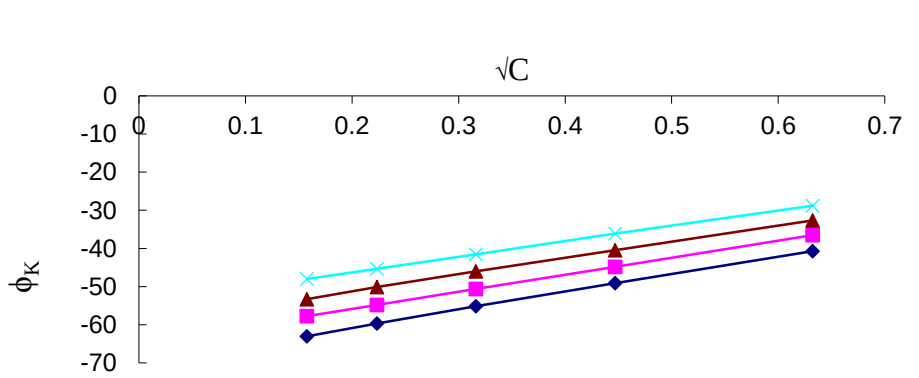

Fig 4. Ploat of ϕK Vs √C of Dextrose in aqueous NaF at 298.15K

Conclusion: - In the present work, density, viscosity and ultrasonic velocity have been measured at temperatures 298.15 301.15, 304.15 and 304.15K for NaF and dextrose system. The parameters such as apparent molar volume (ϕ_v) slope (S_V) and coefficients A and B of Jones- Dole equation and B by using modified Jones- Dole equation, adiabatic compressibility (β_{ad}), limiting apparent molar compressibility (ϕ^0_k), apparent molar compressibility (ϕ_k), specific acoustic impedance (Z), relative association (RA) have been determined and employed to explore the molecular interactions present in the system. The significant solute-solute, solute-solvent and solvent-solvent interactions are present in the system under consideration. It enhances with concentration but decreases with temperature.

Acknowledgement: - Authors are very much thankful to the Head, department of Chemistry and the Principal, LVH College, Panchavati, Nashik for providing laboratory and library facilities.

Conflict of Interest:- Authors declare no conflict of interest.

Ultrasonic and thermodynamic studies of interactions in ternary solutions containing glycerol or sorbitol and aqueous electrolytes

References:-

1. Vishnu, Wadhwani R & Akhtar Y, Ultrasonic and thermodynamic studies of interactions in ternary solutions containing glycerol or sorbitol and aqueous, Indian J.Chem (1995), (34) 954.
2. BoerioGoates J, Heat-capacity measurements and thermodynamic functions of crystalline s-D-glucose at temperatures from 10 K to 340 K, J.Chem. Thermodyn. (1991), (23) 403.
3. Putnam R.L &Boerio-Goates J, Heat-capacity measurements and thermodynamic functions of crystalline sucrose at temperatures from 5 K to 342 K. Revised values for $\Delta_f G^o_m$(sucrose, cr, 298.15 K), $\Delta_f G^o_m$(sucrose, aq, 298.15 K), S^o_m(sucrose, aq, 298.15 K); and $\Delta_r G^o_m$(298.15 K) for the hydrolysis of aqueous Sucrose, J.Chem. Thermodyn. (1993), (25) 607.
4. Goldberg R.N, Tewari Y.B &Ahluwalia J.C, Thermodynamics of hydrolysis of sucrose, J. Biol.Chem. (1989), (264) 9901.
5. Marsh K.N. Recommended materials for the realization of physic-chemical properties, Blackwell Scientific Publication, Oxford(1987).
6. Kim J.S,ParkY,& Lee H, Densities and Viscosities of the Water + Lithium Bromide + Ethanolamine System, J.Chem.Eng.Data, (1996), (41) 678.
7. Kim J.S, & Lee H, Solubilities, Vapor Pressures, Densities, and Viscosities of the LiBr + LiI + HO(CH2)3OH + H2O System, ,J.Chem.Eng.Data, (2001) (46) 79.
8. Nikam P.S.,Jagdale B.S.,Sawant A.B.& Hasan M, Densities and Viscosities for Binary Mixtures of Benzonitrile with Methanol, Ethanol, Propan-1-ol, Butan-1-ol, Pentan-1-ol, and 2-Methylpropan-2-ol at (303.15, 308.15, and 313.15) K, J.Chem.Eng. Data. (2000), (45) 214.
9. McDonald RE, Avery DR, George KS. Dental caries in the child and adolescent. In: McDonald RE, Avery DR, and Dean JA: Dentistry for the Child and dolescent. 8th

ed. St. Louis: Mosby; 2004. 205-32.

10. Clarkson JJ, McLoughlin J. Role of flouride in oral health promotion. Int Dent J, 50 :(2000)119–28. [PubMed].
11. Nowak AJ, Call JJ. Prevention of dental disease. In: Pinkham JR, Casamssimo PS, Fields HW, Nowak AJ: Pediatric Dentistry: Infancy through Adolescence. 4th ed. St. Louis: Elsevier Saunders; (2005) 513-9.
12. Volker JF, Russle DL. The prevention of dental caries with fluoride. In: Finn SB: Clinical Pedodontics. 4th ed. Philadelphia: Saunders; (1998) 495-516.
13. Barone G, Physical chemistry of aqueous solutions of oligosaccharides, Thermo. Chim. Acta. (1990), (162) 17-30.
14. Zhuo K, Wang J, Cao Y& Lu J, Thermodynamics of the interaction of HCI with D- fructose in water at 278.15- 318.15K, J.Phys.Chem. B. (1988) (102) 3574- 3577.
15. Thirumaran S and K..Job Sabu, Ultrasonic investigation of amino acids in aqueous sodium acetate medium. Ind. J.Pure, Appl. Phys. (2009) (47) 87-96.
16. Redlich O and Meyer D M, The Molal Volumes of Electrolytes, Chem Rev, (U.S.A.), (1964) (64) 221.
17. Jahagirdar D V and Pankanti S U, Density studies of Sugar Solutions, Indian J Chem, (1983) (A22)195.
18. Stokes J M and Stokes R H, The Conductances of Some Electrolytes in Aqueous Sucrose and Mannitol Solutions at 25°, J. Phys .Chem, (1958) (62) 497.
19. Comesana J F, Otero J J, Carcia E and Correa A, Viscosity Studies of Sugar Solutions, J. Chem. Eng. Data, (2003) (48) 362.
20. Kim J S, Park Y and Lee H, Densities and Viscosities of the Water + Lithium Bromide + Ethanolamine System, J. Chem. Eng. Data, (1996) (41) 678.
21. Song J H, Park S B, Yoon J H and Lee H, Densities and Viscosities of Monoethanolamine + Ethylene Glycol + Water, J. Chem. Eng. Data, (1996) (41) 1152.
22. Jahagirdar D.V, Arbad B.R, Patil S.C and ShankarwarA.G, Studies in acoustic properties, partial molar volume, viscosity, B- coefficient of lithium chloride in aqueous medium at five temperatures, Ind. J. Pure, Appl. Phys ,(2000), (38) 645-650.

23. Riyazudden and Khan Imran, Interactions in L-alanine-/ L-proline -/ L- valine - / L- leucine – aqueous KCI/KNO_3 systems at different temperatures: An isentropic compressibility study, J. Thermochimica. Acta, (2009) (45) 483.
24. Syal V.K, Lal G, Bisht P and Chauhan S, Ultrasonic measurements of some 1: 1 electrolytes in chlorobenzene + methanol mixtures, J. Mol. Liquids(1995), (63) 317-328.

Paper-8

CONCENTRATION-DEPENDENT DIFFUSION CONSTANT FOR MASS TRANSPORT THROUGH MEMBRANES

[1]Dr. Surekha. V. Munde, [2]Dr. Kranti Zakde, [3]Dr. A. R. Khan, and [4]Dr. Y. H. Shaikh

[1]Assistant Professor, P.E.S College of Engineering Aurangabad,

[2]Assistant Professor, MGM's Javaharlal Nehru College of Engineering, Aurangabad,

[3]Head of Department of Computer Science, Dr. Rafiq Zakaria Campus, Maulana Azad College, Rauza Bagh, Aurangabad,

[4]Associate Professor, Shivaji Arts, Commerce and Science College Kannad,

[1]Dr. Surekha. V. Munde, Assistant Professor, P.E.S College of Engineering Aurangabad[1], India

***Abstract*:**

Diffusion is a significant process in many biological and industrial processes. The diffusion constant (D) of ensemble particles in liquid from a higher concentration region to the lower concentration region is important. In the diffusion of particles from a higher concentration region to the lower concentration region, the Diffusive mass transfer through membrane for evaluation study of diffusion coefficient (D) through different membranes is important. Diffusion coefficients are traditionally measured using integrated solutions of Fick's law for systems with well-defined boundary conditions. A theoretical derivation of the concentration dependent diffusion coefficient equation suitable for mass transfer through membrane for different concentrations of ionic solution on a thickness of membrane by this method, gives the correct form and values for Diffusion coefficient (D) considerably found fine experimentally.

INTRODUCTION

Diffusion is the random motion of the ensemble particles from the higher concentration region to the lower concentration region or the net movement of a substance or from a region of higher concentration to a region of a lower concentration, due to random molecular motion [1-2]. Diffusion is a widespread important process which occurs in both living and non-living organisms [3]. Because diffusion occurs under different situations, conditions. Diffusion [4] is of different types like active diffusion, passive diffusion, simple diffusion, facilitated diffusion, Dialysis, Osmosis etc. shown in following figure 4.1.

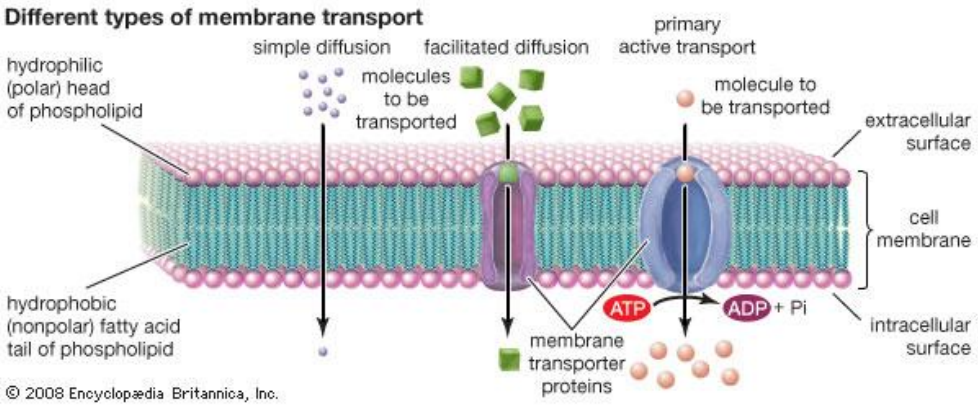

Figure 1: Different types of membrane transport

This paper focuses the evaluation study of diffusion through different membranes. For this purpose the diffusion equation is modified. The drug transport across bio membranes takes place through the pores in the membrane [5-6]. Also concentration [7] of the aqueous solution plays an important role in the diffusion Particularly to this study the diffusion of aqueous solution through the bio-membrane is studied by measuring the conductivity [8] with the help of conductivity meter.

EXPERIMENTAL

Present work aims at the study of diffusion through membranes with emphasis of diffusion through bio-membranes. Study of diffusion through bio-membranes is of importance because of the fact that there is an increasing interest in the field of medicine and drug delivery [9-10] to administer drugs and medicines employing non-conventional techniques that radically enhance performance [11]. There is increasing trend to administer drug through skin in the form of patches containing medicine like Insulin. The advantage of such an approach is that administering drug at specific timings is important and any departure from this seriously affects the performance and patient compliance is usually poor and all this can be taken care by administering drug in a controlled manner [12-13]. The trans-dermal drug delivery through the dosage-form like patches [14] is very useful in such cases. The scope is vast and possible cases of study are very large, therefore the work presented here attempts study of a single molecule namely NaCl through membranes. To study the transport of a molecule in a solution across a membrane, solution with a known concentration is kept on one side of the membrane and the other side of the membrane is pure solvent. Intentionally we selected a water soluble molecule (NaCl) and thus on one side of the membrane we kept NaCl solution in water

of a known concentration and on the other side of membrane pure water is used. The concentration of the molecule in the second compartment (water side) is monitored with time to determine the mode of transport of the molecule across the membrane.

In the actual set up of the experiment, it contains a Franz cell with two arms; in one arm of Franz cell a conductivity cell is inserted. The cell constant of the conductivity cell is one that makes the calculation simple. The upper compartment (Donor compartment) of Franz cell is filled with the NaCl solution of known concentration (on one of the side of membrane) and in the lower compartment (Acceptor compartment) distilled water is placed (on the other side of membrane). As diffusion of solute in the upper compartment takes place, the concentration of solute in the lower compartment starts increasing. This diffused solute tends to remain closer to the diffusing membrane surface and the distribution of solute throughout the lower cell is not uniform. Because of this, to allow for the uniform distribution of the solute in the lower compartment, the Franz cell is kept on a magnetic stirrer and associated pin in the lower compartment. This allowed even and uniform spreading of the NaCl solution diffused through the membrane in the lower acceptor compartment of the Franz cell. Conductivity meter used for measurement of conductivity with the help of conductivity cell inserted into the arm of the Franz cell. The conductivity of the diffused solute of NaCl on the other side of membrane is measured at successive time intervals using stop watch.

Set of readings of conductivity measurement with different membranes, bio-membranes are taken for particular time durations and by using mathematical treatment the diffusion constant was obtained. Here the solution for Fick's law [15-16] is used and some mathematical formulae are obtained suitable for the experimental set up is given below.

As at large concentration differences of the solutions, while the transport across the membrane will be due to advection while diffusion across the membrane will be predominant at lower concentration differences [17-19] Diffusion of NaCl was studied by using bio-membranes and synthetic membrane of different thickness of different concentration. Initially NaCl solute taken was of 1 Molar and 2 Molar concentrations.

As the molecular weight of NaCl is 58.44 gm/mol by using the formula

$$Weight\ \ required = \frac{\mathrm{M} \times \mathrm{Molecular\ weight} \times \mathrm{Volume}}{1000} \qquad [1]$$

Where, M: is molar weight

By this initially weight required is obtained and after that the solute is dissolved in the solvent for example water [20].

For example for preparation of 100 ml of 1 Molar NaCl solution in water, the amount of sodium chloride required is,

$$Weight\ \ required = \frac{1 \times 58.44 \times 100}{1000} = 5.84 \qquad [2]$$

Therefore for 1 Molar NaCl solution 5.84 gm NaCl is dissolved in the pure water to have 100 ml of Sodium Chloride solution. In the similar way other solutions of different molarities can be prepared for the experimentation of conductivity measurement. The prepared NaCl solution is filled in the upper compartment of Franz cell. In the lower compartment of Franz cell pure (distilled) water was filled. In between upper and lower compartment the membrane is placed. From the arms of the Franz cell conductivity meter cell was inserted and connected to conductivity meter. The diffusion of solute was monitored for 60 minutes by the duration of one minute. For monitoring stop watch was used. For the purpose so that the solute should mix evenly in lower compartment the Franz cell was kept on the magnetic stirrer.

DIFFUSION CONSTANT EQUATION

The main interest is to determine the mass transfer of solute through the membrane [21]. For the measurement diffusion constant [22-29], concentration of the solute in the lower compartment we used a simple method of measuring conductivity of the solution.

The standard table of readings of relation between conductivity and concentration (% w/w) of NaCl solution in the conductivity range of 0.0001 to 2 mS is given below.

Table 1: Relation between conductivity and concentration (% w/w) of NaCl solution in the conductivity range of 0.0001 to 2 mS.

NaCl % w/w	Normality	Conductivity micro symen	Conductivity mili Symen
0.0001	1.72414E-05	2.2	0.0022
0.0003	5.17241E-05	6.5	0.0065
0.001	0.000172414	21.4	0.0214
0.003	0.000517241	64	0.064
0.01	0.001724138	210	0.21
0.03	0.005172414	617	0.617
0.1	0.017241379	1990	1.99
0.3	0.051724138	5690	5.69
1	0.172413793	17600	17.6
3	0.517241379		48.6

The conductivity versus concentration relationship is linear for sodium chloride [30]. The exact relationship obtained from the graph shown in Figure 4.4 is

$$Conductivity(mS) = 19.966 \cdot concentration\ of\ \ NaCl\ (\%w/w) \qquad [3]$$

In figure 4.4, the points plotted represent actual standard data and the straight line joining those points is the best fitting straight line and the equation of the straight line is shown in the inset.

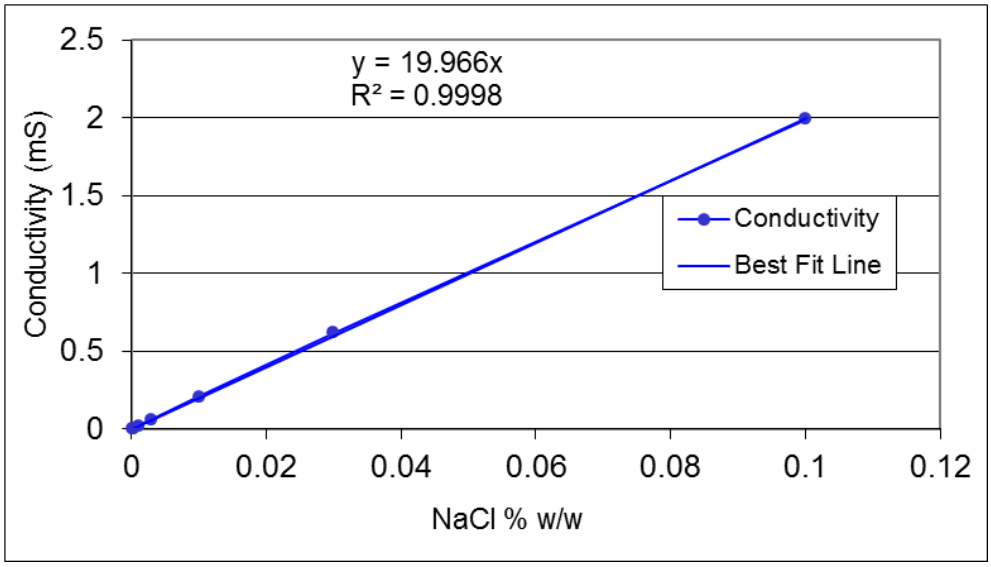

Figure 2: Relation between conductivity and concentration (% w/w) of NaCl solution in the conductivity range of 0.0001 to 2 mS.

During the study concentration of NaCl in the lower compartment (accepter compartment) was monitored for 60 minutes by measuring the conductivity with time and converted finally to the concentration using the above relationship.

If (ϕ_1) is the mass transfer through the membrane and (ϕ_2) is the concentration of the solution in the upper compartment at any time T, then the Driving force $\partial\phi/\partial$x is given by the relation

$$\frac{\partial \phi}{\partial x} = \frac{(\phi_2 - \phi_1)}{(x_2 - x_1)} \qquad [4]$$

$(\phi_2 - \phi_1)$ is the concentration difference between the concentration in upper compartment and concentration in lower compartment

$(x_2 - x_1)$ is the thickness of membrane.

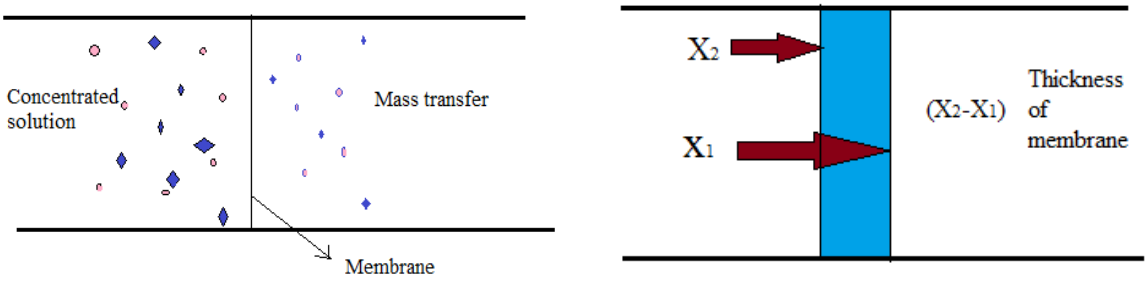

Figure 3: Mass transfer through membrane and schematic to show Thickness of membrane

The diffusion flux J in a particular direction is directly proportional to the Driving force in the same direction i.e. $\frac{\partial \phi}{\partial x}$

$$\therefore J \propto \frac{\partial \phi}{\partial x} \qquad [5]$$

$$OR \quad J = \quad -D \times \frac{\partial \phi}{\partial x} \qquad [6]$$

Where D is Diffusion constant and it is a property of membrane which depends on many factors like type of solution, type of membrane, Concentration etc. [31].

At time t_1 the mass transferred in the lower compartment through the membrane is m_1 and the conductivity measured is C_1 and at time t_2 the mass transferred in lower compartment through the membrane is m_2 and the conductivity measured is C_2 then, mass flow through the membrane per unit time is given by,

$$Mass\ \ flow\ \ per\ unit\ time = \quad \frac{(m_2 - m_1)}{(t_2 - t_1)} \qquad [7]$$

Diffusion flux J can be given by Mass flow per unit time per unit area

$$Flux\ J = \quad \frac{\left[\frac{(m_2 - m_1)}{(t_2 - t_1)}\right]}{(\mathrm{A})} \qquad [8]$$

As for all the conductivity measurements membrane used is cylindrical in shape therefore above equation can be written as,

$$Flux\ J = \frac{\left[\frac{(m_2 - m_1)}{(t_2 - t_1)}\right]}{(\pi r^2)} \qquad [9]$$

Therefore Diffusion constant D is given by

$$D = \frac{-J}{\left[\frac{\partial \phi}{\partial x}\right]} \qquad [10]$$

Equation (10) is for Diffusion Constant.

STUDY OF DIFFUSION THROUGH SOME BIO-MEMBRANE

Diffusion constant is dependent on the thickness of membrane, molarity of the solution and also on the type of drug which is to diffused through bio-membrane. The diffusion constant for mass diffused through membranes of different thickness for different molarities solution obtained using above equation is studied and the results obtained were good.

CONCLUSION

The differential form of Fick's law have been used to determine the diffusion coefficient of diffusive mass through membrane. The technique is a simple alternative to a complicated integrated form of Fick's law. It provides accurate diffusion coefficient values. The method could be extended to various diffusion cases where the boundary conditions are not well defined or the diffusion equation does not have a simple integrated solution.

REFERENCES

[1] H. J. V. Tyrrell, K. R. Harris, (1984), Diffusion in Liquids 1st Edition a Theoretical and Experimental Study. eBook, ISBN: 9781483100890 *Imprint: Butterworth-Heinemann Published.*

https://www.elsevier.com/books/diffusion-in-liquids/tyrrell/978-0-408-17591-3.

[2] E. L.Cussler, (1999), Diffusion: Mass Transfer in Fluid Systems. Third Edition, Cambridge University Press.

http://assets.cambridge.org/97805218/71211/frontmatter/9780521871211 _frontmatter.pdf

[3] Alessandro Gajo, Benjamin Loret, (2004), Mass Transfer Through Membranes and Generalized Diffusion. Print ISBN 978-3-211- 1323-0 Online ISBN 978-3-7091-2778-0, 462, Springer Vienna

DOI :10.1007/978-3-7091-2778-0_9

[4] J. W. Ayres, F.T. Lindstrom, (1977), Diffusion model for drug release from suspensions.I: Theoretical considerations. J. Pharm. Sci. 66, 654–662.

[5] W. Stein, (1967), The Movement Of Molecules Across Cell Membranes. eBook ISBN: 9780323152679 Imprint: Academic Press.

https://www.elsevier.com/books/the-movement-of-molecules-across-cell-membranes/stein/978-0-12-664650-4

[6] Endre Nagy, (2011), Basic Equations of the Mass Transport through a membrane Layer eBook ISBN: 9780123914255 Hardcover ISBN: 9780124160255 Paperback ISBN: 9780323165365 Imprint: Elsevier Published.

https://www.elsevier.com/books/basic-equations-of-the-mass-transport-through-a-membrane-layer/nagy/978-0-12-416025-5.

[7] Henrik Stenlund, (2011), Three Methods for Solution of Concentration Dependent Diffusion Coefficient. *Visilab Signal Technologies Oy. Finland*.

http://www.visilab.fi/bolmatano.pdf.

[8] Chang Liua, Hyeonseok Leea, Ya-Huei Changa, Shien-Ping Fenga, (2016), The Study of Electrical Conductivity and Diffusion Behavior of Water - Based and Ferro/Ferricyanide - Electrolyte-Based Alumina Nanofluids. *Journal of Colloid and Interface Science*. 469, 17–24.

DOI: http://dx.doi.org/10.1016/j.jcis.2016.02.001

[9] J. W.Ayres, F.T. Lindstrom, (1977), Diffusion model for drug release from suspensions.I: Theoretical considerations. *J. Pharm. Sci*.. 66, 654–662.

[10] J. Siepmann, N.A. Peppas, (2001), Modeling of drug release from delivery systems based on hydroxypropyl methylcellulose (HPMC). *Adv. Drug Deliver. Rev*. 48, 139–157.

[11] J. Siepmann, N.A. Peppas, (2000), Hydrophilic matrices for controlled drug delivery: An improved mathematical model to predict the resulting drug release kinetics (the "sequential layer" model). *Pharm. Res*. 17, 1290–1298.

[12] Azad Khan, Mohd Yasir, Mohd Asif, Iti Chauhan, Alok P. Singh, Rajat Sharma, Pradeep Singh and Shubham Rai, (2011), Iontophoretic drug delivery: History and applications. *Journal of Applied Pharmaceutical Science.* 01 (03), 11-24.

[13] Prasanjeet Patnaik, (2011), a thesis entitled, Development of Iontophoretic Delivery system. submitted to Department of Biotechnology & Medical Engineering National Institute of Technology Rourkela 769008.

[14] Patricia Connolly, Christopher Cotton, Fabrice Morin, (2002), Opportunities at the Skin Interface for Continuous Patient Monitoring: A Reverse Iontophoresis Model Tested on Lactate and Glucose, IEEE Transactions On Nanoscience, 1:1, 37-41.

[15] Fick A 1855 U¨ ber diffusion Ann. Phys., Lpz. 23 59.

[16] B Ph van Milligen, P D Bons, B A Carreras, R S anchez, (2005), On the applicability of Fick's law to diffusion in inhomogeneous systems. *Eur. J. Phys.* 26, 913–925.

DOI:10.1088/0143-0807/26/5/023

[17] B. A. Puthenveettil, J. H. Arakeri, (2005), Plume structure in high Rayleigh-number convection. *J. Fluid. Mech*. 542, 217–249.

DOI:10.1017/S002211200500618X

[18] B. A. Puthenveettil, J. H. Arakeri, (2008), Convection due to an unstable density gradient across a permeable membrane. *Jl. Fluid. Mech.* 609, 139–170.

DOI: https://doi.org/10.1017/S0022112008002334

[19] G. V. Ramareddy, Baburaj A. Puthenveettil, (2010), The Pe regime of pe convection across a horizontal permeable membrane. *J. Fluid Mech.*

https://apm.iitm.ac.in/fmlab/raj/index_files/RamaReddy-Baburaj-Revised.pdf

[20] Preparing Chemical Solutions.

https://www.sciencecompany.com/Preparing-Chemical-Solutions.aspx

[21] D.R. Paul, S. K. McSpadden, (1976), Diffusional release of a solute from a polymeric matrix. *J. Membr. Sci.* 1, 33–48.

DOI: 10.1016/S0376-7388(00)82256-5.

[22] J. Crank, (1979), The mathematics of diffusion. *Oxford University Press. Oxford.* 2edition.

[23] J. Siepmann, F. Siepmann, (2008), Mathematical modeling of drug delivery. *Int. J.Pharm*. 364, 328–343.

DOI:10.1016/j.ijpharm.2008.09.004.

[24] Jean Philibert, (2005), One and a Half Century of Diffusion: Fick, Einstein, before and beyond. *Diffusion Fundamentals* . 2 ,1.1 - 1.10 .

[25] Richard DiDomizio, Afina Lupulescu, Martin E. Glicksman, (2006), Simulation of Fick's Verification of the 2nd Law. *Diffusion Fundamentals*. 4, 2.1 - 2.14.

[26] B. Baeumer, M. Kovcs, M. Meerschaert, (2008), Numerical solutions for fractional reaction-diffusion equations. *Comput. Math. Appl*. 55, 2212–2226.

[27] E. Abad, S. B. Yuste, K. Lindenberg, (2010), Reaction-subdiffusion and reactionsuper diffusion equations for evanescent particles performing continuous-time random walks. *Phys. Rev.* E 81, 031115.

[28] Surekha V. Munde, S.K. Kapsae, GulamRabbani, Shaikh Yusuf H, (2014), Microcontroller Based Data Acquisition System. Journal of Chemical, Biological and Physical Sciences.4(3),3593-3597.

[29] C.-M. Chen, F. Liu, I. Turner, V. Anh, (2007), Fourier method for the fractional diffusion equation describing sub-diffusion. *J. Comp. Phys*. 227, 886-897.

[30] Conductivity ordering Guide.

http://myweb.wit.edu/sandinic/research/conductivityvconcentration

[31] Diffusion.

https://engineering.dartmouth.edu/~d30345d/courses/engs43/ Diffusion Equation.pdf.

Paper-9

AN ASSESSMENT OF DISTRICT-WISE URBANIZATION GROWTH OF MAHARASHTRA

Dilip D. Muluk[1]
Associate Professor
Dept. of Geography,
Hutatma Rajguru Mahavidyalaya, Rajgurunagar.

Dr. Arjun H. Musmade[2]
Research Guide
Asso. Prof. & Head, Dept. of Geography,
T. J. College Khadki, Pune.

Abstract:

In order to understand the concept of urbanization, and the process, it is important to look at how and where a place grows. In this research paper, district wise analysis of urbanization in Maharashtra has been done. Maharashtra is first in India in terms of total urban population. Maharashtra has a very high rate of urbanization in India. The availability of employment opportunities and livelihood in Maharashtra attracts many people. The urban population of Maharashtra has increased tremendously due to the migration from the entire country as well as the rural areas of Maharashtra to the urban areas. The western part of Maharashtra has a higher urban population than the eastern part. Marathwada and Vidarbha in Maharashtra have the lowest level of urbanization. In the last two decades (1991 to 2011), the urban population in the state of Maharashtra has increased by 23.67 percent, which is very high. In the future, Maharashtra will continue to be one of the most urbanized states of India. Various problems created due to rapid urbanization will have to be faced in the future. Therefore, it is very important to study the population in the context of urbanization. Such a study would provide guidelines for planning future demographic aspects.

Key Words: urbanization, urban centers, population growth, industrialization.

Introduction:

The word urbanization is derived from the English word urban. The word urban is derived from the Latin word *urbs*. In Latin, the word *urbs* means city or town. In order to understand the concept of urbanization, and the process, it is important to look at how and where a place grows. According to Nelson Anderson, "urbanization is a change in the way in which industries (factories) develop more and the way of life is different than in rural areas." Places that have made great strides in modern times have become hubs of industry. Many people from different parts of the country come to such places to seek employment. Therefore, new and different ways of life are created by changing the old way of life of that place. This

method is different from the village. This is because most of the people in the place of business are engaged in secondary sector business. People in rural areas are engaged in agribusiness and other primary activities. So, the lifestyle in the city is different than in the rural areas. The percentage of urban population is increasing in the states of India (Mundhe, 2014),(Klasen 2006). The growth of urban population in a state is the most important indicator in the analysis of regional development (Bhagat, 2019), (Bhagat & Mohanty, 2009). The growth of the urban population plays an important role (Chhabra et al., 2007) in the analysis of social and economic development (Onda et al., 2019). In 2011, Maharashtra had a total population of 11,23,72,972 (9.29 per cent), second only to Uttar Pradesh in terms of population (Chandrasekhar2015), (Sassen et al., 1998). Maharashtra's population has increased by 17.8 million in the last two decades (Mohanty et al., 2021). From 1991 to 2011, the urban population of Maharashtra has increased from 30.54 million to 50.83 million (Agarwal, 2011). The urban population of Maharashtra has increased tremendously due to the migration from the entire country as well as from the rural areas of Maharashtra towards the urban centers of the Maharashtra (Salunke, 2020), (Nadu, 2001). The growth in terms of urbanization in Maharashtra is very heterogeneous (Iyer et al., 2005), (Han et al., 2009). The urban population seems to have increased more in the western part of Maharashtra than in the eastern part (Linard et al., 2012). Marathwada and Vidarbha in Maharashtra have the lowest level of urbanization (Waghmare, 2016). Besides this, industrialization, information technology and educational advancement have led to rapid changes in the level of urbanization in the cities and districts such as Mumbai, Pune, and Nagpur. Mumbai and the suburbs of Mumbai seem to be 100 percent urbanized. In contrast, Sindhudurg and Gadchiroli districts have the lowest level of urbanization (less than 15 percent). Mumbai and its suburbs have a combined population of over 1.84 crores. Maharashtra has a total of six urbanized regions, with Mumbai, Pune, Nagpur, Nashik, Vasai Virar and Aurangabad, having a population of more than one million each (Rain et al., 2007b). The main reasons for the increase in population in the cities of Maharashtra are the guarantee of employment, education and a high standard of living which attracts people from different parts of the country and all corners of Maharashtra (Rain et al., 2007). Maharashtra ranks fifth in India in terms of urbanization. But in comparison to the total population, Maharashtra's population of 50.83 million is the largest urban population of any state in India (Cohen, 2006). Therefore, Maharashtra ranks first in India in terms of total urban population. Maharashtra alone accounts for 13.5 percent of India's total urban population. After Maharashtra, Uttar

Pradesh has 11.8 percent of total urban population of India. No other state in the rest of India has more than 10 per cent of urban population of India.

Objectives:

The present study has been undertaken with the following specific objectives:

1. To examine the trend of urbanization in Maharashtra.
2. To analysis district-wise urban growth of Maharashtra.

Database and Methodology:

This paper is based on secondary data sources. To fulfill the objectives of this research, data regarding urbanization of Maharashtra is obtained from the Census of India. The analysis and interpretation of data has been done from the geographical point of view. MS-Excel was used to process, analyze and represent the demographic data. Very high, high, moderate and low urbanization patterns in Maharashtra were examined in detail. ArcGIS software was used to prepare the maps.

Result and Discussion:

Trend of Urbanization in Maharashtra from 1901 to 2011:

By observing the graph 1 below, the urban population of Maharashtra has been steadily increasing since 1901 with two exceptions (1911 and 1961). In 1901, the percentage of the urban population was 16.59 percent. This was slightly reduced to 15.13 percent in 1911. Since 1921, the percentage of urban population has been steadily rising except during 1961. According to the Census report of 1951, after independence of India in 1947, the urban population of Maharashtra grew by 7.64 percent to reach 28.75 percent from 21.11 percent. This was the highest decadal increase in the percentage of urban population of Maharashtra. This was followed by a slight decrease of 0.53 percent in 1961. After 1961, however, the urban population of Maharashtra has been growing. In 2011, the percentage of the urban population in Maharashtra was 45.22. This proportion is higher than the proportion of India's urban population. According to the Policy Commission's (*Niti Aayog*) 2021 report, Maharashtra will have more than 51 percent population of the state living in urban areas.

Table 1: Rural and Urban population in Maharashtra (%) from 1901 to 2011

Census Year	Urban Population (%)	Rural Population (%)
1901	16.59	83.41
1911	15.13	84.87
1921	18.50	81.50
1931	18.60	81.40
1941	21.11	78.89
1951	28.75	71.25
1961	28.22	71.78
1971	31.17	68.83
1981	34.99	65.01
1991	38.73	61.31
2001	42.43	57.57
2011	45.22	54.77

Source: Census Reports - 1901 to 2011

Graph 1: Percentage of Urban and Rural Population of Maharashtra from 1901 to 2011

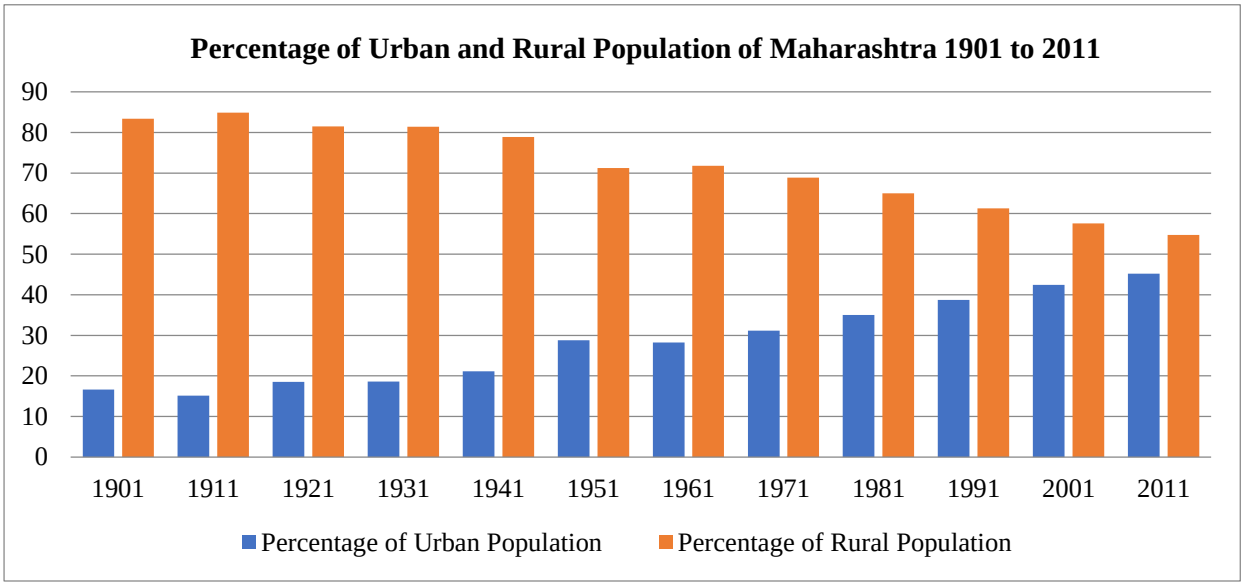

District-wise Urbanization in Maharashtra:

According to the 2011 Census report, the trend of district-wise urbanization in Maharashtra shows that the urban population of Mumbai Suburban, Thane, Pune, Nagpur, Mumbai and Nashik together is more than 25 lakhs. These districts are followed by Aurangabad, Solapur, Jalgaon, Kolhapur and Amravati with a population of over one million each. The two districts of Greater Mumbai and Mumbai are 100 percent urbanized. According to the 2011 Census report, Thane (85,03,094) district has the highest urban population, followed by Mumbai and Mumbai Suburban. After that is Pune district which has the population of Pune and Pimpri Chinchwad as well as other urban areas of the district

(57,93,716). The district having the lowest urban population in Maharashtra is Sindhudurg (1,06,998) and the percentage of the urban population in Sindhudurg district is only 12.60 percent. The percentage of urban population is the lowest in Gadchiroli district i.e. 11 percent. Hingoli district has an urban population of 15.17 percent, Washim 17.69 percent and Gondia 17.07 percent. Although the percentage of urban population growth in the districts of eastern Maharashtra is higher, the overall population growth rate is very low. The districts of Maharashtra are categorized by the percentage of urban population as follows:

1) Very High Urbanization (75 to 100 percent):

Maximum growth of urban areas in Maharashtra has taken place in the area around the Mumbai metropolitan city. The districts with more than 75 percent urban population are Mumbai, Mumbai Suburban and Thane. Out of these, Mumbai and Mumbai Suburban are 100 percent urbanized. Thane district near Mumbai has 76.92 percent urban population. According to the 2011 Census report, the level of urbanization is highest in Mumbai and its environs. Mumbai, Mumbai Suburban and Thane are all close to each other. These areas have eight of the 27 largest Municipal Corporations in Maharashtra. The reason for the high rate of urbanization in Mumbai and its environs is that many people migrate to Mumbai from different parts of the country, not just Maharashtra. Increased urbanization and industrialization in and around Mumbai provides employment opportunities to many people, so the population in and around Mumbai is growing very rapidly. The increase in urbanization in the adjoining districts of Palghar and Raigad is also astonishing. The population density of Mumbai and its environs is also very high. This has created various problems related to the environment. The city of Mumbai has to deal with issues such as transportation, water supply, power supply, waste management, sewage disposal, public sanitation, health facilities, crimes, air pollution, noise pollution and congestion. The number of slums in Mumbai and adjoining areas has also increased rapidly. Dharavi in Mumbai is the largest slum in Asia.

2) High Urbanization (50 to 75 percent):

Regions with more than 50 percent but less than 75 percent urban population are categorized as highly urbanized regions. In Maharashtra, Nagpur and Pune districts have more than fifty percent urban population. Nagpur district has achieved 68.3 percent urbanization and Pune district has 60.89 percent urban population. Nagpur is the sub-capital of Maharashtra and an important administrative city in the Vidarbha region. As Nagpur district has more employment opportunities than other districts of Vidarbha, so the flow of migrants from other districts of Vidarbha to Nagpur city is higher. Pune district is known as the cultural capital of

Maharashtra. Large-scale industrialization has taken place in the Pune district. Along with Pune and Pimpri Chinchwad, Chakan, Talegaon, Ranjangaon, Sanaswadi, Jejuri and Baramati have witnessed rapid industrialization. The industrial sector in this area has created many employment opportunities for the people in the surrounding regions. Also, the growing population has created many employment opportunities in the construction, education and other services sectors as well. Overall, this has created employment opportunities in different areas of the Pune district, which has resulted in the high level of urbanization in Pune district.

Table 2: District wise Distribution of Population in Maharashtra (Total, Rural, Urban) in 2011

Sr. No.	District	Total	Rural	Urban	Percentage of Urban Population	Decadal Growth Rate of Urban Population (2001 – 2011)
1	Nandurbar	1,646,177	1,370,995	275,182	16.72	35.78
2	Dhule	2,048,781	1,477,034	571,747	27.91	28.23
3	Jalgaon	4,224,442	2,880,984	1,343,458	31.80	27.61
4	Buldhana	2,588,039	2,038,650	549,389	21.23	16.06
5	Akola	1,818,617	1,096,768	721,849	39.69	15.04
6	Washim	1,196,714	985,058	211,656	17.69	18.61
7	Amravati	2,887,826	1,851,134	1,036,692	35.90	15.24
8	Wardha	1,296,157	875,284	420,873	32.47	29.48
9	Nagpur	4,653,171	1,474,977	3,178,194	68.30	21.60
10	Bhandara	1,198,810	965,053	233,757	19.50	33.02
11	Gondia	1,322,331	1,096,631	225,700	17.07	57.36
12	Gadchiroli	1,071,795	953,858	117,937	11.00	75.34
13	Chandrapur	2,194,262	1,424,424	769,838	35.08	15.75
14	Yavatmal	2,775,457	2,176,252	599,205	21.59	31.06
15	Nanded	3,356,566	2,442,734	913,832	27.23	32.62
16	Hingoli	1,178,973	1,000,102	178,871	15.17	16.13
17	Parbhani	1,835,982	1,266,112	569,870	31.04	17.45
18	Burn	1,958,483	1,581,251	377,232	19.26	22.53
19	Aurangabad	3,695,928	2,079,327	1,616,601	43.74	48.70
20	Nashik	6,109,052	3,510,885	2,598,167	42.53	34.10
21	Thane	11,054,131	2,551,037	8,503,094	76.92	44.06
22	Mumbai Suburban	9,332,481	--	9,332,481	100	8.01
23	Mumbai	3,145,966	--	3,145,966	100	5.75
24	Raigad	2,635,394	1,662,585	972,809	36.91	81.89
25	Pune	9,426,959	3,687,243	5,739,716	60.89	36.63
26	Ahmednagar	4,543,083	3,630,012	913,071	20.10	13.61
27	Beed	2,585,962	2,071,277	514,685	19.90	32.97
28	Latur	2,455,543	1,830,085	625,458	25.47	27.58
29	Osmanabad	1,660,311	1,378,713	281,598	16.96	20.72
30	Solapur	4,315,527	2,917,088	1,398,439	32.40	14.13
31	Satara	3,003,922	2,433,694	570,228	18.98	43.23
32	Ratnagiri	1,612,672	1,349,062	263,610	16.35	37.15
33	Sindhudurg	848,868	741,870	106,998	12.60	29.98
34	Kolhapur	3,874,015	2,644,119	1,229,896	31.75	17.09
35	Sangli	2,820,575	2,101,143	719,432	25.51	13.62
	Maharashtra	**112,372,972**	**61,545,441**	**50,827,531**	**45.23**	**23.67**

Source: Census Report of Maharashtra, 2011

Graph 2: Distribution of District wise Urban Population and Decadal Growth of Urban Population in Maharashtra, 2011

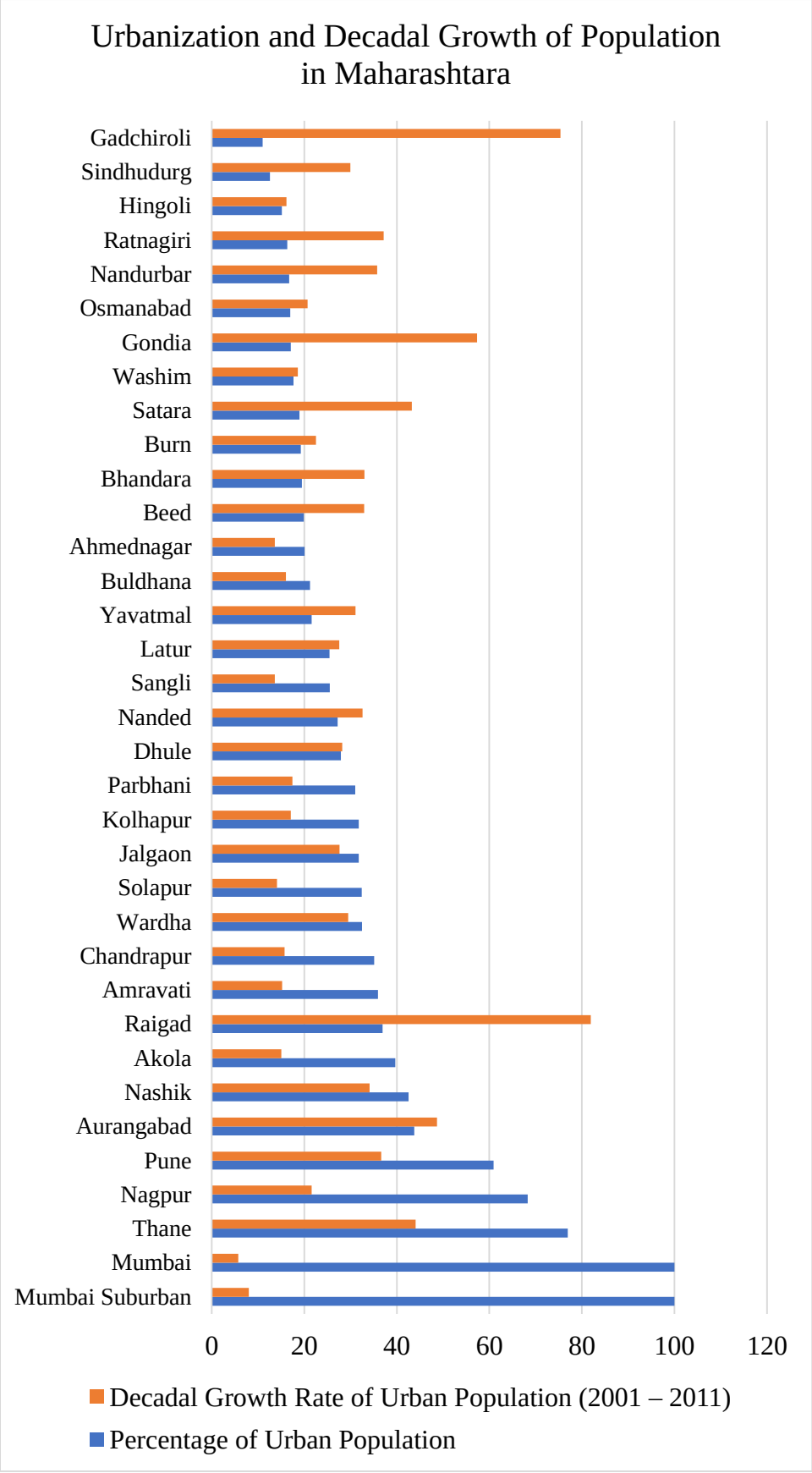

3) Moderate Urbanization (25 to 50 percent):

According to 2011 Census report, the urban population of Aurangabad is 43.74 percent, Nashik 42.53 percent, Akola 36.69 percent, Raigad 36.91 percent, Amravati 35.9 percent, Chandrapur 35.8 percent, Wardha 32.47 percent, Solapur 32.4 percent, Jalgaon 31.8 percent, Kolhapur 31.75 percent, Parbhani 31.04 percent, Dhule 27.91 percent, Nanded 27.23 percent, Sangli 25.51 percent and Latur 25.4 percent. These fifteen districts have more than 25 percent and less than 50 percent urban population each which corresponds to the moderate level of urbanization. Aurangabad and Nashik districts have more than 40 percent urban population. Nashik is an important cultural center in Western Maharashtra, so the population of Nashik district is growing rapidly. Also, Aurangabad is a major industrial city in Marathwada. Due to migration from other parts of Marathwada to Aurangabad city, the population and urbanization rate of Aurangabad district are increasing rapidly. The remaining districts of Western Maharashtra such as Solapur, Kolhapur and Sangli are basically agricultural and to some extent industrial, so their population is increasing. Also, due to the proximity of Raigad district to Mumbai, the urban population is increasing very rapidly in Raigad district. Due to the migration of the educated community from the rural areas of the district to the urban areas, the urban population of these districts is increasing. As a result, the total urban population in all these districts is slowly increasing.

4) Low Urbanization (0 to 25 percent):

The level of urbanization is low in the districts which have less than 25 percent urban population. There are 15 districts in Maharashtra with less than 25 percent urban population. These are Yavatmal (21.59 percent), Buldhana (21.23 percent), Ahmednagar (20.1 percent), Beed (19.9 percent), Bhandara (19.5 percent), Jalna (19.26 percent), Satara (18.98 percent), Washim (17.69 percent), Gondia (17.07 percent), Osmanabad (16.96 percent), Nandurbar (16.72 percent), Ratnagiri (16.35 percent), Hingoli (15.17 percent), Sindhudurg (12.7 percent) and Gadchiroli (11 percent). The level of urbanization in these districts is very low, due to unfavorable geographical conditions and low availability of employment opportunities, as well as primary activities based economy. Among the districts with low levels of urbanization, Gadchiroli, Hingoli, Nandurbar, Gondia and Washim are the districts with high tribal population. The total population is low due to migration from these districts to other districts, and the rate of urbanization in these districts is also low. The level of urbanization is low in the Sindhudurg and Ratnagiri districts of Konkan. Due to the lack of industrialization in Konkan and lack of employment opportunities, most of the people in Konkan migrate to Mumbai, Thane and surrounding areas. This seems to have affected the total population and urban

population of these districts. The level of urbanization is very low in all these districts. The educated community in these districts appears to be migrating to the big cities for jobs and to secure a better life. Out of all these districts, migration to Mumbai, Pune, Nashik, Nagpur and Aurangabad is higher. Overall, the growth rate of urban population in these districts is very low.

Map 1: Proportion of Urban and Rural Population in Maharashtra, 2011

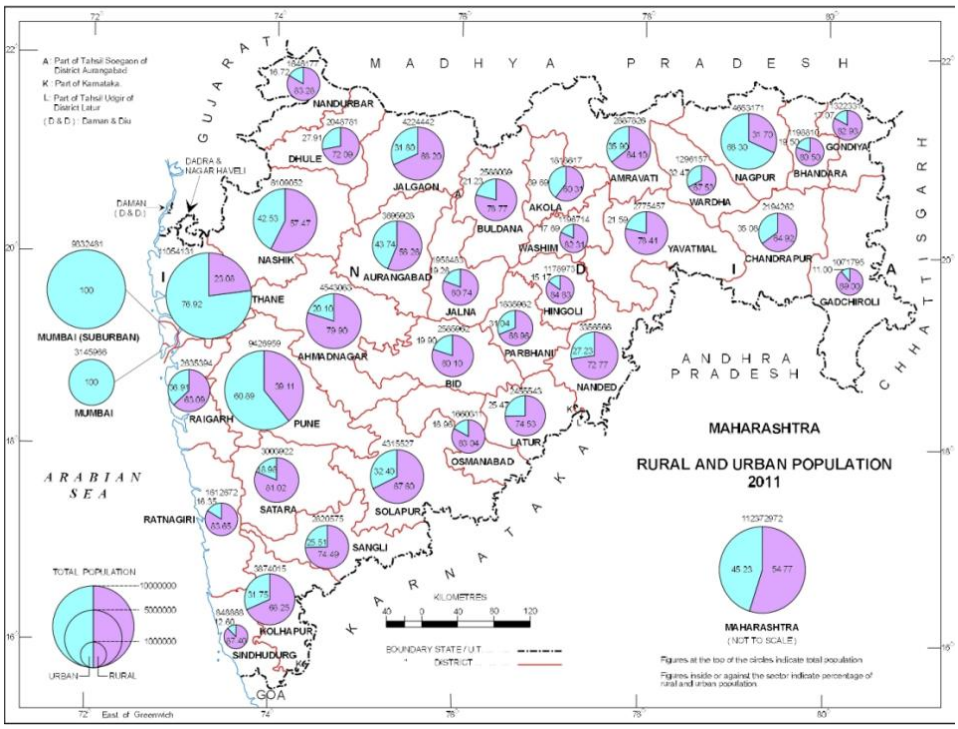

Source: Census Report of Maharashtra, 2011

Growth in the last decade in the districts of Maharashtra

Graph 2 shows the urban growth in the last decade (2001 to 2011). Between 2001 and 2011, the highest urban population growth rate (UPGR) has been observed in the following districts: Raigad (81.89 percent), Gadchiroli (75.34 percent) and Gondia (57.36 percent). Although Raigad, Gadchiroli and Gondia districts have a very high percentage increase in the urban population, their overall urban population is less. Raigad district has recorded an high increase rate in urban population (81.89 percent), with a total population of 9,72,809. However, in Thane (44.06 percent UPGR), Pune (36.63 percent UPGR) and Nashik (34.1 percent UPGR) districts, the urban population seems to have increased significantly. Among the districts with an increase of urban population between 25 and 50 percent are Aurangabad, Thane, Satara, Ratnagiri, Pune, Nandurbar, Nashik, Bhandara, Beed, Nanded, Yavatmal, Sindhudurg,

Wardha, Dhule, Jalgaon and Latur. In the remaining 16 districts, the increase in urban population is up to 25 percent. In the last two decades, the urban population in the state of Maharashtra has increased by 23.67 percent. Maharashtra has 19 districts with more than the state's average percentage increase in the urban population.

Map 2: Change in Urbanization between 2001 and 2011 in Maharashtra

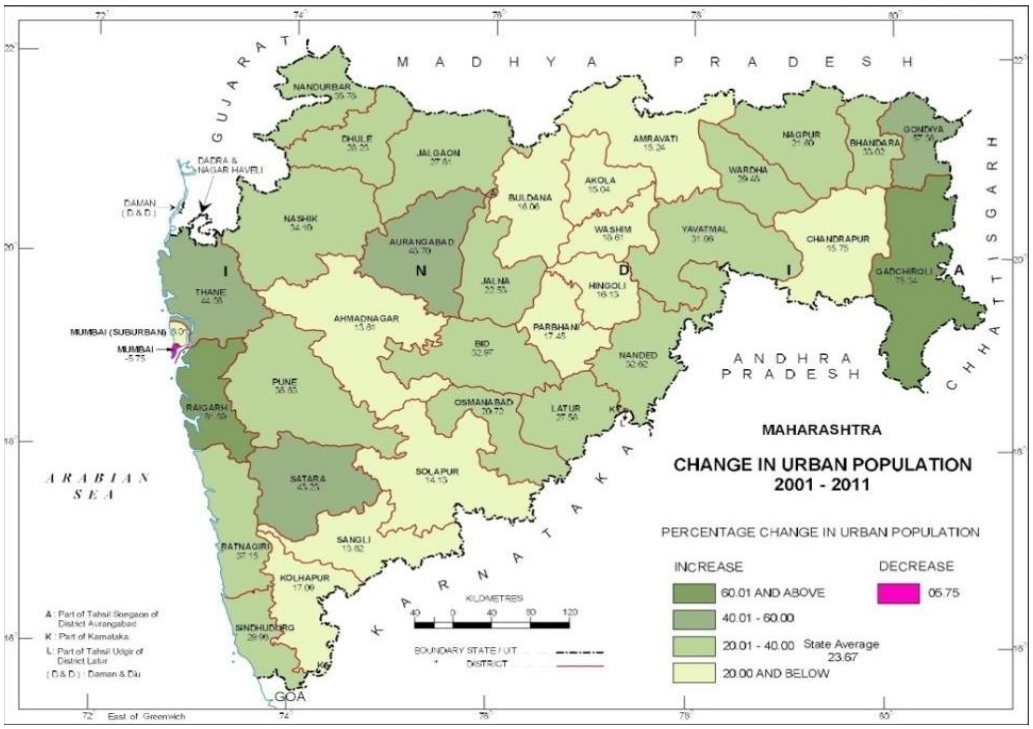

Source: Census Report of Maharashtra, 2011

Conclusion:

Maharashtra has the highest number of million cities in India. Maharashtra has the highest urban population in India. Maharashtra alone accounts for 13.15 percent of the total urban population in India. Maharashtra ranks first in India in terms of the total urban population. Maharashtra ranks second in terms of total population after Uttar Pradesh. Maharashtra's population has increased by 17.8 million in the last two decades (1991 to 2011). From 1991 to 2011, the urban population of Maharashtra has increased from 30.54 million to 50.83 million. The urban population of Maharashtra has increased tremendously due to the migration from the entire country as well as the rural areas of Maharashtra to the urban areas. The growth in terms of urbanization in Maharashtra is very heterogeneous. The western part of Maharashtra has a higher urban population than the eastern part. Marathwada and Vidarbha

in Maharashtra have the lowest level of urbanization. Mumbai and its suburbs in Maharashtra are 100 percent urbanized. Sindhudurg and Gadchiroli districts have the lowest level of urbanization. According to the 2011 Census report, the urban population of Mumbai, Mumbai Suburban, Thane, Pune, Nagpur, Nashik is more than twenty five lakhs. Greater Mumbai and Mumbai are two districts that are 100 percent urbanized. In the last two decades (1991 to 2011), the urban population in the state of Maharashtra has increased by 23.67 percent, which is very high. The level of urbanization in Maharashtra is increasing rapidly. By the end of 2021, the urban population in Maharashtra will be more than 52 percent. After analyzing the demographic data, in the future, the rate of urbanization in Maharashtra will increase rapidly. Various problems created due to rapid urbanization will have to be faced in the future. Therefore, it is very important to study the population in the context of urbanization. Such a study would provide guidelines for planning future demographic aspects.

References:

1. Agarwal, S. (2011). The state of urban health in India; comparing the poorest quartile to the rest of the urban population in selected states and cities. *Environment and Urbanization*, *23*(1), 13–28. https://doi.org/10.1177/0956247811398589
2. Bhagat, R. B. (2019). Emerging Pattern of Urbanisation in India there. *Economic and Political Weekly*, *46*(34), 10–12. http://www.jstor.org/stable/23017782
3. Bhagat, R. B., & Mohanty, S. (2009). Emerging pattern of urbanization and the contribution of migration in urban growth in India. *Asian Population Studies*, *5*(1), 5–20. https://doi.org/10.1080/17441730902790024
4. Chandrasekhar, S., & Sharma, A. (2015). Urbanization and Spatial Patterns of Internal Migration in India. *Spatial Demography*, *3*(2), 63–89.
5. Chhabra, P., Nair P., Gupta, A., Sandhir M., & Kannan, A. T. (2007). Immunization in urbanized villages of Delhi. *Indian Journal of Pediatrics*, *74*(2), 131–134. https://doi.org/10.1007/s12098-007-0004-3
6. Cohen, B. (2006). Urbanization in developing countries: Current trends, future projections, and key challenges for sustainability. *Technology in Society*, *28*(1–2), 63–80. https://doi.org/10.1016/j.techsoc.2005.10.005
7. Han, J., Hayashi, Y., Cao, X., & Imura, H. (2009). Application of an integrated system dynamics and cellular automata model for urban growth assessment: A case study of Shanghai, China. *Landscape and Urban Planning*, *91*(3), 133–141.
8. Iyer, S., Kitson, M., & Toh, B. (2005). Social capital, economic growth and regional

development. *Regional Studies*, *39*(8), 1015–1040.

9. Klasen, S., & Nestmann, T. (2006). Population, population density and technological change. *Journal of Population Economics*, *19*(3), 611–626.
10. Linard, C., Gilbert, M., Snow, R. W., Noor, A. M., & Tatem, A. J. (2012). Population distribution, settlement patterns and accessibility across Africa in 2010. *PLoS ONE*, *7*(2). https://doi.org/10.1371/journal.pone.0031743
11. Mohanty, S. K., Bhagat, R. B., Sharma, S. K., Nair, A., & Mishra, R. (2021). Development disparities across urban localities of Maharashtra: a multilevel analysis. *SN Social Sciences*, *1*(7), 1–20. https://doi.org/10.1007/s43545-021-00182-x
12. Mundhe, N. N. (2014). A study of urbanization in pune district using geoinformatics approach abstract : introduction : *International Journal of Advance and Applied Research (IJAAR)*, *2*(1), 45–55.
13. Nadu, T. (2001). *Regional dimensions of urbanisation : A Quick Analysis of the Census 2001*. *8*(6), 25–31.
14. Onda, K., Sinha, P., Gaughan, A. E., Stevens, F. R., & Kaza, N. (2019). Missing millions: undercounting urbanization in India. *Population and Environment*, *41*(2), 126–150. https://doi.org/10.1007/s11111-019-00329-2
15. Rain, D. R., Long, J. F., & Ratcliffe, M. R. (2007). Measuring population pressure on the landscape: Comparative GIS studies in China, India, and the United States. *Population and Environment*, *28*(6), 321–336.
16. Rain, D. R., Long, J. F., & Ratcliffe, M. R. (2007). Measuring population pressure on the landscape: Comparative GIS studies in China, India, and the United States. *Population and Environment*, *28*(6), 321–336. https://doi.org/10.1007/s11111-007-0055-4
17. Salunke, V. S. (2020). *Study of urbanization trends in western maharashtra*. *June*.
18. Sassen, S., Gugler, J., & Pattnayak, S. R. (1998). The Urban Transformation of the Developing WorldGlobalization, Urbanization, and the State. *Contemporary Sociology*, *27*(1), 86.
19. Waghmare, P. B. (2016). *Trends of Urbanization in Nanded District of Maharashtra State Trends of Urbanization in Nanded District of Maharashtra State*. *May*.

Paper-10

An Analysis of the Determinants of Rural and Urban migration in Maharashtra state

Dr. Deshmane Jini Subhash
Assistant Professor
Department of Zoology

Dr. Prakash Rajaram Chavan
Head &Assistant Professor
Department of Statistics

Smt. Kasturbai Walchand College, Sangli
Affiliated to Shivaji University, Kolhapur, Maharashtra

ABSTRACT

In rural areas, less employment opportunities, low wages, drought, lack of basic amenities, landlessness, are the factors contributes towards the rural to urban areas. However, in urban areas, more employment opportunities, higher income, better wages, better facilities activities are pull factors for migrants. However, there are some consequences of migration. The influx of workers in urban areas increases competition for the job, houses, school facilities, etc. Having large population puts too much pressure on natural resources, amenities and services. we analyze the collected data by using statistical tools.

Key Words: - Rural Migration, Urban Migration, Statistical Analysis.

1 Introduction

The problem of rural to urban migration is a relatively old and ubiquitous phenomenon globally. However, in recent years, it has become a cause of concern at the global, regional and national levels. The unprecedented levels of urbanization characteristic to most developing countries have resulted in the movement of people from rural to urban areas subsequently resulting in the emergence of slums and informal settlements. Like many developing countries, Rwanda has been facing increasing challenges related to rural to urban migration. It is in this context that the broad objective was to analyze factors that determine rural youths' decision to migrate to urban areas in Nyabihu (Western Province) and Burera (Northern Province). A combination of non-probability and probability sampling methods were used to select a total of 113 for

inclusion into the survey. Structured questionnaires were used as the principal data collection instruments. Secondary data was used to complement primary data collected in this study. The study was pillared on two hypotheses. The study also postulated that the desire for better employment opportunities explains the likelihood to migrate. The results of the study showed that youths who are likely to migrate are predominantly aged between 17 to 22 years, and earn incomes of less than 34129Frw per month, are male, have primary education, are currently not employed. Youths migrate for a number of reasons which include the need for temporary and permanent job opportunities, access to social services and infrastructure, as well as schooling opportunities. Factor analysis showed that there are three factors which are critical in rural to urban migration and these are availability of social services in rural areas, which is likely to deter youths from migrating.

2. Methodology

Descriptive Statistics are used to describe the basic features of the data in a study. They provide simple summaries about the sample and the measures. Together with simple graphics analysis, they form the basic virtually every quantitative analysis of data.

VARIANCE: Variance is a measure of dispersion which explains the distribution of values around the mean it is the square of S.D. We can calculate variance by dividing the sum of squared deviation of all measured values by the number of all measured value.

$$\sigma=\sum(Xi-\overline{X})^2/\mathrm{N}$$

Defination of F-Test:

F-Test is described as a type of hypotheses test, that is based anSnedecor's F-distribution under the null hypothesis. The test is performed when it is not known whether the two populations have some variance.

F-Test can also be used to check if data confirms to regression model, which is acquired through least square analysis. When there is multiple linear regression analysis, it examines the overall validity of model or determines whether any of independent variables is having a linear relationship with the dependent variable. A number of prediction can be made through, the comparisomon of the two data set. The expression of the F-Test value is in ratio of variances of the two observation which is shown as under

$F_{\text{value}} = \sigma_1^2/\sigma_2^2$ Where, σ^2 = Variance

- The assumptions on which F-test relies are:
- The population is normally distributed.
- Samples have been drawn randomly.
- Observation are independent.
- H_0 may be one sided or two sided.

F-test Analysis : Graphical Analysis

PARAMETER	RURAL	URBAN
EMPLOYMENT	1790	5115
WORK	38	155
EDUCATION	212	392
MARRIAGE	10691	4177
AFTER BIRTH	3105	2004
WITH FAMILY	2603	4585
OTHER	4011	2837
TOTAL	22450	19265

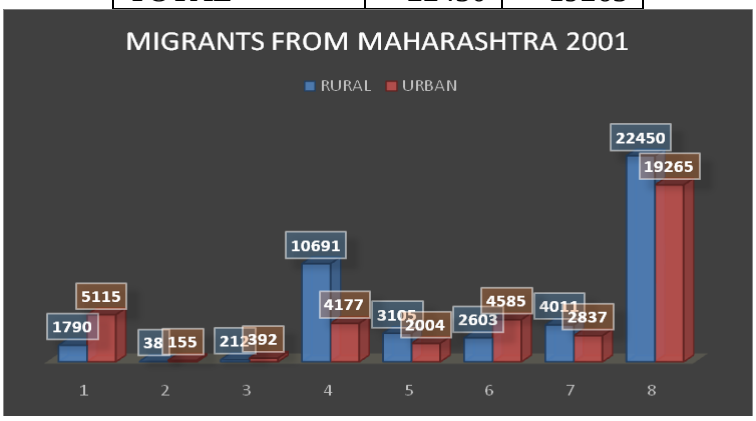

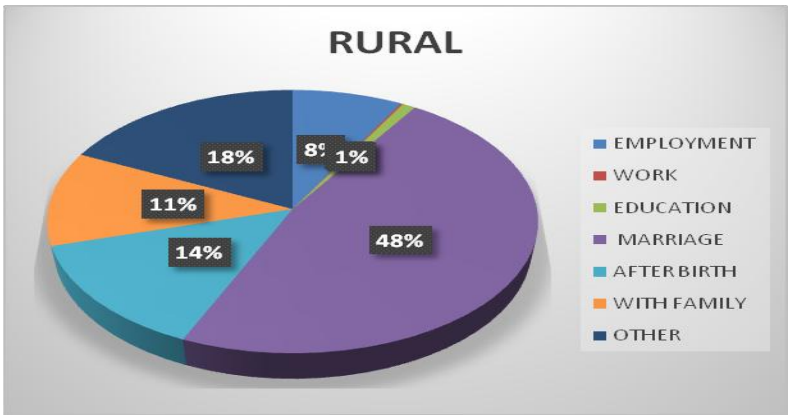

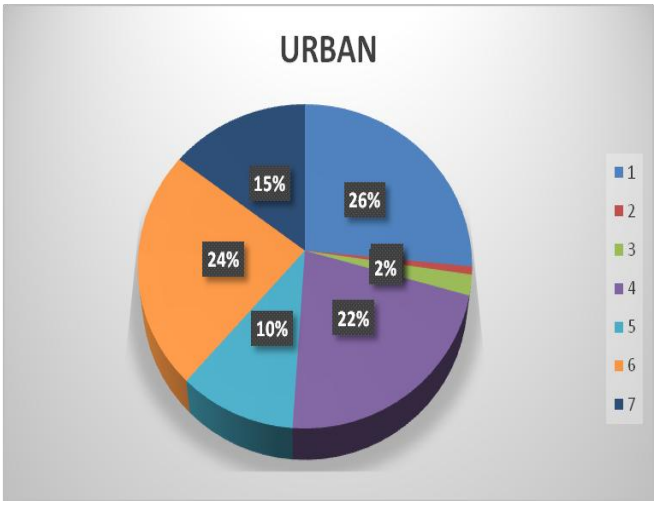

PARAMETER	MALE(In lakhs)	FEMALE(In lakhs)
EMPLOYMENT	62.32	6.73
WORK	1.67	0.26
EDUCATION	4.41	1.63
MARRIAGE	1.14	147.54
AFTER BIRTH	31	20
WITH FAMILY	29.74	42.14
OTHERS	37.26	31.26

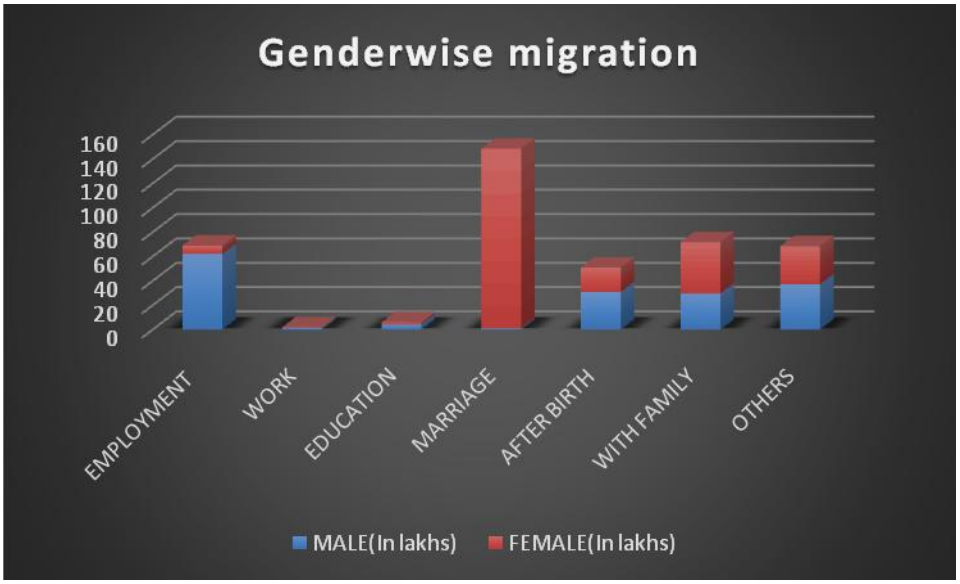

PARAMETER	Total
EMPLOYMENT	69.05
WORK	1.93
EDUCATION	6.04
MARRIAGE	148.68
AFTER BIRTH	59.09
WITH FAMILY	71.88
OTHERS	68.48

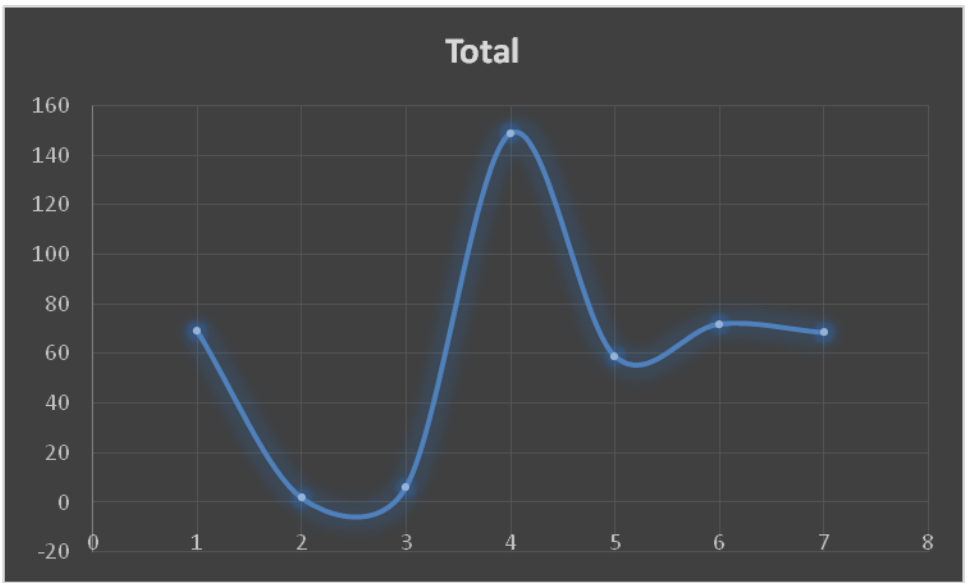

PARAMETER	X_1	X_2	X_1^2	X_2^2
EMPLOYMENT	1790	5115	3204100	26163225
WORK	38	155	1444	24025
EDUCATION	212	392	44944	153664
MARRIAGE	10691	4177	114297481	17447329
AFTER BIRTH	3105	2004	9641025	4016016
WITH FAMILY	2603	4585	6775609	21022225
OTHER	4011	2837	16088121	8048569
TOTAL	22450	19265	150052724	76875053
MEAN	3073.167	2752.143		

3. Calculations: We have, $n_1 = n_2 = 7$, $\bar{X}_1 = 3207.1428$, $\bar{X}_2 = 2752.1428$

$? X_1^2 = 150052694 \sum X_2^2 = 76875053$

HYPOTHESIS : $H_0 = s_1^2 = \sigma_2^2$ V/S $H_1 = \sigma_1^2 \neq \sigma_2^2$

$\sigma_1^2 = 1/n_{1-1} [\sum X_1^2 - n_1 \bar{X}_1^2] = 13008744.19$ Similarly, $\sigma_2^2 = 3975854.99$

$F_{cal} = \sigma_1^2 / \sigma_2^2$ $F_{cal} = 3.2719$

$F_{tab} = F_{[6,6,0.05]} = 4.284$

$F_{cal} < F_{tab}$

RESULT : We accept H_0. We reject H_1.

$H_0 = s_1^2 = \sigma_2^2$

4. Concluding Remarks-

1. There is equality of variance of migration in rural and urban areas.
2. Female migrants are more in number than male migrants due to marriage parameter.
3. There is no significant difference between observed and expected frequency. Hence we accept null hypothesis.

5. References-

1. Bhagat RB. Conceptual Issues in Measurement of Internal Migration in India. IUSSP XXVth International Conference, Contributed Papers, France, 2005, 18-23.
2. Census of India. Soft copy, India D-series, Migration Tables. Registrar General and Census commisioner, India, 2001-2011.
3. Chakravarty B. The Census and the NSS Data on Internal Migration, in Ashish Bose, 1997,
4. Chatterjee Atreyi, Ashish Bose. Demographic Data on Internal Migration and Urbanisation from Census and NSS – An Appraisal, in Ashish Bose, Davendra B. Gupta, and Gaurisankar Raychaudhuri (eds.), Population Statistics in India. New Delhi: Vikas Publishing House Pvt. Ltd, 1977.
5. Davendra B Gupta, Gaurisankar Raychaudhuri (eds.). Population Statistics in India. New Delhi: Vikas Publishing House Pvt. Ltd